Norwegian University of Life Sciences
Faculty of Environmental Science and Technology
Department of Mathematical Sciences and Technology

Master Thesis 2014
60 credits

The Changing Arctic Sea Ice Cover- Regional and Seasonal Aspects

Rebekka Jastamin Steene

The changing Arctic sea ice cover regional and seasonal aspects

Department of Mathematical Sciences and Technology (IMT)

NMBU, Norwegian University of Life Sciences

Rebekka Jastamin Steene

December 2014

Preface

This thesis marks the final work of my Master of Science degree in Environmental Physics and Renewable Energy at The Norwegian University of Life Sciences (NMBU). I was pleased to be able to round up the years as a student by putting acquired understanding of physics into the context of Arctic climate change, as I have been writing my thesis in the field of climate dynamics.

I would like to express my gratitude to Tor Eldevik who welcomed me at the Centre for Climate Dynamics (SKD) and agreed to become my supervisor. Thank you for great advices and helpful guidance along the way. To Ingrid Onarheim who also provided helpful supervision, thank you for comments and feedback of high value.
I would also like to thank my main supervisor Arne Auen Grimenes, who supported my choice of thesis and helped me realize it. Thank you for your supervision and encouragement. You have the most marvelous ability to make anything sound like a walk in the park.

To who ever initiated the week of Pakistani food in the cafeteria at Samfunnet, I know I speak for at least three students, including myself, when I say thank you for the nutritional highlight of final weeks as master students.

Additionally I would like to thank Helene for sending me thoughts of goats and cabins, reminding me of the most joyful things awaiting out there.
And last but not least I would like to thank my fellow students at TF211. The cheerful fellowship will be greatly missed in the aftermath. A special thanks to Maria and Frida for shearing struggles and sorrows to the very end.

Rebekka Jastamin Steene,
Ås, 14th of December 2014

Abstract

As global climate changes are becoming increasingly evident, increasing air temperatures, melting glaciers, rising sea levels, and decreasing biodiversity is observed at increasing rates worldwide. The Arctic sea ice cover has has become a key indicator of the ongoing global climate change through its substantial decline in both extent and thickness.

In this study we show how the observed regression of the Northern Hemisphere sea ice is distributed over different regions of the Arctic Ocean and adjacent seas. We further provide an evaluation of to what extent the regions are reflecting changes during summer or winter seasons, exemplified by the months of September and March. We also relate the changes to observed atmospheric and oceanographic conditions. Data from passive microwave satellite measurements are used to investigate regional and seasonal time series of ice extent.

All regions except one show a decreasing trend throughout the data record. It is found that six of twelve regions has seen an accelerated decline during the last decade. This is either caused by an increasingly smaller summer minimum, or by a prolongation of the regional summer season.

It is further found that summer melting is initiated by atmospheric heat in the areas where the recession of ice extent most prominent. The process of freezing during winter is found to be particularly sensitive to the oceanic temperatures in the regions receiving currents of warm Atlantic Water.

Contents

List of Figures

List of Tables

Chapter 1

Introduction

One of the present times greatest global concerns is the ongoing changes of the Earths climate. These changes arise from a warming of the globe, and are observed in numerous ways worldwide. Increasing air temperatures, melting glaciers, rising sea levels, and decreasing biodiversity are just some examples. Induced by human activity, the revolting climate also poses severe challenges for humanity. The much needed reactions can include both limitation of and adaption to the consequences. Either way it is crucial for the outcome of our efforts that we have the best possible understanding of the processes of our surrounding nature and how they are invoked by a changing climate.

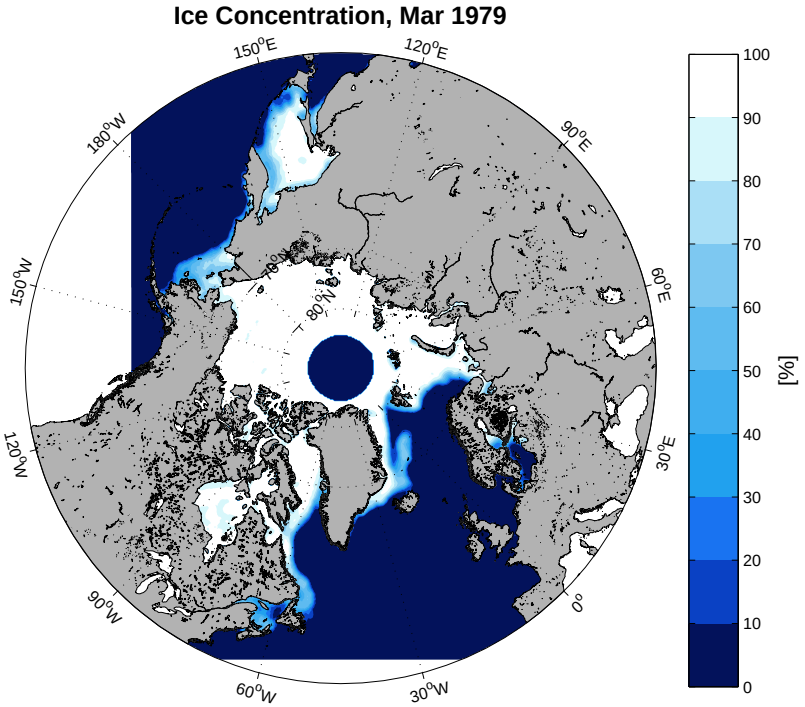

Figure 1.1: *Sea ice in the Arctic, ice concentration in March 1979.*

1.1 Retreating Sea Ice extent

The Arctic sea ice cover, manifesting as a white blanket covering much of the Arctic Ocean and adjacent seas (Fig. 1.1), has in resent years been broad-casted as one of the clearest indicators of the ongoing climate change. According to the latest report by the International Panel on Climate Change (IPCC) the summer minimum ice extent has decreased with 11.5 $\pm$ 2.1% per decade over the period from 1979 to 2012 (Stocker and Qin, 2013). The report also states, with high confidence, that the ice extent has seen a declining trend in every season and between every successive decade over these 34 years. It can hereby be said that the Arctic sea ice extent undoubtedly is subject to a steady retreat. Time series of sea ice extent and related variables, as those presented by Cavalieri and Parkinson (2012), clearly illustrates that deviations are becoming more negative, and the extent itself smaller.

The observed downward trends have shown to be largest in September (Fig. 1.2), the month when we commonly experience the minimum extent of the year (Serreze et al., 2007). To date, the smallest extent on record was seen in September 2012 (Parkinson and Comiso, 2013). In Figure 1.3 the ice cover for this month of minimum extent is depicted in comparison to the ice cover of September 1979, the first year of our longest satellite record of sea ice. The observed decrease has made rise to the question of if, and in that case when, we will see a seasonally ice-free Arctic (e.g. Smedsrud et al., 2008; Wang and Overland, 2012). Subsequently prospects are made regarding which consequences this might entail (e.g. Notz, 2009; Eisenman and Wettlaufer, 2009).

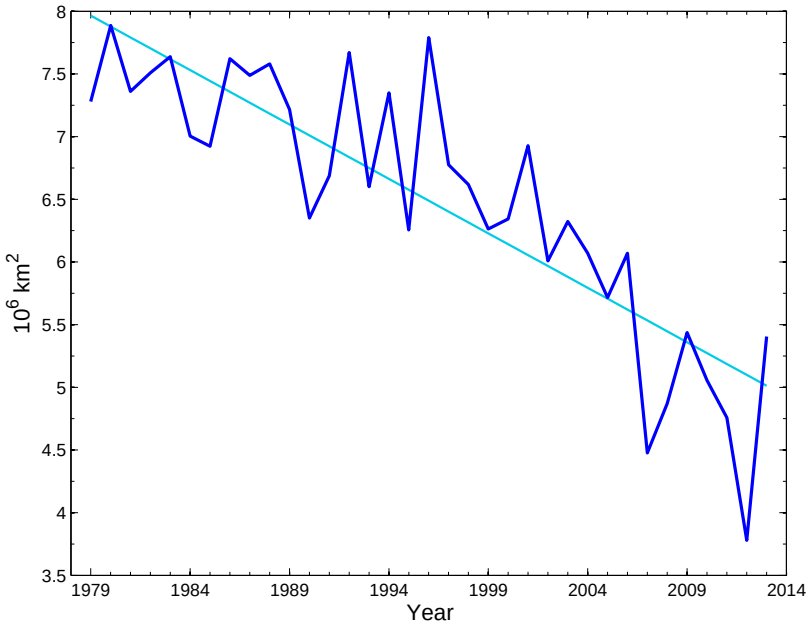

Figure 1.2: *Arctic Sea Ice in decline, September ice extent 1979-2013.*

Overland and Wang (2007) undertook an assessment of the models used by the International Panel on Climate Change (IPCC) in their Fourth Assessment Report (AR4). They investi-

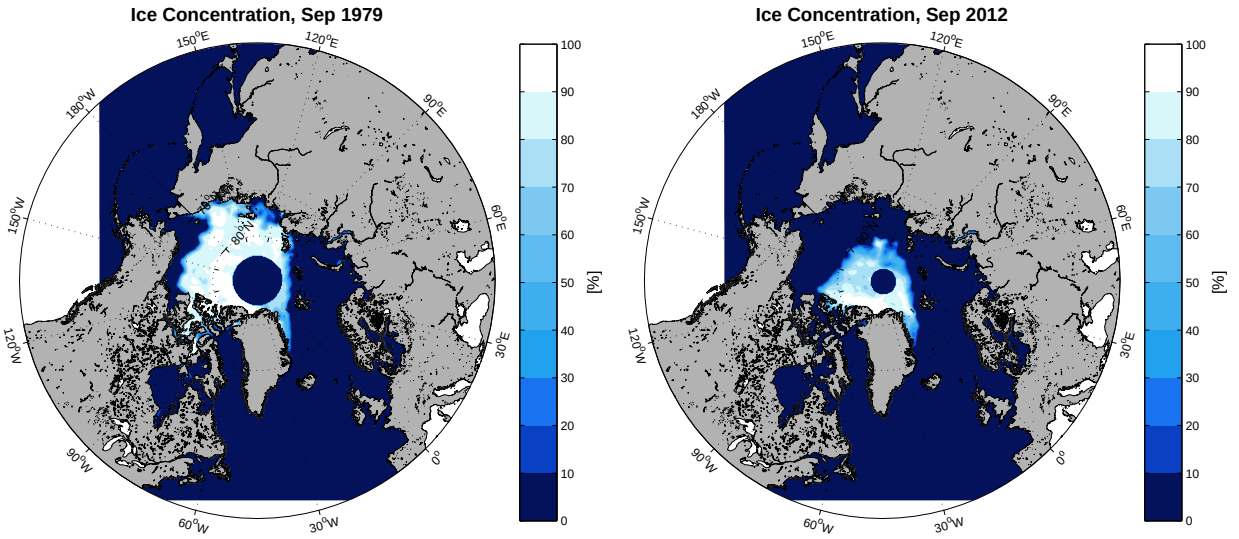

Figure 1.3: *Arctic Sea Ice in decline, ice cover in September 1979 and 2012.*

gated their performance regarding sea ice projections on a regional level, with the intention to discuss the evolution of ice extent through the 21st century. The findings of Overland and Wang (2007) suggested a future summer sea ice area loss of more than 40% by 2050 in the marginal seas of the Arctic basin. Also in the adjacent seas of Bering, Okhotsk and Barents, although with less confidence, their results suggested a similar decline of 40% by 2050 in winter sea ice area.

Cavalieri and Parkinson (2012) addressed the evolution of the Arctic sea ice using observational data. Applying a regional division in the same manner as Overland and Wang (2007), although not making the same areal selections, they enabled a comparison of ice extent and area between different geographical areas. Using data from polar orbiting satellites they investigated the development of the Arctic sea ice over a temporal span of 32 years, primarily discussing yearly and seasonal trends. They found that for all their individual regions, except for the Bering Sea, the trends in yearly sea ice extent were negative. In accordance with what they found for the Northern Hemisphere as a whole.

1.2 Part of a changing climate

The global climate system consists of an immense amount of different variables, all interacting at various levels. As a part of this system the sea ice is influenced by a vast variety of factors. Most prominent are temperatures, insolation, wind, waves, and ocean currents. Being part of the closely coupled air-ice-sea system the sea ice works as an insulator between the ocean and atmosphere. The layer of frozen water restricts heat fluxes between ocean and atmosphere with its low heat conductivity, and also inhibits exchange of mass, momentum and chemical constituents. As the ice reduces its presence exchange patterns, both between and within

atmosphere and ocean, are altered. Changes that in turn can have nested effects throughout the global climate system.

The concept of feedback mechanisms, in a climatic context, is by now a well known phenomenon. Implying that a perturbation to the climate system, leading to a change in either positive or negative direction, does not end its effect on the climate by this. But instead leads to changes in other parts of the system giving new perturbations to the climate. The ice-albedo feedback (Notz, 2009) is one such mechanism.

It is also worth to note that our comprehension of the future climate relies entirely on projections made by climate models. The broader our understanding of the physical processes involved is, the better we can represent them in model designs, and consequently the more reliable our model outputs will be. Hence it is obvious that an increased understanding of the physics of climate will be beneficial in further development of climate models, and hereby contribute to clarify the picture of anticipations of our common global future.

1.3 The significance of a decreasing Arctic sea ice cover

Although a vital part of the global climate system, this is not the only concern to which the Arctic sea ice is influential. The Arctic Ocean, itself with an area of approximately 9.4 million square km (Jones, 2001) and including adjacent seas covering more than 14 million square km, is almost encircled by the shorelines of major continents. Hence vast areas are directly influenced by and sensitive to the presence of sea ice in these oceans.

Local communities build upon hunting and fishing, may experience an alteration of their life basis as a consequence of a retracting ice cover. Remote areas where people depend on certain means of transportation to connect with the outer world may see need for adaptation to new conditions. Shipping can face refreshing opportunities by opening of new sea routes, but unpredictable ice conditions may give rise to a new challenges. The access to resources entrained in these areas will be altered by changing ice conditions. Not addressing the ethics or politics of petrol exploitation here, it is an unavoidable fact that an opening of the Arctic Ocean also makes available new reservoirs of fossil recourses, opening yet another possible pathway for the future development of the Arctic region.

Apart from the human community, other inhabitants of the Arctic ecosystem are equally worth some concern. Many species are carefully adapted to the marginal conditions of which they are reliant on. Rapid changes in surrounding environment can be crucial if the new conditions does not give room for some continuation of previous ways of living. Adaptation takes time, but the rate of decay of Arctic sea ice seems to outrun many of the characteristic lifeforms living of it. Measures of adaptation, both in favor of human benefits as well as ecological preservation, requires good predictions and extensive insight in the climate system to be conducted adequately.

1.4 Objectives

Although there is a clear overall decreasing trend in the extent of the Arctic sea ice cover, there are obvious observable disparities between different regions (Parkinson and Cavalieri, 2008). Neither in the context of climate change, nor for the local interests in the Arctic, is this a matter of trivial character. The main goal for this work is therefore to identify these regional differences, with a similar approach, but using updated observational data compared to that of Cavalieri and Parkinson (2012). It is also of interest to put our findings in the context of regional projections like those carried out by Overland and Wang (2007). We further strive to point out possible reasons for more or less pronounced characteristics in the temporal evolution of the ice cover. Beyond this it is an aim to investigate the seasonal variabilities in the ice cover, and hereby strive to detect the regional significance of summer melting as opposed to lack of winter freezing.

Thus this thesis hereby aims to:

- describe the regional and seasonal differences in evolution of distribution/prevalence of Arctic sea ice during the satellite record from 1979 to 2013.
- evaluate how the temporal variance of the ice cover for the different regions can be related to summer melting versus winter freezing processes.

Chapter 2

Theoretical background

2.1 Air-Ice-Sea interactions

The climatic state of the Arctic Ocean region is highly dependent on the relation between atmosphere, ocean and, when present, the sea ice. Atmospheric and hydrospheric conditions are on their own crucial to the existence of ice in the first place, but at the same time the interaction with ice is also influential for the condition of adjacent masses of air and ocean throughout the region. Heat, mass and momentum are transported across the boundaries between atmosphere, hydrosphere and cryosphere, and these constant interactions are what sets the basis for variability of the sea ice. When studying the coupling between different parts of the climate system we define so called boundary layers within the atmosphere and ocean. Spanned by the vertical range of air and sea for which the interaction with an adjacent mass has noteworthy influence. These layers are respectively called the atmospheric boundary layer (ABL) and the oceanic boundary layer (OBL), or when ice is present referred to as the under-ice boundary layer (UBL) (McPhee and Morison, 2001). Along with other constituents heat and momentum are transported vertically in these boundary layers through turbulent mixing. The physical processes of these boundary layers have direct impact on the concerned spheres dynamics, and are hence profound drivers for the entire climatic system. In the interaction between ice and ocean the most essential variables are temperature, salinity, density and momentum.

2.2 Sea Ice formation and growth

Sea water with a salinity of 34 psu has a freezing point of -1.86°C (Eicken, 2003). When the ocean air interface reaches this temperature the process of sea ice formation starts. In the Arctic the salt contents of the water normally lies between 31 - 34 psu in the upper layers of the water column (Jones, 2001), approaching 35 psu at greater depths. Thermal mixing, that is vertical eddies generated by temperature gradients, ensures that freezing does not

start until the entire surface layer of some depth has reached the freezing point.

While forming, the ice is constantly transmitting energy to its surroundings in terms of latent heat of freezing. Thus the growth rate of the ice can be determined by evaluating the heat budget at the interfaces. In the search for a net heat flux the energy balance at both the upper and lower ice interface of the ice needs to be taken into account, not to forget the thermal properties of the ice. After the initial formation, the thermodynamics of sea ice can be described by the classical heat conduction equation in one dimension (as stated by e.g. Leppäranta (1993)).

$$\partial/\partial t(\rho_i c_i T) = \partial/\partial z(\kappa_i \partial T/\partial z) + q \tag{2.1}$$

Here t is the time, ρ_i the ice density, c_i the specific heat of ice, T is the ice temperature, z the vertical stretch, κ_i is the heat conductivity of ice, and q is an internal source therm. To fully describe the heat conduction through ice, and the evolution of ice thickness, we depend upon the boundary conditions determined by the heat flux to the atmosphere at the top (Eqn. 2.2), the continuous bottom temperature (Eqn. 2.3), and the dynamic lower boundary level, driven by the latent heat related to melting and freezing (Eqn. 2.4).

$$-\kappa_i \partial T/\partial z = Q_T \tag{2.2}$$

$$T = T_f \tag{2.3}$$

$$\rho_i L dH/dt = -\kappa_i \cdot \partial T/\partial z|_{bottom} - Q_w \tag{2.4}$$

As H is the thickness of ice, this provides the means to estimate ice growth, dH/dt, with time. Here Q_T is the heat flux at the air-ice interface, T_f is the freezing point temperature, L is the latent heat of freezing and Q_w is the oceanic heat flux into the ice. This set of equations were the basis for the development of the first analytical models of sea ice. Such as Stefan's Law from 1891 (Leppäranta, 1993), which is still widely referred to today. The oceanic heat flux, Q_w, is either assumed to be known or to be found from the turbulent heat flux in the under-ice boundary layer, expressed as

$$\overline{w'T'} = w_0 L + \kappa_i \cdot \partial T/\partial z|_{bottom} \tag{2.5}$$

Here $w_0 = -(\rho_i/\rho_w)dH/dt$ is the isostatically balanced ice melt rate. The prime marks denotes fluctuations in the properties of temperature, T and vertical velocity, w, and hence $\overline{w'T'}$ equals the covariance of these.

During ice formation and growth much of the original salt content of the water is excluded from the ice through brine release. This is then convected vertically in the water column by turbulent eddies, setting up a salt flux described as

$$\overline{w'S'} = w_0(S_0 - S_i) \tag{2.6}$$

where S_0 is salinity at the interface and S_i is salinity of the ice (McPhee et al., 2008), and as above the prime marks indicate fluctuations in the properties. Thus the turbulent motions in the UBL does not only promote an upward flux of heat (2.5), but also governs a downward convection of salt. This facilitates a second approach for estimation of growth rate, through coinciding measurements of salinity and vertical velocity.

2.3 Processes of sea ice melt

In the situation contrary to that discussed in the previous section, when temperatures rices above the freezing point, the process of melting becomes pertinent. Sea ice has the potential to undergo melt initiated from each of the two interfaces (atmosphere and ocean).

Since the temperature where ice meets ocean always will be at the freezing point When the heat flux from the ocean into the ice exceeds the outgoing conductive heat flux, the result is a net melting and a recession of the ice from underneath. The oceanic heat flux Q_w can be estimated from turbulent boundary layer theory (McPhee, 1992), and expressed as done by Leppäranta (2011)

$$Q_w = \rho_w c_w C_{wH}(T_w - T_f)|\mathbf{U}_w - \mathbf{u}| \tag{2.7}$$

Here ρ_w and c_w is the density and specific heat of seawater, C_{wH} is the ice-water heat exchange coefficient, $\mathbf{U}_w$ is the water velocity and $\mathbf{u}$ velocity of the ice. The water temperature, T_w, will always be higher than the freezing point temperature, and hence the oceanic heat flux is, without exceptions, positive towards the ice. This implies a melting process that is active all year around. Even mid winter, when the net growth of ice is unequivocal, there is a continuous cyclic process of freezing and thawing.

At the upper interface though, the ice is openly exposed to air of which temperatures can be much lower than the freezing point, and consequently a net positive heat flux alone is not enough to enable melting at the upper ice surface. It will rather result in warming of the ice, and associated melting on microscopic scales, but will not influence the ice thickness until the temperature reaches the bulk melting point of ice. At this stage surface ablation is initiated. For this reason melting initiated from the air-ice interface is first seen when entering the more temperate seasons, and the air temperatures at ground level can be elevated above the freezing temperature.

The relative importance of the two ablation processes is not firmly stated, but ice loss in the Arctic is assumed to have been dominated by surface melting. The later observed changes in the Arctic climate system has though been associated with an increase in importance of bottom melting (Thomas and Dieckmann, 2009).

2.4 Marginal ice zone (MIZ)

In the Arctic ice formation mainly happens in the Marginal ice zone (MIZ), marking the zone of transition between ice cover and open water. Generally defined as the ice within a distance to the open ocean small enough for the ice to feel the impact of the ocean directly (e.g. Wadhams, 1986; Leppäranta, 2011; Squire, 2007). More tangible referred to as an area stretching about 100 m from the ice edge. Due to the yearly cycle of melting and freezing the location of the MIZ shifts constantly throughout the year, reaching its southernmost location in March, when the ice has its largest extent. From there it retreats southwards until the minimum extent is seen in September. The MIZ is by far the most active region when it comes to thermal growth and recession of sea ice as air-ice-sea interactions are most intensive here. The ice edge also marks a front in temperature and salinity of the ocean, and the MIZ is important for the induction of the characteristic layering of the Arctic Oceans.

2.5 Ocean currents and circulation

As is illustrated in Figure 2.1 the Arctic Oceans has two main connections to other regions of the word oceans. One being the gateway between the European continent and the coast of Greenland, where water masses are exchanged with the Atlantic Ocean. The other being where the American and the Asian continents boarder each other, and the Bering Sea and Bering Strait define the port to the Arctic from the Pacific Ocean. This is a relatively narrow and shallow strait, limiting interoceanic mass exchange in this part of the Arctic Ocean. On the opposite side on the other hand, the North Atlantic current drives an important exchange of water masses. Flowing along the Norwegian coast, and entering the Arctic Ocean through the eastern Fram Strait and the Bering Sea it carries warm water from the tropical regions of the west Atlantic Ocean to the Arctic Oceans. This is an important heat flux into the Arctic region.

In the upper layer (also known as the Polar Mixed Layer (PML)), water originating from the incoming Atlantic Water (AW) flows eastwards from the Fram Strait and Barents Sea, towards Laptev Sea, before it turns to cross the Arctic Basin and exits again through western Fram Strait. The colder Pacific originating water parts in two branches after entering through the Bering Strait. One branch continuing north, meeting up with, and to some extent mixing with, the Atlantic originating current as it traverses the Arctic Basin to eventually reach the Fram Strait. The other branch sticks to the coast of North America, allowing some of it to exit through the Canadian Arctic Archipelago, while a fraction follows the margin of the basin all the way to western Fram Strait (e.g. Jones, 2001).

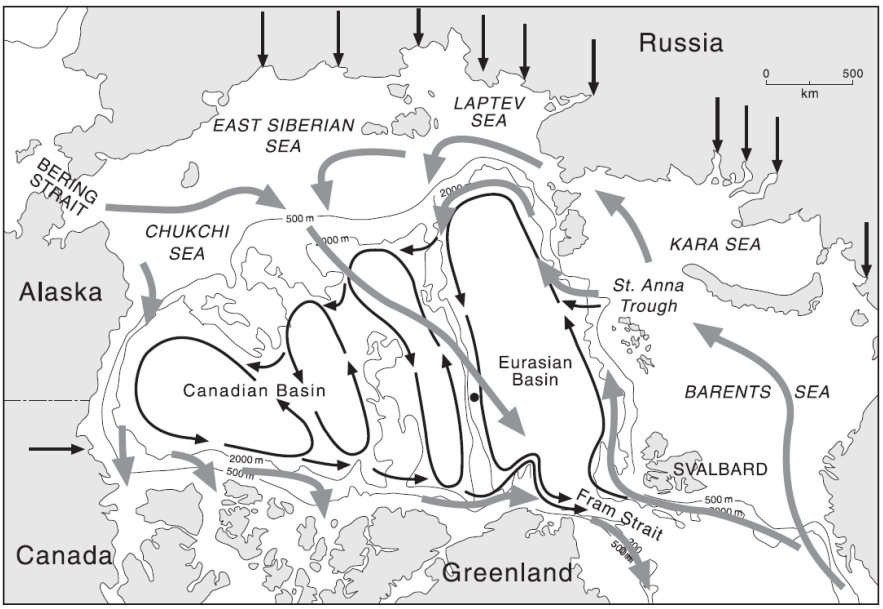

Figure 2.1: *Currents of the Arctic Ocean. Gray arrows shows circulation of upper layer water, while black arrows represent the Atlantic Layer and water down to 1700 m. Straight arrows indicates mouths of major rivers. Figure from Jones (2001).*

2.5.1 The Arctic cold halocline

An important feature of the Arctic Oceans is the Arctic cold halocline (e.g. Aagaard et al., 1981; Rudels et al., 1996), separating an upper Polar Mixed Layer (PML) from the underlying Atlantic Layer. A halocline is a prominent vertical gradient in salinity. The Arctic cold halocline is named so because it refers to segment of the vertical profile of the ocean with a continuous increase in salinity with depth, while the temperature remains low, close to the freezing point. As low temperatures leads to a sea water density mainly determined by the salinity, the steep halocline also defines a pycnocline (a strong density gradient). This leads to a stable stratification of the water masses, restricting vertical mixing in the water column and hereby hampering any upward heat transport. For the ice cover this is an important feature, promoting winter sea ice growth and contributing to the retainment of a stable ice cover (Thomas and Dieckmann, 2009).

The Cold Halocline Layer (CHL) is generally seen at depths between 50 m and 200 m (Aagaard et al., 1981). It is thought to be formed and maintained by a selection of physical processes (Kikuchi et al., 2004). Steele and Boyd (1998) among others describes the advective and convective mechanisms of cold halocline formation (Fig. 2.2). The advective formation involves shelf water, which is growing colder and more saline during ice formation in winter. It eventually becomes so dense that, when flowing off the shelf, it penetrates under the Polar Mixed Layer, settling as a boundary layer between this and the underlying Atlantic Layer. In the convective the upper incoming Atlantic Water (AW) cools to the freezing point, and when ice formation starts brine release and salination of the under-ice

water induces vertical mixing by convection. Hence a well mixed layer of relatively saline water at freezing point temperature is created. With input of fresher water from ice melt or river runoff, a new layer of fresher water forms and mixes downwards. Leaving a halocline where the water column transits to the winter mixed layer.

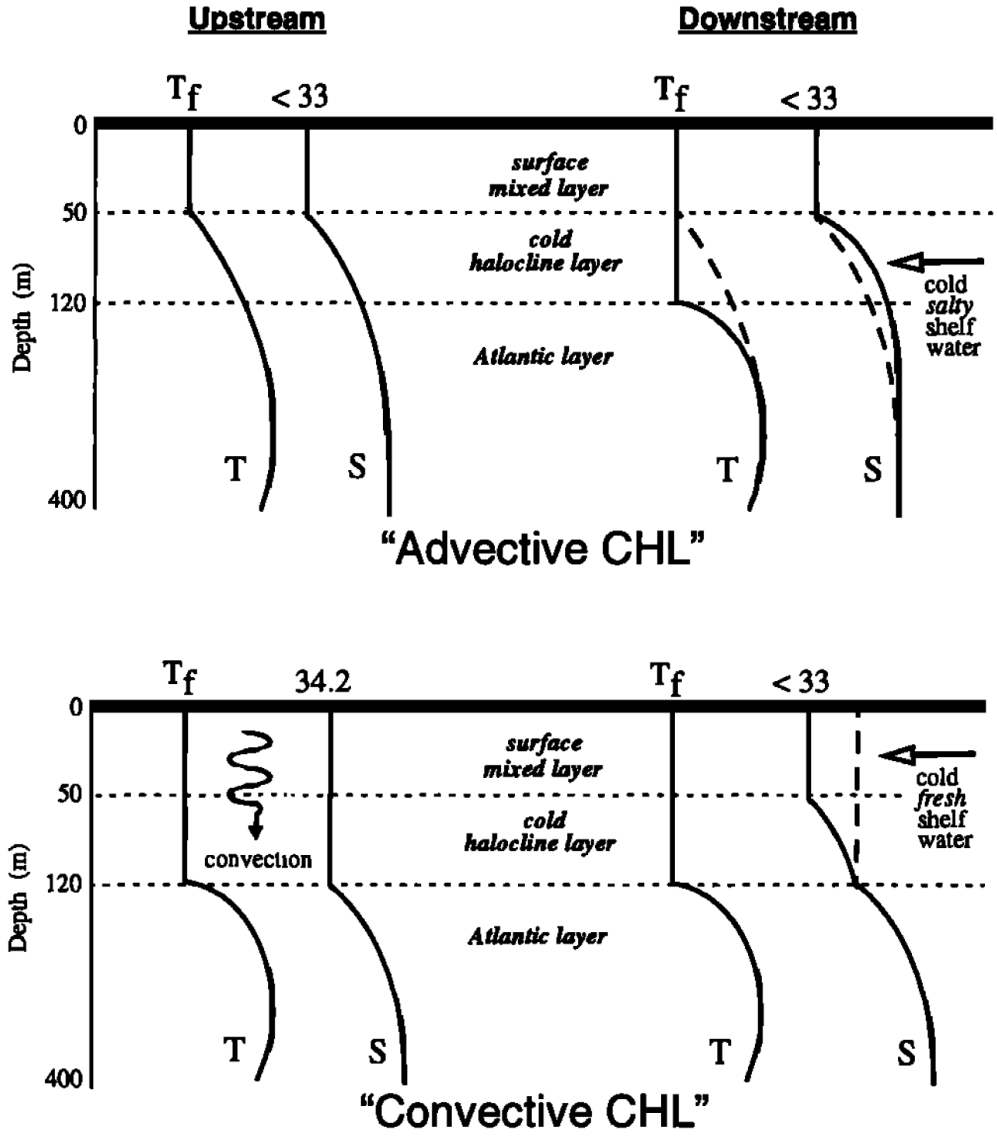

Figure 2.2: *Illustration of the process of advective and convective cold halocline formation. Figure from Steele and Boyd (1998).*

2.6 Transport of sea ice

Sea ice extent is not only controlled by the growth and decay, but also by movement of the ice masses. Although this study focuses on thermodynamic effects on the ice cover also the dynamic processes are essential to bear in mind when evaluating the larger picture. Even though a superficial glance can give the impression of a seemingly settled body of mass, the sea ice (except the smaller land fast segments) is undoubtedly in frequent motion. Driven by both ocean currents, atmospheric winds and internal inertia, ice masses are distributed around the oceans. The force balance controlling the motion (Thorndike and Colony, 1982) is given by

$$C + \tau_a + \tau_w + T = 0 \tag{2.8}$$

where τ_a is atmospheric stress, τ_w is stress from the ocean, T is the pressure gradient force due to sea surface tilt, and C is the Coriolis force, an apparent force invoked by the rotation of the Earth. Here internal forces are neglected, assuming they are equalized to zero, in what is known as the free drift assumption (Rothrock, 1975; Ogi et al., 2008). As long as we are far enough from the shorelines this is a reasonable assumption.

The drift of sea ice does not only redistribute ice masses within the Arctic Ocean, but also leads to export of ice to southern-more latitudes. The ice drifting southwards is facing inevitable melt, and hence the ice area flux leaving the Arctic region represents a net sink of ice mass. This implies that an increased export rate can be of utter importance to the evolution of the Arctic sea ice cover. The Arctic Ocean is connected to the circulation systems of the world oceans through the Barents Sea, the Fram Strait, the Davis Strait and the Bering Strait. The main exit for sea ice entrained in the Arctic Ocean is through the Fram strait northeast of Greenland (e.g. Kwok et al., 2004; Smedsrud et al., 2011). It was long a common assumption that this ice flux accounted for close to all of the ice mass leaving the Arctic by mechanical drift. Later studies have though suggested that the export directed through the channels and straights of the Canadian Arctic Archipelago, leading in to the Baffin Bay, is not entirely negligible (Münchow et al. (2006) and Kwok et al. (2010)). Nevertheless, the mechanisms and conditions determining if the ice flux here is significant is not yet throughly mapped.

2.6.1 Wind forcing

As atmospheric stress is part of the force balance determining ice motion, winds have profound impact on the drift vector. Recognized since early oceanographic studies (Ekman, 1905) is a theoretical relation suggesting that the ice floes with a speed of 2 % of the surface wind speed, directed 45° to the right relative to the wind. Surface winds are however highly variable, in both space and time. A characteristic making it less suitable for large scale analyses. In this regard a similar relation between ice velocity and geostrophic wind has been examined (e.g. Thorndike and Colony, 1982).

Geostrophic wind occurs when there is a balance between the Coriolis force and the pressure

gradient force, and it is not affected by the friction of the ground. This is mainly a theoretical situation, but still geostrophic wind serves as a highly useful variable since it can be calculated from gradients in sea level pressure. Thorndike and Colony (1982) found that the mean ice drift over a time span of several months is directly related to the geostrophic wind. Assuming ocean currents to be equally important, the combination of the two was seen to explain the average ice drift. On shorter time scales Thorndike and Colony (1982) found the geostrophic wind to account for as much as 70 % of the variance in drift velocity. Expressing ice drift velocity, $\mathbf{u}$, on the form

$$\mathbf{u} = A\mathbf{V}_g + \overline{\mathbf{V}}_w + \boldsymbol{\varepsilon} \tag{2.9}$$

where $\mathbf{V}_g$ is the geostrophic wind vector, $\overline{\mathbf{V}}_w$ is the mean ocean current and A is stating the relative drift velocity, while $\boldsymbol{\varepsilon}$ represents a varying nonlinear component of the drift.

2.6.2 Convergence and divergence

When in motion the ice may break up into floes, and can further be subject to utterly compression or expansion. In the case of convergence, if ice floes are crammed together it will lead to mechanical ice growth. The ice piles up to form areas of ridges and hummocked ice. These dynamic processes can make the ice far thicker than if it had just been subject to thermodynamical growth. On the other hand, divergence in the ice cover promotes thermodynamical ice growth during wintertime. This is because it generates cracks, leads and polynyas, where the unveiling of open water enables new ice to form. Hence a diverging drift regime will enhance ice production and favor a thin but extensive ice cover.

2.7 Ice thickness distribution

When evaluating sea ice, the lateral area covered has often been the predominant concern, and this is also what is evaluated in this study. But the total volume of the ice is also of uttermost importance. By increased melting the ice can undergo substantial diminishing of the total ice mass, but perturbations to change in area covered is only seen where the entire vertical span is depleted. The Arctic ice cover has proven to be far from a uniform body of mass. Both thickness and structure vary greatly between regions. The main distinction in ice characteristics is usually made between first-year (FY) ice and multi-year (MY) ice (Maslanik et al., 2007), the latest being ice of which has lived through at least one melt season. While FY ice is newly formed and typically has quite even surfaces and constrained thickness, MY ice has experienced several growth seasons and is additionally thought to have undergone more ridging and rafting making it comparably thicker. The thickest ice is found in the areas north of Greenland and the Canadian Archipelago, where the ice piles up against the coast, only released through the straits and sounds of the Canadian Arctic Archipelago.

As part of the observations indicating a changing Arctic climate also the ice-thickness distribution has seen a severe shift. According to recent studies with global climate models the

transition to a seasonal nearly ice-free Arctic can to occur within three decades (Wang and Overland, 2009, 2012). A portion of ice situated where we today find our thickest ice cover is likely to remain beyond this time span (hence nearly ice-free), but we are evidently facing an open Arctic Ocean during summer in a foreseeable future. It is also a stated concern that seasonal forecasting is growing more uncertain as the ice cover grows thinner.

2.8 Other aspects of influence to sea ice

There is of course a vast web of mechanisms influencing the sea ice. Even though not the major drivers, many factors may still be of high importance to the large scale picture regarding evolution of the Arctic sea ice cover (Stroeve et al., 2012). The impact of changes in these conditions can be hard to quantify, and the relevant impact may change as the characteristics of the ice cover changes. The presence or lack of snow can invoke both surface radiative properties and ice-air heat transfer (Maykut, 1978; Overland and Guest, 1991). Cloud cover is influencing the incoming part of the radiative budget (Curry et al., 1996), and changes in the appearance and quantity of clouds can hence also have influence on the ice cover (Kapsch et al., 2013). Similar effects are seen from changes in atmospheric humidity, and Kapsch et al. (2013) advocate that enhanced transport of humid air from southern latitudes not only facilitates increased cloud formation, but also enhances the greenhouse effect directly. The fresh water content of the water masses is also a relevant factor for sea ice. The salinity has implications for the formation of ice, but more importantly the fresh water content, and especially runoff from larger rivers can invoke the stratification and circulation patterns of the ocean (Aagaard and Carmack, 1989; Serreze et al., 2006). This can in turn lead to locally altered heat budgets, with consequences for the growth and decay of sea ice (Ekwurzel et al., 2001).
The above mentioned are all some of the many factors that can contribute to perturbations in the ice cover evolution. Although important these variables are however all beyond the scope of this thesis.

Chapter 3

Data and Methods

The data used in this study results from satellite observations of the Arctic region over a period of 35 years (1979-2013). Presented as time series the quantified data works as a base for evaluation and comparison of the variability in sea ice cover between different regions of the Arctic Ocean as well as different seasons of the year.

3.1 Passive microwave remote sensing of sea ice

3.1.1 Dataset

The sea ice quantities used are based on data material from remote sensing of the sea ice concentration by satellite. The data set is acquired from the North-American NSIDCs (National Snow and Ice Data Center) database (Cavalieri et al., 1996). These measurements goes back to October 1978 and thereby make a good basis for further investigations of changes and variability in the sea ice cover through time series analysis. The data set consists of passive microwave measurements gathered by NIMBUS-7 and DMSP (Defense Meteorological Satellite Program) satellites. Sensors used are SSMIS (Special Sensor Microwave Imager/Sounder) SSM/I (Special Sensor Microwave/Imager) and SMMR (Scanning Multichannel Microwave Radiometer), which all measures the surface brightness temperature. The dataset has a resolution of 25 km $\times$ 25 km, provided in a polar stereographic projection.

3.1.2 Advantages and disadvantages

Microwave satellite data is among the methods of remote sensing that is most advantageous for large scale data collection in the Arctic regions. Due to special conditions both in insolation, temperatures and weather patterns, scientific observations in the polar regions has always posed challenges not seen in other parts of the world. Passive microwave, in remote

sensing terminology, means observing the long wave radiation emitted from the earth it self. Hence it does not depend upon sunlight, and data can be collected 24 hours a day. This means that it is also operational during polar night in the Arctic and Antarctic regions. Using spectral bands in the microwave range the long wavelengths makes it possible to "see through" clouds, ensuring that overcast conditions will not hamper the ability of data acquisition.

Although following what is called a polar orbit, the satellites does not pass exactly over the poles. Their orbit is designed so that it has a slight tilt relative to the Earth axis. As an effect of this there is a circular area around the North Pole from which it is not possible to achieve measurements. During the first eight years of measurements the area afflicted by this inability of data collection was at it largest, measuring 1.19×10^6 km^2. This was consistent until July 1987, when the shift to the first DMSP satellite reduced the area to 3.11×10^5 km^2 (visualized in Fig. 3.1). Further, there were some disruptions during the first week of May 1995, leading to three days with discrepancies in size of the data void. In the Arctic this has to date not been a tremendous drawback, because the vicinity of the North Pole has shown to be subject to a persistent total ice cover all year around. The development seen the latest years though, indicates that this can rise as a greater problem in the future, as the ice melts in a somewhat unforeseen rate (Stroeve et al., 2007). Conditions, even in the midst of the Arctic Ocean, may not be stable for very long. And the potential changes in this region will then be of utter interest to monitor in the coming years.

For temporal analyses it is desirable with a dataset of substantial length. A 35 year long time series makes it likely that the data can provide significant results. Even though some of the newer satellites and instruments provide measurement methods of sea ice concentration of more accuracy (e.g. Aqua (AMSAR-E) and CryoSat (SIRAL)), none of these can provide historical data in the range of the dataset processed by NASA/NSIDC. Therefore the combined dataset from NIMBUS-7/DMSP satellites is still crucial to studies of long term sea ice development.

3.1.3 Algorithm for conversion to sea ice concentration

Brightness temperature is a measure of the Earths emitted intensity, quantified as the temperature it would have if it was a black body in thermal equilibrium. This can generally be used to investigate a variety of different quantities. To make the conversion from brightness temperature to sea ice concentration algorithms assigned for this purpose are utilized. A multiple of such algorithms exists, developed by different research communities, and giving somewhat different results (e.g. Ivanova et al., 2014; Andersen et al., 2007). The data set used in this study consists of grids of sea ice concentration calculated by the NASA Team algorithm. This algorithm is developed by the Oceans and Ice Branch, Laboratory for Hydrospheric Processes at NASA Goddard Space Flight Center (GSFC). As seen in the work of Ivanova et al. (2014) the NASA Team algorithm lies in the lowest range of available algorithms when it comes to output in ice area and extent. The extent is still within one standard deviation of the mean of the eleven sea-ice algorithms evaluated by Ivanova et al. (2014). But when it comes to area it is by far the lowest. Nevertheless, the variability is in general

similar for all investigated algorithms. Since the main objective in this work is evaluation of variation, the choice of algorithm should not be crucial to the result.

3.2 Processing

3.2.1 Sea ice extent and area

The data is, in this study, further processed in several steps. The sea ice concentration is a quantification of the fraction or percentage of each grid cells area that is covered by ice. Due to the polar stereographic projection of the gridded data set a scaling mask is applied to get the correct surface estimates. This mask is provided by NSIDC.

The estimates for sea ice extent is calculated by setting a concentration limit of 15%, a threshold commonly used for quantification of sea ice (see Parkinson and Cavalieri, 2008, for reasoning). Any area with a concentration below this limit is not defined as ice covered, while the area within the limit is summed up to express the total sea ice extent. Ice extent is in other words calculated as the cumulated area with an ice concentration of 15% or more. The ice edge is defined as the line along this 15% threshold. Ice area differ from ice extent by expressing the true ice covered area. While still only considering concentrations of 15% or more, the extent of each grid cell is multiplied with the respective ice concentration, then the cumulated sum denotes the ice area for a region.

The data lacking region around the North Pole is simply treated as ice covered area. For an ice extent calculation this means that an ice concentration above 15% is assumed throughout the region lacking data. While for ice area calculations the corresponding assumption is an ice cover of 100% concentration for the entire data lacking region. If the compilation of the ice cover is altered the assumption of continuous ice cover is more persistent than the assumption of consistent hundred percent concentration. Hence, for a study such as conducted here, ice extent comes forward as a more reliable quantification compared to ice area. It is also to be mentioned that the data void does wary in size between the different satellites of whose measurements are compiled in this dataset.

3.2.2 Concentration anomalies and trends

Downloaded as daily values, the matrices of sea ice concentration were computed into monthly averages. The concentration data facilitates calculations of gridded anomalies. This is done by, for each grid point, subtracting the 30-year climatology, which is the 1981-2010 mean value. The base 1981-2010 is used for the sake of consistency with the classical standard for defining climate normals, which is taking averages of climatological variables over 30 years. The World Meteorological Organization (WMO) currently defines 1961-1990 as their climate normal, but for historically limited records it is common to use the three latest complete decades. Gridded trends are also estimated. For each grid point a linear trend in time (Eqn.

3.1-3.2) is calculated based on data from the entire series. These calculations enables the map presentations shown in Chapter 5.

3.2.3 Time series of extent

Time series are constructed for monthly mean values of ice extent and area (Sec. 3.2.1). The gridded ice concentration data were first divided into specified regions (see Sec. 3.2.5). Daily extent and area values were first calculated from daily concentration grids, before averaging over the months. Even though monthly mean concentrations were already computed (Sec. 3.2.2), these were not used because of an aspiration to avoid propagation and enhancement of possible erroneous data. Regional values were conducted by first extracting daily concentration data for the separate regions by masking. Further the calculations of daily then monthly extent values were conducted. As for the gridded concentration anomalies, extent anomalies are taken from the mean of the respective month over a period of 30 years, from 1981 to 2010 (cf. Sec. 3.2.2). Time series were created both for ice extent and area, but only extent results are presented and discussed here. Deviations from area outcome may be commented upon. In general, although ice area gives lower values, the outline and variations of the time series does not differ much.

3.2.4 Annual cycle and trends in extent

The time series of sea ice extent were in addition used to compose annual cycles. By dividing the time series in 12 month segments cycles for each year was obtained. Further taking an average for each month of the year the compilation resulted in a mean annual cycle. This was done for the time series of all regions. In addition monthly trends were computed for the extent values of each region. Considering values for one month of the year at a time, a linear least square fit (Eqn. 3.1-3.2) was used to obtain the trend for the month in question.

3.2.5 Regional division

Based on existing definitions of seas of the Arctic, whilst conveniently modified, a division of the Arctic Ocean and adjacent seas as illustrated in Figure 3.1 is used in this study. These are the same boarders as used by the MASIE-NH (Multisensor Analyzed Sea Ice Extent - Northern Hemisphere) dataset (Fetterer et al., 2010). From the boarder definitions gridded masks were made to extract data from each region. This provided the necessary basis to create regional time series, using the procedure described above (Sec. 3.2.3). The characteristics of each region are given a more in-depth description in Chapter 4.

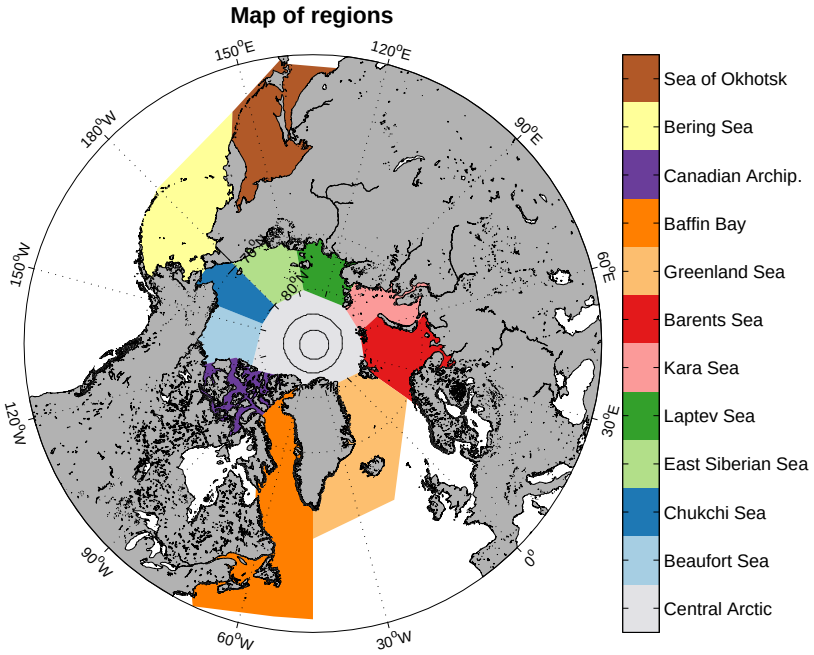

Figure 3.1: *The area of study is divided into several regions as shown here. The division is based on existing definitions of seas of the Arctic, with some modifications, resulting in boarders equal to those used in the dataset of Fetterer et al. (2010). As the satellite data is lacking measurements in an area around the North Pole the dashed circles indicates the smallest and largest extent of this area (Sec. 3.1.2).*

3.3 Additional data sets

To facilitate a discussion of mechanisms behind variability an trends in ice cover, it is necessary to include other influential climate variables in the interpretation of sea ice data. With this in mind, presumably relevant variables were acquired for compilation with, and further assessment of our findings.

3.3.1 Oceanic data

Ocean temperatures were obtained from the Ocean Climate Laboratory (OCL) at the National Oceanographic Data Center (NODC) (Levitus et al., 2012). This gridded data set, with a resolution of 1.0° × 1.0°, consist of vertically averaged temperature anomalies (respective to a 1955-2006 mean) for the upper 100 meters of the water column. These data are downloaded as seasonally averaged values, meaning that it is provided in January-March, April-June, July-September and October-December means. When compared with monthly sea ice data this needs to be kept in mind. However, as the ice extent at a certain time is the result of the rate of melting and freezing over a preceding time span, we regard the seasonal

means as advantageous in this study. As the co-variability is evaluated the to seek a causal relation, using temperature data averaged over a period of two moths prior to the ice data will predominantly make any assumptions about causality increasingly plausible. We therefore use January-March mean in co-evaluation with ice extent for March, and accordingly the July-September mean is used together with the ice extent for September.

3.3.2 Atmospheric data

Monthly mean atmospheric temperatures were retrieved from ERA-Interim reanalysis (Berrisford et al., 2011). The data used are gridded temperature estimates at 2 meters height, with a resolution of $0.75° \times 0.75°$. When used in this study computed anomalies with a 1981-2010 base were made. To ensure consistency with the data for ocean temperatures three month seasonal averages were created also here. After which they were averaged over the regional areas to form time series matching those of ice extent.

3.4 Time series analyses

To enable comprehension of the time series attained, they were evaluated and analyzed by statistical methods. The aim was to build an understanding of the complex picture and to grasp the essence of the data, regarding origin of variability in the ice extent. The approaches used are described in the following sections.

3.4.1 Trends

A temporal trend describes the general development of a variable as time evolves. Trends are estimated by the least-square method, mimicking the outline of the respective variables evolution as well as possible. Different trend profiles, such as linear, polynomial and logarithmic, can be chosen based on the shape of the data attained. In this study linear trends are estimated. Not because they are believed to make the best fit to the data, but to give a common base for interregional comparison, and possibly make the results comparable to other studies. The linear trend line can be expressed as

$$\hat{y} = \hat{\alpha} + \hat{\beta}x \tag{3.1}$$

$$\hat{\beta} = \frac{\sum_{i=1}^{n}(x_i - \overline{x})(y_i - \overline{y})}{\sum_{i=1}^{n}(x_i - \overline{x})^2} = r \cdot \frac{S_Y}{S_X} \qquad \hat{\alpha} = \overline{y} - \hat{\beta}\overline{x} \tag{3.2}$$

where x_i and x_i are observations of the two compared variables, and $\overline{x}$ and $\overline{y}$ are the respective means of all observations (Løvås, 2013).

3.4.2 Correlation

Correlation addresses how separate quantities vary according to each other, and is commonly referred to when detecting and discussing co-variability. To quantify the co-variability the correlation coefficient r, a dimensionless parameter, is a useful and widely applied tool. It is expressed as the relation between covariance, S_{XY}, and the product of standard deviations for each variable, denoted S_X and S_Y (Løvås, 2013):

$$r = \frac{S_{XY}}{S_X \cdot S_Y} = \frac{\sum_{i=1}^{n}(x_i - \overline{x})(y_i - \overline{y})}{\sqrt{\sum_{i=1}^{n}(x_i - \overline{x})^2} \cdot \sqrt{\sum_{i=1}^{n}(y_i - \overline{y})^2}} \tag{3.3}$$

Here x_i and y_i is observations of the two compared variables, and $\overline{x}$ and $\overline{y}$ are the respective means of all observations.

In this study mutual correlation between the regional time series of ice extent were done, after first performing detrending and standardising. Correlation of regional ice extent time series to their corresponding time series of air and ocean temperature were also conducted. Statistical significance of correlations can be tested based on a calculated p-value. In this study correlations are tested to a level of 0.95, and it is in each case indicated if the null-hypothesis of no correlation is rejected.

Chapter 4

Study regions

The areas looked upon in this study are the Arctic Ocean and adjacent seas. This comprises the ice influenced regions of the Northern Hemisphere. There are however some areas in the Northern Hemisphere which, although known to see seasonal ice cover, are not included in this study. These are the Cook Inlet, Yellow Sea, Baltic Sea and Hudson bay. They are left out mainly due to limited areal coverage and geographical separation from the remaining study regions, and thus less anticipated relevance for the Arctic ice cover as a whole. Although in the ensemble category, Northern Hemisphere, these areas are included as well. In the following the different regions, as can be viewed in Figure 3.1, are given a brief introduction. Note that the areal extents given in the descriptions are the areas of the regions used in this study, and they may therefore differ from other sources although the same names are used. For instance many of the regions in the interior of the Arctic Ocean are typically stretched further north in this study than what the official definition (IHO, 1953) states.

4.1 Central Arctic

The Central Arctic region is here defined as an area of $3.51 \cdot 10^6$ km^2, encircling the North Pole. Although not completely circular it generally incorporates the area north of 80°N. It has coastal contact where it is confined by the northern edge of Greenland, and along its boarder to the Canadian Arctic Archipelago. These coast bordering areas of the Central Arctic holds the thickest ice found in the Arctic Ocean. It is also assumed that this will be the last ice holding areas when presumably approaching a seasonally nearly ice free Arctic. The region also stretches down to the northern coasts of Svalbard and Franz Joseph Land. Note that this is the region holding the area of missing satellite data. However, as argued in Section 3.1.2 this is not thought to be a problem in this study.

4.2 Beaufort Sea

The Beaufort Sea is adjacent to the northern coast of Canada and Alaska. Covering an area of $1.10 \cdot 10^6$ km^2 it boarders the Chukchi Sea in the west and the Canadian Arctic Archipelago in the east. The region incorporates areas between 65°N and 80°N. The largest and longest river of Canada, the Mackenzie River, has its outlet here, providing an additional input of freshwater. Beaufort Sea is known to have substantial reservoirs of petroleum and natural gas, which has been the basis for the main human activity in this region.

4.3 Chukchi Sea

Chukchi Sea lies north of the Bering Strait, and is hence the first region of the Arctic Ocean to meet the inflowing water from the Pacific. Its southern limit being the narrowest part of the Bering Strait, the region stretches as far north as 80°N, covering a total area of $9.68 \cdot 10^5$ km^2. The Chukchi Sea is not a sea of great depths, and contains areas as shallow as 50 m.

4.4 East Siberian Sea

The East Siberian Sea lies north of the far eastern Russia, shearing boarders to with Chukchi Sea in the east and Laptev Sea in the west. This region with an area of $1.05 \cdot 10^6$ km^2, reaches up to 80°N where it meets the Central Arctic region. As a shelf sea it sees depths as limited as 25 m. The main current from both the Atlantic and the Pacific enters this region briefly, before they turn north to cross to the other side of the Arctic Ocean. Hence the intrusion of these currents to the inner shelf areas is minimal. Along the coast several rivers flow into the region, providing important sources for freshwater input.

4.5 Laptev Sea

Laptev Sea is situated west of the East Siberian Sea. It comprises of an ocean area of $8.06 \cdot 10^5$ km^2, bordered in the south by the Siberian coast. While this region lies between the East Siberian Sea in the east and Kara Sea in the west most of its oceanic input consists of Atlantic water masses entering from the Kara Sea. Among the rivers having their outlet in this ocean region the largest is the Lena River.

4.6 Kara Sea

The Kara Sea is an area of $9.13 \cdot 10^5$ km^2. It is sheltered by the Russian archipelago Severnaya Zemlya in the east, marking its boarder to the Laptev Sea. The western boarder is denoted by the Novaya Zemlya islands continuing in a line stretching north from these till it encounters the archipelago of Franz Josef Land. Also in this region there are important rivers having their outlets along the coast, of these Ob and Yenisei are the largest.

4.7 Barents Sea

The Barents Sea, along with the Greenland Sea, marks the entrance to the Arctic Ocean from the Atlantic side. Off the northern coast of Norway, Finland and Russia it comprises of an area stretching up to 81°N, Franz Josef Land and the Svalbard archipelago forming its vertices. In total the region is covering $1.56 \cdot 10^6$ km^2. Atlantic Water enters the Arctic through this region, traveling with the North Atlantic Current, and for a major part of the Atlantic inflow the Barents Sea (for large periods of the year) represents the first encounter with the ice edge.

4.8 Greenland Sea

Greenland Sea lies off the east coast of Greenland. In this study the region of Greenland Sea is extended southwards, stretching to 55°N south of the Cape Farewell. It also includes extended areas to the east, in all covering $3.73 \cdot 10^6$ km^2. In the north of the Greenland Sea region we find the Fram Strait, forming the connection to the Arctic Ocean. The East Greenland Current flows from here continuing south along the coast of Greenland, making it an important region for transport of water mases from, not excluding to, the Arctic Ocean.

4.9 Baffin Bay

When addressing the Baffin Bay region in this study we refer not only to the commonly defined Baffin Bay, restricted by a southern limit of 70°N, but also include both the Davis Strait, Labrador Sea and the Gulf of St. Lawrence. This means the region stretches down to a latitude of 38°N at the most, including an area of $4.85 \cdot 10^6$ km^2. In the north the Baffin Bay region is linked to the Arctic Basin by the Nares Strait, and also through various straits and sounds of the Canadian Arctic Archipelago.

4.10 Canadian Arctic Archipelago

The Canadian Arctic Archipelago, for convenience often only referred to as the Canadian Archipelago, is situated north-east of the Canadian mainland. The sea in this area is composed of numerous straits and sounds surrounding the Canadian Arctic islands. In all the ocean areas are adding up to $7.72 \cdot 10^5$ km^2. This region is characterized by a total cover of land fast ice in mid winter, shifting to more dynamic drift ice regime as the ice melts during the warmer periods of the year.

4.11 Bering Sea

The Bering sea marks the gate to the Arctic Ocean from the Pacific Sea. Meeting Chukchi Sea in the Bering Strait, its connection with the Arctic Ocean is not more than 82 km wide. In all the Bering Sea region covers an area of $3.17 \cdot 10^6$ km^2, with longitudinal limits formed by the Russian coast in the west and the Alaskan coast in the east. From the Bering Strait at 65°N it extends south to approximately 47°N. Lying outside the Arctic Ocean one may to a lesser extent expect similar behavior with other regions.

4.12 Okhotsk Sea

Along with Bering Sea the Okhotsk Sea region represent the Pacific outer regions of the Arctic Oceans adjacent seas. The Sea of Okhotsk itself is a semi-enclosed sea west of the Kamchatka Peninsula of Russia. The region in this study stretches south to additionally include northern parts of the Sea of Japan. In total this covers an area of $2.23 \cdot 10^6$ km^2, with a latitudinal extent between 66°N and 39°N.

Chapter 5

Results

In this chapter the obtained data is presented in various manners, aiming to grasp some core features of the variability and evolution of the Arctic sea ice cover. Gridded data is included to give a spatial conception, and time series of quantified data aims to give an understanding of the temporal evolution. March and September are chosen in particular as months of exemplification. This is because they are known to be the months of general maximum and minimum ice extent in the Arctic, and are on this basis regarded to be useful representatives for the winter and summer seasons. The hope is that a study of these two extremes can contribute to the give a deeper insight in mechanisms of the changing ice cover.

5.1 General overview

From the processed satellite data maps with gridded linear trends of sea ice concentration were made. In Figure 5.1 the trends throughout the 35 year long (1979-2013) study period is displayed. It appears that the trends to a large extent are negative, and the steepest decadal trends are found in areas of the Barents and Kara Seas (See display of regions in Fig. 3.1). Pronounced trends are also seen in a belt crossing the regions of Beaufort, Chukchi and East Siberian Sea. While the eastern part of the Bering Sea reveals the only area of slight positive trends. Figures 5.2a and 5.2b show the linear trend in mean March and September concentrations, respectively. In March (Fig. 5.2a) the trends are seen in areas known to comprise the marginal ice zone (MIZ) (definition in Chap. 2.4) of the winter sea ice cover. This is areas from the Labrador Sea stretching north across Davids Strait towards Greenland. Areas off the west coast of Greenland extending north of Iceland towards Svalbard. Also including large fractions of the Barents Sea, where in fact the strongest negative trends are seen. On the Pacific side trends are located throughout the Sea of Okhotsk and in the Bering Sea. As in Figure 5.1 the trends observed in the Bering Sea are positive, forming an arc south of the Bering Strait. The positive trends are stronger and more extensive for calculations based on March values only, than for the overall trend throughout the period. In September (Fig. 5.2b), the computed linear trends are found to be negative throughout most of the

Arctic region. The only detectable exception being a fraction of minor positive trends off the north-east coast of Greenland. A larger area, covering most of the Beaufort, Chukchi, East Siberian and Laptev Seas, are characterized by negative trends of 20 % per decade or more.

In the same manner as for the gridded trends results from calculations of concentration anomalies, relative to the mean of the period 1981-2010, are shown in Figures 5.3a-5.3b. As 2012 was a year of record low summer ice extent in the Arctic (e.g. Parkinson and Comiso, 2013), the anomalies for this year is included to form a picture of how extremes of the later years deviates from an observed climatology. An interesting aspect is in what regard this year of all time low relates to the long term trends. It is also worth noting that although an extreme, 2012 still serves as a good exemplification of the pattern of concentration anomalies seen the latest years. In March 2012 (Fig. 5.3a) the anomalies indicates low values of ice concentration in the Barents Sea and adjacent areas. Less ice relative to the climatology is also traced along the east coast of Greenland and in the Labrador Sea. Though in the outskirts of Baffin Bay a region of positive anomalies are located. Positive anomalies are also seen in the Okhotsk Sea and markedly in the Bering Sea. In the later a profound belt of increased concentrations of more than 50 % is evident. In September (Fig. 5.3b) there are strong negative anomalies in a large part of the Polar Basin. This signal extends from the Canadian Archipelago throughout the Beaufort, Chukchi, East Siberian and Laptev Seas, and intrudes into the Central Arctic region north of the Kara and Barents Seas. The only regions of positive anomalies are a section off the northernmost part of the East-Greenland coast, and an entrained section in the midst of the Arctic Basin.

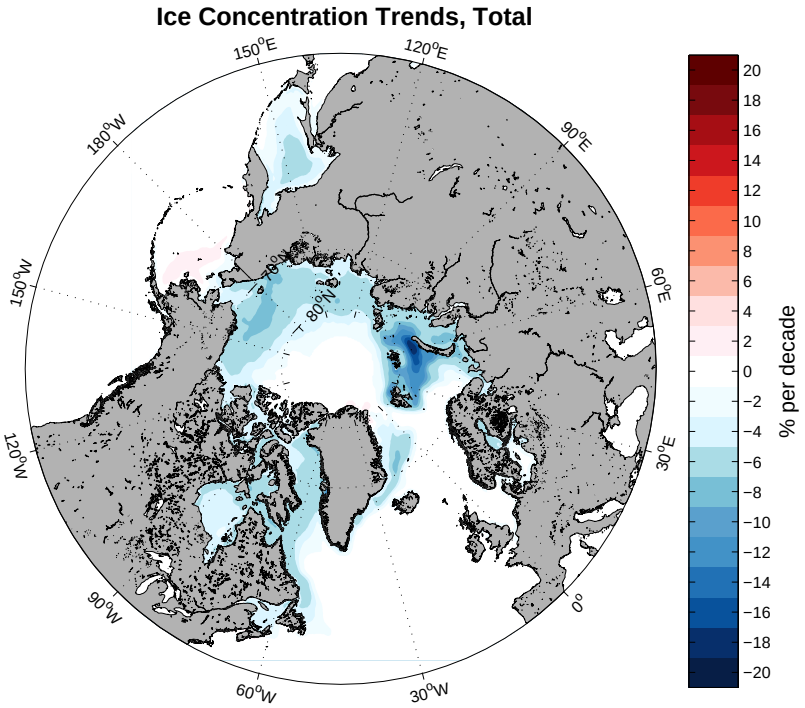

Figure 5.1: *Linear trends in monthly mean sea ice concentration for the satellite record from 1979 throughout 2013.*

To enhance our understanding of the climatological processes affecting the Arctic region and its sea ice cover it is advantageous to study the ice in context of other climate variables. Therefore gridded linear trends of air temperature is displayed in Figure 5.4. The trends are based on data from ERA-Interim reanalysis, given as air temperatures at 2 m height (cf. Sec. 3.3.2). The computed trends are based on three month averages, and presented are the results for January-March (a) and July-September (b). These are the same averages used for the time series of atmospheric temperatures presented later in this chapter.

For the winter months (Fig. 5.4a) we see a cooling trend over the Bering Sea, and regions of cooling trends north of the Canadian Archipelago and off the north and northern east coast of Greenland. Most of the remaining regions subjected to sea ice are characterized by positive trends. Concentrating on the areas with underlaying ocean the Barents Sea stands out with strong positive trends. During the summer months (Fig. 5.4b) negative trends are still observed north of Greenland. There are additionally negative trends over the Laptev Sea, and over parts of the Kara and Barents Sea. Remaining areas of interest mainly depicts positive trends. Over the Baffin Bay region particularly strong trends are depicted. There is also positive trends of high values off the southern east coast of Greenland.

In Figure 5.5 trends for oceanic temperatures are shown. This data, attained through the Ocean Climate Laboratory (OCL), are gridded averages of upper 100 m ocean temperatures (cf. Sec. 3.3.1). In the figure the trends for the January-March mean (a) and the July-September mean (b) is shown.

The winter months (Fig. 5.5a) reveals that the regions on the Atlantic side of the Arctic are predominantly denoted by positive trends. The Bering Sea is split, holding positive trends in the east and negative trends in the west. For the summer months (Fig. 5.5b) we see stronger trends stretching further north. Of the areas holding most pronounced positive trends are the regions in the vicinity of Svalbard, and a region on the east coast of Greenland.

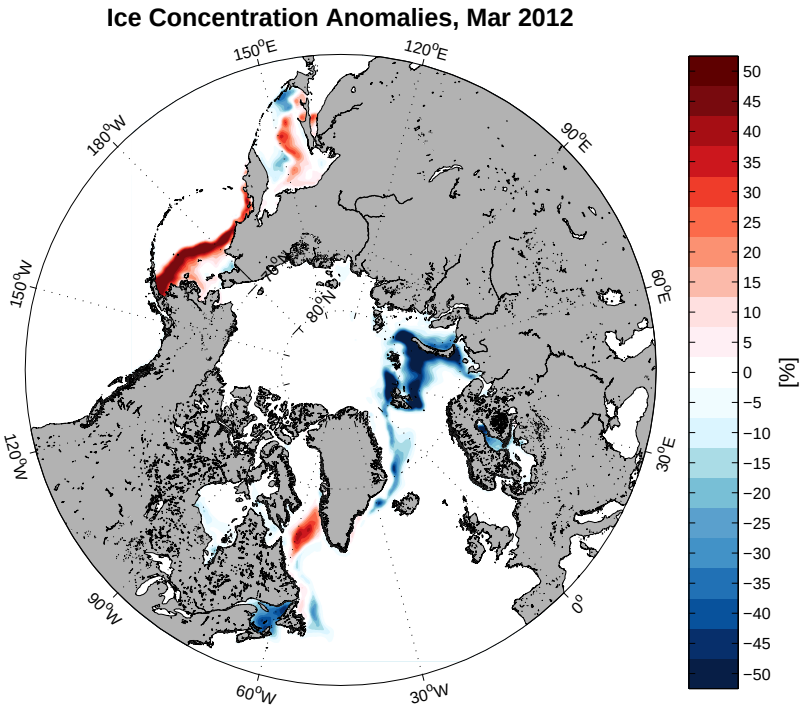

(a)

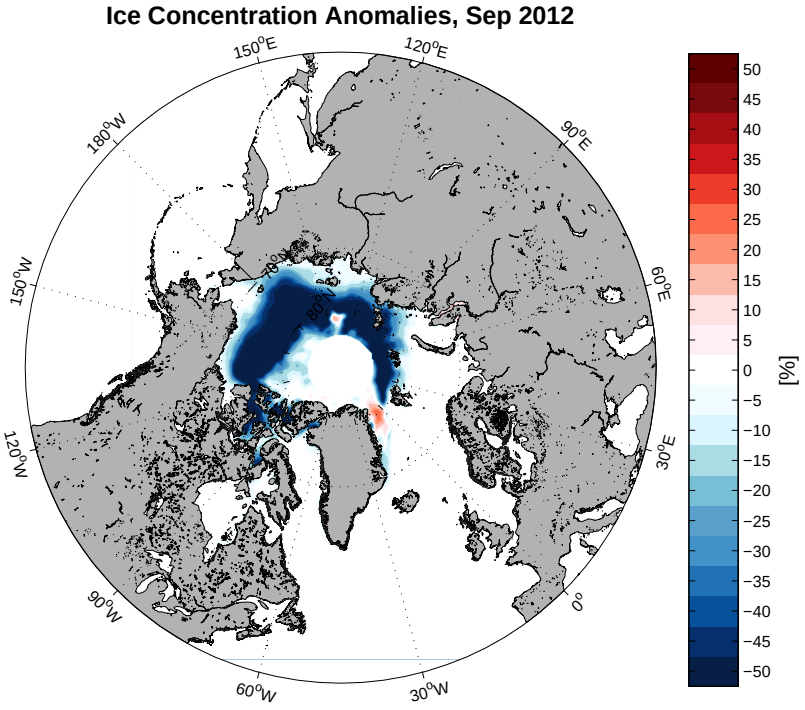

(b)

Figure 5.3: *Anomalies of monthly mean sea ice concentration from a 1981-2010 mean, for March 2012 (a) and September 2012 (b).*

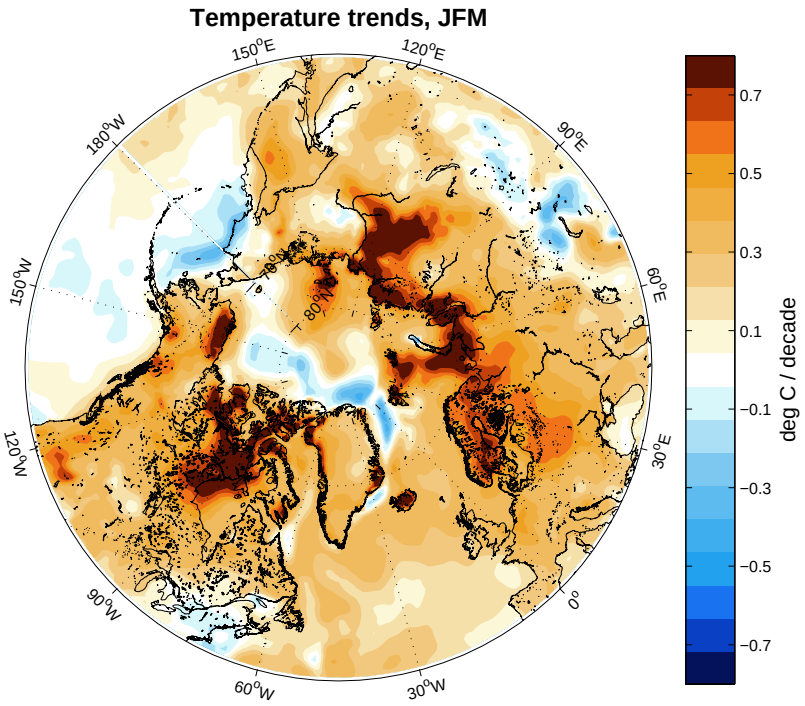

(a)

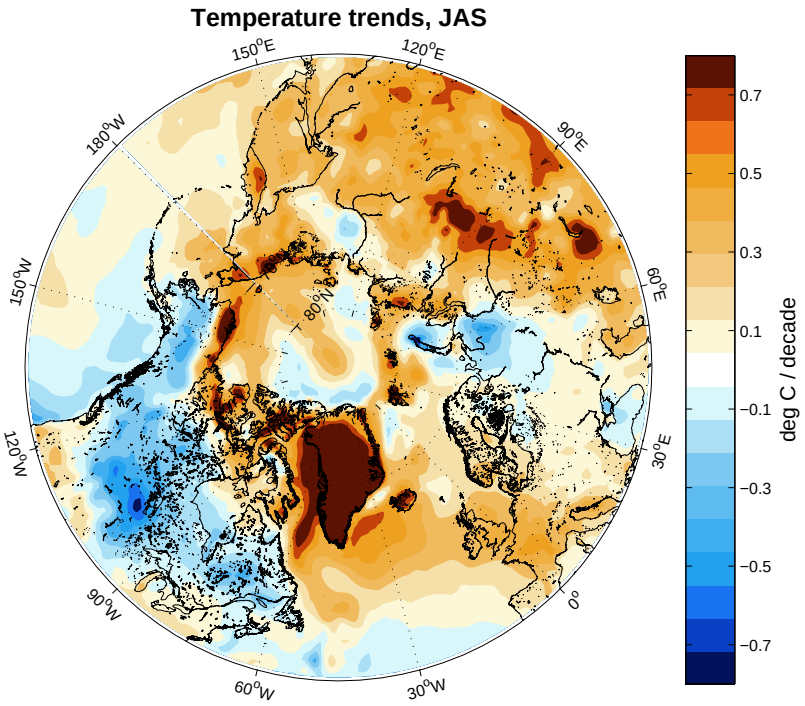

(b)

Figure 5.4: *Linear trends in air temperature (2 m height) from 1979-2013 for the average over the months January-March (a) and July-September (b).*

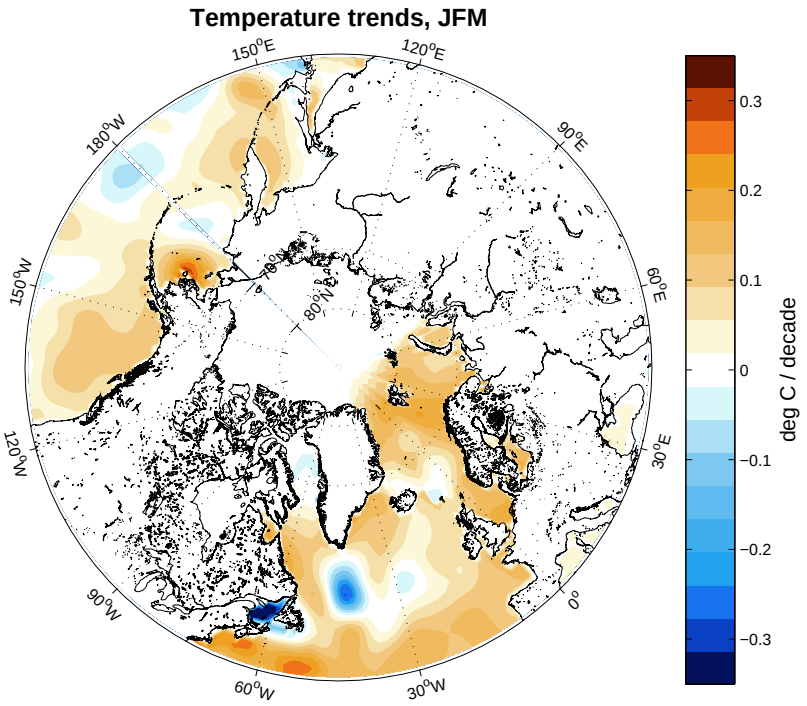

(a)

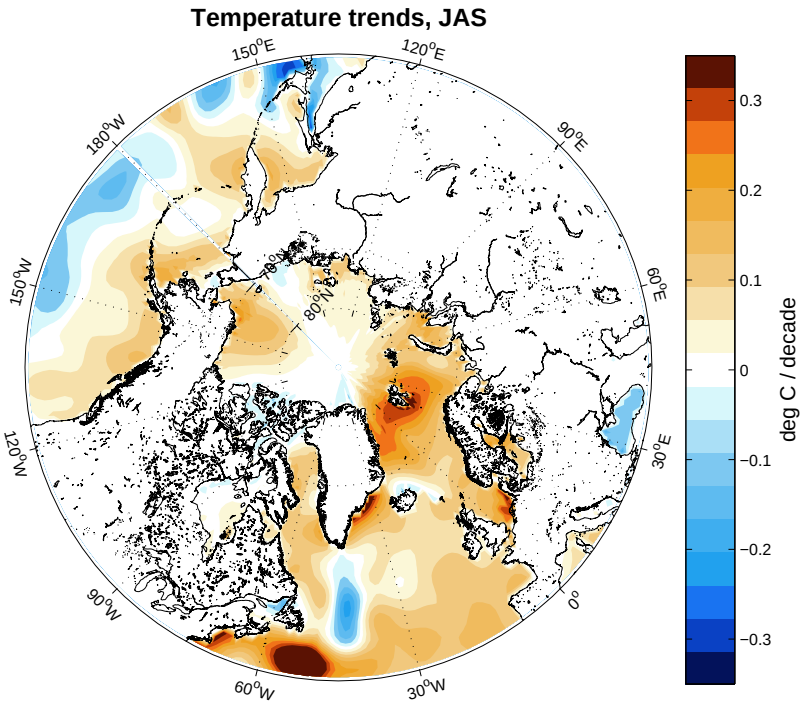

(b)

Figure 5.5: *Linear trends in ocean temperature (upper 100 m) from 1979-2013 for the average over the months January-March (a) and July-September (b).*

5.2 Annual cycles and monthly trends

Exploring the evolution of the ice cover in closer detail the monthly mean ice extent (calculated as described in Section 3.2) is used as base for the various time series presented in this chapter. To start of with a general overview the annual cycle of ice extent is plotted for the Northern Hemisphere as a whole in Figure 5.6a. The black line is drawn from the mean of each month, while the cycle for each single year is given in blue, colored lighter as years go by. A sinusoidal wave emerges, and the shape seen in the annual cycle is also quite consistent for all years, although there is a shift towards lower extent values for the later years (lighter colored lines). In Figure 5.6b we see linear trends calculated for each month of the year, represented by bar plots for the different regions. The negative trends for all months are confirming the downwards shift in ice extent through the years observed in the annual cycle (Fig.5.6a). The bars are scaled relative to the strongest decreasing trend of $-8.68 \cdot 10^4$ km^2/yr seen in September. September being the extreme, with a yearly decrease roughly corresponding to 22 % of the Norwegian land area, the figure reveals that the strongest trends are all found in the months close to late summer. July, August, September and October are the most pronounced. While still negative, the trends for the months from November to June are not as strong. The least remarked trend is found in May, with a magnitude of $-3.16 \cdot 10^4$ km^2/yr.

In the proceeding parts of this chapter we first lay out the annual cycle and monthly trends for all study regions, to see how the outline of these vary inter-regionally. Then we present in further detail the temporal evolution for each region.

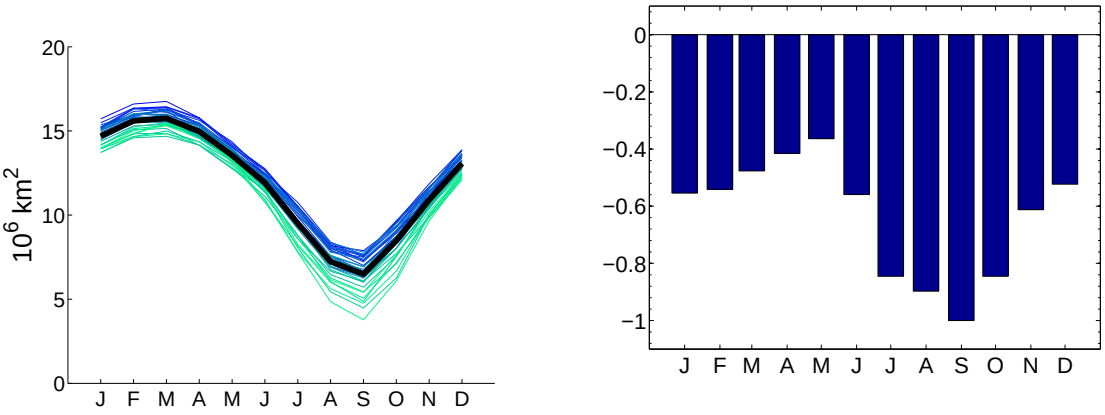

(a) *Annual cycle* **(b)** *Monthly trends*

Figure 5.6: *(a) Mean yearly cycle of sea ice extent in the Northern Hemisphere (black line), with the single years drawn in blue (lighter color indicating later years). (b) Trends in sea ice extent for each month of the year for the Northern Hemisphere, computed from time series over the period 1979-2013. Values are scaled relative to the September trend for the Northern Hemisphere of* $-8.68 \cdot 10^4$ km^2/yr.

Figure 5.7 shows the annual cycle in ice extent for each of the study regions. It appears that a selection of the regions experiences a total ice cover during parts of the year. This is recognized by a flat maximum stretching over several of the winter months and happens in the Beaufort Sea (b), Chukchi Sea (c), East Siberian Sea (d), Laptev Sea (e) and the Canadian Arctic Archipelago (j). And, although not entirely consistent for all years, it is also seen in the Kara Sea (f) and Central Arctic (a). Regions who does not see a total ice cover has an annual cycle with a shape more resembling the sinusoidal pattern of the entire Northern Hemisphere (Fig. 5.6a). Another feature to note is that the annual cycle of some regions reaches a minimum of no notable ice extent. This is the case for the Bering (k) and Okhotsk (l) Seas, where we most years do not see ice during the months from July to September. In general we can classify the regions in two groups from the outline of their mean annual cycle. Letting the first class, C1, be regions with a general cycle of total freeze up during winter months, and a sharply defined minimum. This criteria applies to the regions (a)-(f) as well as the Canadian Archipelago (j). These regions in the C1 class all reach their mean annual minimum in September, with few deviations from this for individual years. The C1 regions are also seen to have the largest spread in yearly values coinciding with the minimum in their yearly mean cycle. The second class, C2, holds regions of varying winter extent as they never see an overall ice cover, and is recognized by more sinusoidally shaped mean cycles. Including the regions (g)-(i), (k) and (l) in 5.7. For these regions the largest discrepancy between years is found during the winter season. All reach their mean maximum in March, except the Barents Sea, (g), peaking in April. However the mean maximums are not particularly defined, and especially for the Barents Sea (g), Greenland Sea (h), and Bering Sea (k), the month of maximum extent varies on a yearly basis. Neither minimum extents are sharply defined, but in the Barents Sea g, Greenland Sea h and Baffin Bay i the mean cycle minimums are all found in September. For the regions seeing ice extinction during the summer months, Bering Sea (k) and Okhotsk Sea (l), this is reached in July and holds throughout September.

Figure 5.8 displays the monthly linear trends for all study regions. Bars are still scaled to the September trend of the Northern Hemisphere as a whole ($-8.68 \cdot 10^4$ km^2/yr) as in Figure 5.6b. Negative trends seems to be the overall rule of thumb, although some negligible positive trends are indicated e.g. in the East Siberian Sea (d) region. The Bering Sea (k) stands out in this regard, as the only region having pronounced positive trends. This is seen in the months of January through May. If, by the same approach as for the mean annual cycles (Fig. 5.7), the regions are to be categorized by the outline of monthly trends, a reasonable classification could be as follows. The first class, T1, is recognized by having the strongest negative trends during summer time, and a general profile where the trends are growing stronger towards the middle of this period. This is the case for regions (a)-(e) as well as (j). A second class, T2, has denoted trends also during winter, with a remarked decrease in extent in the first months of the year. Hereunder are regions (g), (h), (i) and (l). Another notable feature, seen particularly in the Barents Sea (g) and in the Baffin Bay region (i), is that we have weaker trends in the low extent months and then a leap in trend magnitude towards neighboring months in both directions. That is, strong trends in the transition seasons between high and low extent. Already having very low summer extents, strong trends in the vicinity of

the minimum season indicates that ice lacking season is evolving to last longer. Melting is over with earlier and freezing starts later. The Kara Sea (f) falls in the middle of these two categories, having very low winter trends it resembles T1, but it lacks the steady decrease towards a defined minimum trend in mid summer. During the last seven months of the year its profile more resembles that of the Barents Sea (g) and in the Baffin Bay (i) regions. With strongest trends in July and October. The Bering Sea turns out to be the only region which does not quite fit with any of these categories. Its positive winter trends making it stand out, and low summer trends not showing any strong characteristics. Since this region has a fairly long ice free season (Fig. 5.7k) the most negative trends in June, November and December can be seen as a temporal prolongation of the ice minimum, corresponding to what is observed in the Barents Sea (g) and Baffin Bay (i).

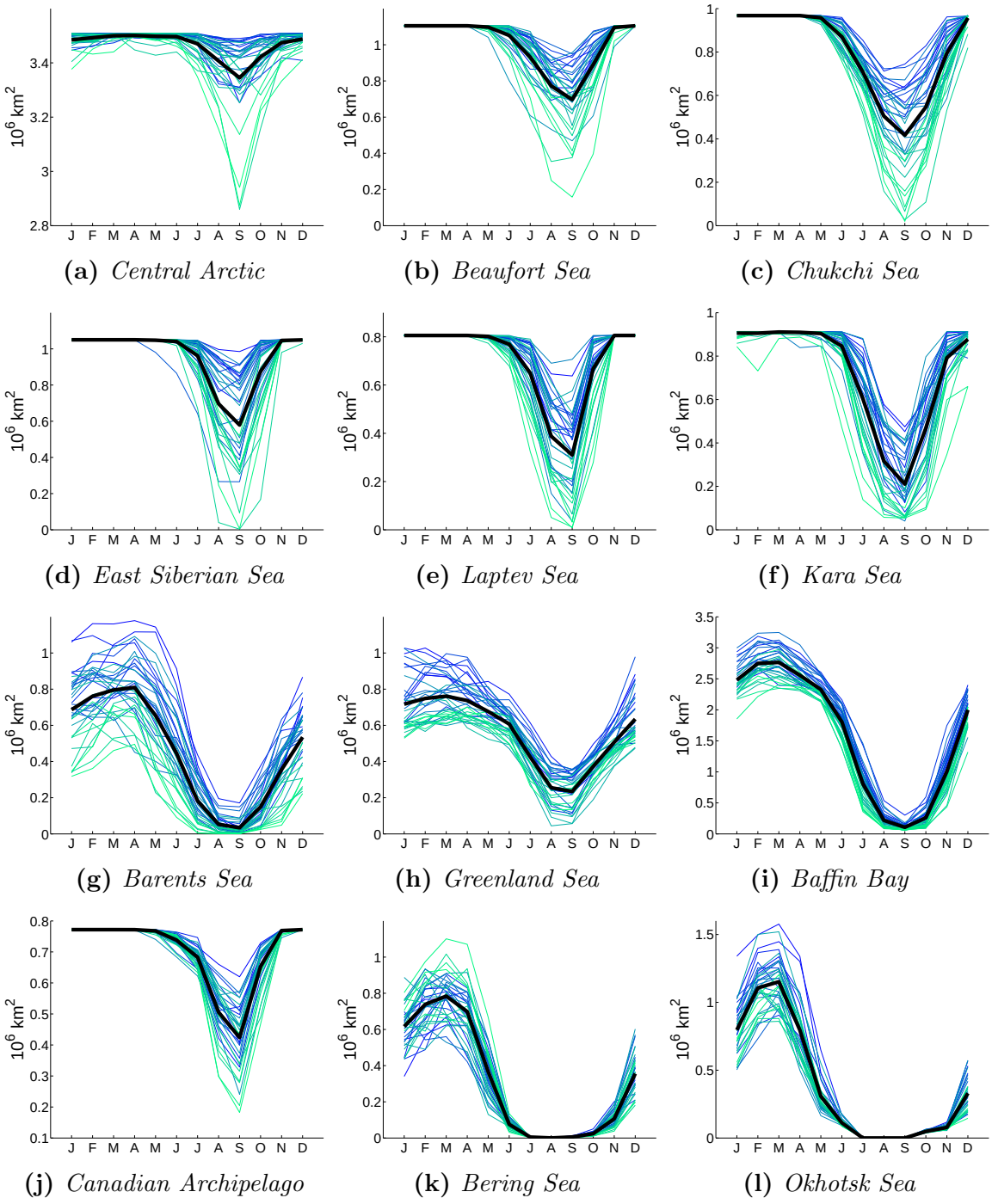

(a) *Central Arctic* **(b)** *Beaufort Sea* **(c)** *Chukchi Sea*

(d) *East Siberian Sea* **(e)** *Laptev Sea* **(f)** *Kara Sea*

(g) *Barents Sea* **(h)** *Greenland Sea* **(i)** *Baffin Bay*

(j) *Canadian Archipelago* **(k)** *Bering Sea* **(l)** *Okhotsk Sea*

Figure 5.7: *Mean yearly cycle of sea ice extent in the different study regions (black line), with the single years drawn in blue (lighter color indicating later years). Note that the range differs between graphs.*

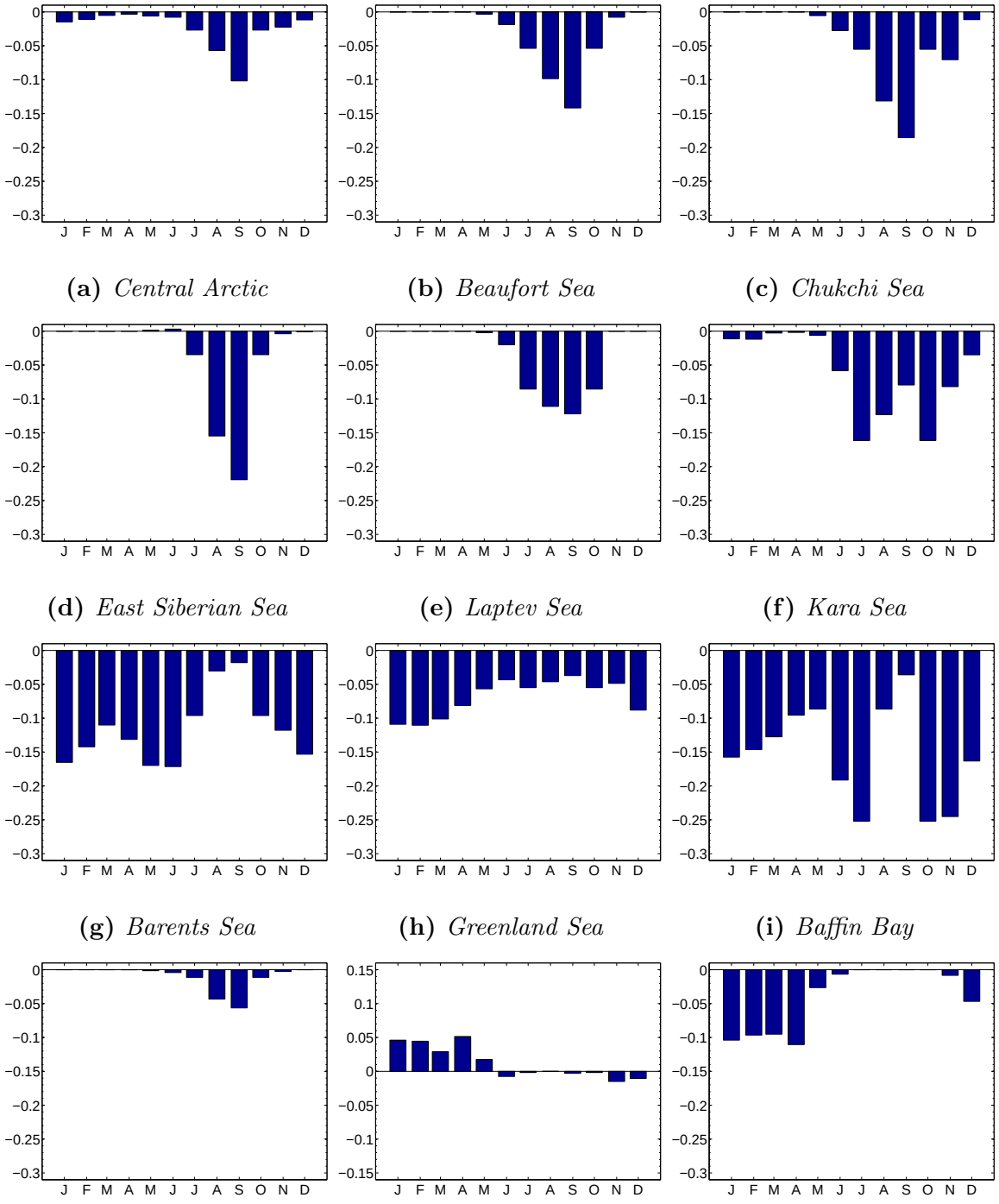

(a) *Central Arctic* **(b)** *Beaufort Sea* **(c)** *Chukchi Sea*

(d) *East Siberian Sea* **(e)** *Laptev Sea* **(f)** *Kara Sea*

(g) *Barents Sea* **(h)** *Greenland Sea* **(i)** *Baffin Bay*

(j) *Canadian Archipelago* **(k)** *Bering Sea* **(l)** *Okhotsk Sea*

Figure 5.8: *Trends in sea ice extent for each month of the year, computed from time series of the different study regions throughout the period 1979-2013. Values are scaled relative to the September trend for the Northern Hemisphere of* $-8.68 \cdot 10^4$ km^2/yr. *Note that (k) Bering Sea has a shifted axes, range and scale are still the same.*

5.3 Northern Hemisphere

In Figure 5.9a the time series of yearly averaged sea ice extent in the Northern Hemisphere is displayed. The averages are taken from January throughout December. Using a winter centered July-June average is a common option for regional sea ice studies. This is often used in regions which does not see ice during summer, allowing the entire process of freezing and subsequent melting to be assembled in one mean. But since this study addresses the entire Arctic, including the variety of regions within, the advantage of this way to partition the year is not unequivocal. Additionally, the way the data is presented in this study, going into detail about the development in both March and September, it is seen as an advantage if the yearly values for these two months correspond to the same yearly average. Because the satellite measurements used started in late October 1978 (Chap. 3) the traditional calender-year-mean allow us to make a full 35-year-long time series also of yearly averages. As would not be possible with a yearly average starting any earlier than October. The yearly averaged time series portrays interannual variability to some extent, but also makes it clear that these fluctuations are outscaled by the overall decrease in ice extent. In the figure the linear trend over the entire data record (cyan) illustrates this decrease. Linear trends over parts of the time series, 1979-2003 (yellow) and 2003-2013 (green), are also displayed.

Further in Figure 5.9b anomalies relative to the mean ice extent of 1981-2010 for the month in question is plotted. The values are substantial both for March (blue) and September (red) in the Northern Hemisphere. The extremes for March are found in 1979 and 2006, with respective deviations of $1.01 \cdot 10^6$ km^2 and $-1.06 \cdot 10^6$ km^2 from the 1981-2010 mean of $15.75 \cdot 10^6$ km^2. For September extremes are seen in 1980 with an extent of $1.29 \cdot 10^6$ km^2 more than the climatology of $6.60 \cdot 10^6$ km^2, and in 2012 when the extent was $2.82 \cdot 10^6$ km^2 less than the climatology. Trend lines for the months in question are also shown. Trends indicated in the figure are given in percent of the monthly climatology per decade, although lines are drawn corresponding to the 10^6 km^2 axis. For metric quantification see Figure 5.6b. In general it appears that anomalies shift from mainly positive to mainly negative around the end of the 1990's. As this shift occurs to the right from the middle of the time span, it implies that there is a greater change rate at the later part of our time series.

Knowing how heat fluxes from the atmosphere and ocean is important for the processes of formation, growth and melt of ice (Chap. 2.2 and 2.3), the relationship between ice extent with air and ocean temperatures may be of interest. To build up an understanding of the observed evolution in ice extent, an assembly with geographically corresponding temperatures are therefore presented for March and September in Figures 5.9c and 5.9d. Ocean temperature anomalies from the Ocean Climate Laboratory (OCL) (see Chap. 3.3.1) are vertically averaged over the upper 100 meters of the ocean. The data set provides seasonal averages, here using the values averaged over January-March and July-September. Atmospheric temperatures acquired from ERA Interim reanalyzes gives temperature data at 2 m above ground. The gridded data is spatially averaged and presented as anomalies with a 1981-2010 base. The time series used here is calculated to three month means, to resemble the oceanic temperature data. The time series shown are for the months of March (left) and

September (right), with atmospheric temperature anomalies in the upper panel, inverted ice extent in the middle and oceanic temperature anomalies in the lower panel. For the Northern Hemisphere both months of March and September reveals a decreasing sea ice extent seen relative to an increase in both atmospheric and oceanic temperatures. The figure also gives an impression of to what extent features of variability in the ice extent are found again in the time series of temperatures.

Proceeding in this chapter the analogous data to that of the above mentioned graphs are, for each of the separate regions, successively presented in the same manner as outlined in Figure 5.9.

5.4 Central Arctic

From Figure 5.7a we know that the Central Arctic region has a close to total ice cover during the winter months, and there is not much differentiating the months of February, March, April, May and June. The lowest extent is found in September. But although a minimum in the mean annual cycle, it does not represent a major modification to the total areal coverage. As this region lies in the midst of the ice influenced regions in the Northern Hemisphere intrusions to the Central Arctic ice extent are limited, and only induced when the ice edge retreats sufficiently to cross the boarder from adjacent regions. Knowing that this region contains the data void around the North Pole, we bear in mind that this void at its largest corresponds to 41.7 % of the minimum regional extent, and at its smallest 10.9 %. The trend bars in Figure 5.8a reveals the strongest negative trend in September. Even though the trends during winter months are an order of magnitude less all months show negative trends. Figure 5.10a displays an overall decrease in the yearly mean ice extent plotted throughout the period, as enhanced by the linear trend (cyan). However, the partitioned trends reveals a more negative trend for the last decade (green) than for previous years (yellow). The largest interannual variations is seen during the latest decade, and in particularly the two latest years stands out as the lowest extents of the time series. This is seen again in the anomalies for September (Fig. 5.10b), where only the year of 2007 surpasses 2012 and 2013 in negative anomalies. It is clear from the figure that anomalies from 2007 and later are heavily decisive for our result when estimating the September trend. This implies that a linear trend through the entire time series may not be the best description of the temporal development. Because of the modest variability during the winter, months anomalies for March are almost not apparent. In Figures 5.10c and 5.10d extent values (mid panels) for March and September are extracted to be displayed as independent time series, and compared with temperatures of atmosphere and ocean. The extents are shown with an inverted y-axis for easier comparison. In March (left) variations in ice extent is negligible compared to the fluctuations seen in September extent (right). Relations between the ice extend, air temperatures at 2 m height (upper panels) and ocean temperatures for the upper 100 m (lower panels) are not striking. But in September we see some extremes in the ice extent which coincides with peaks in the air temperature. This is the case in 2005, 2007 and 2012. Correlation coefficients with ice extent are also indicated in the panels.

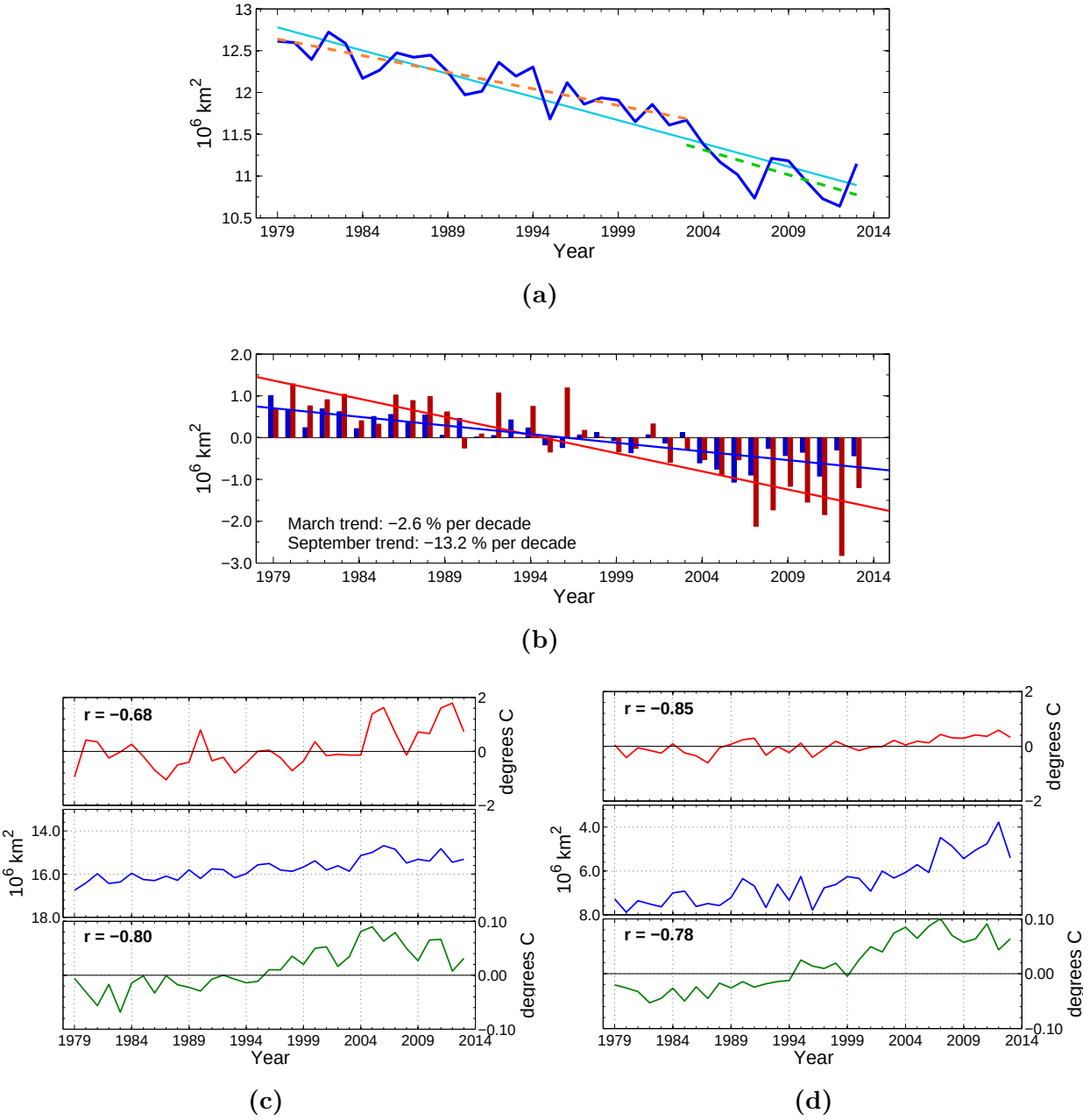

Figure 5.9: *Northern Hemisphere sea ice extent, anomalies and temperatures. (a) Time series of annual mean sea ice extent wit linear trends. (b) Anomalies of sea ice extent relative to the 1981-2010 mean. Bars show values for the month of March (blue) and September (red), while lines show the corresponding trends throughout the study period. Note that quantification of trends is given as percentage of the 1981-2010 climatology. (c) and (d) Air (2 m height) and ocean (upper 100 m) temperature anomalies (top and bottom panels respectively) compared with sea ice extent (mid panel) for March (c) and September (d). Temperatures from gridded data sets are spatially averaged over the region. Correlation, r, between temperatures and ice extent is indicated. Note that ice extent is inverted for easier comparison.*

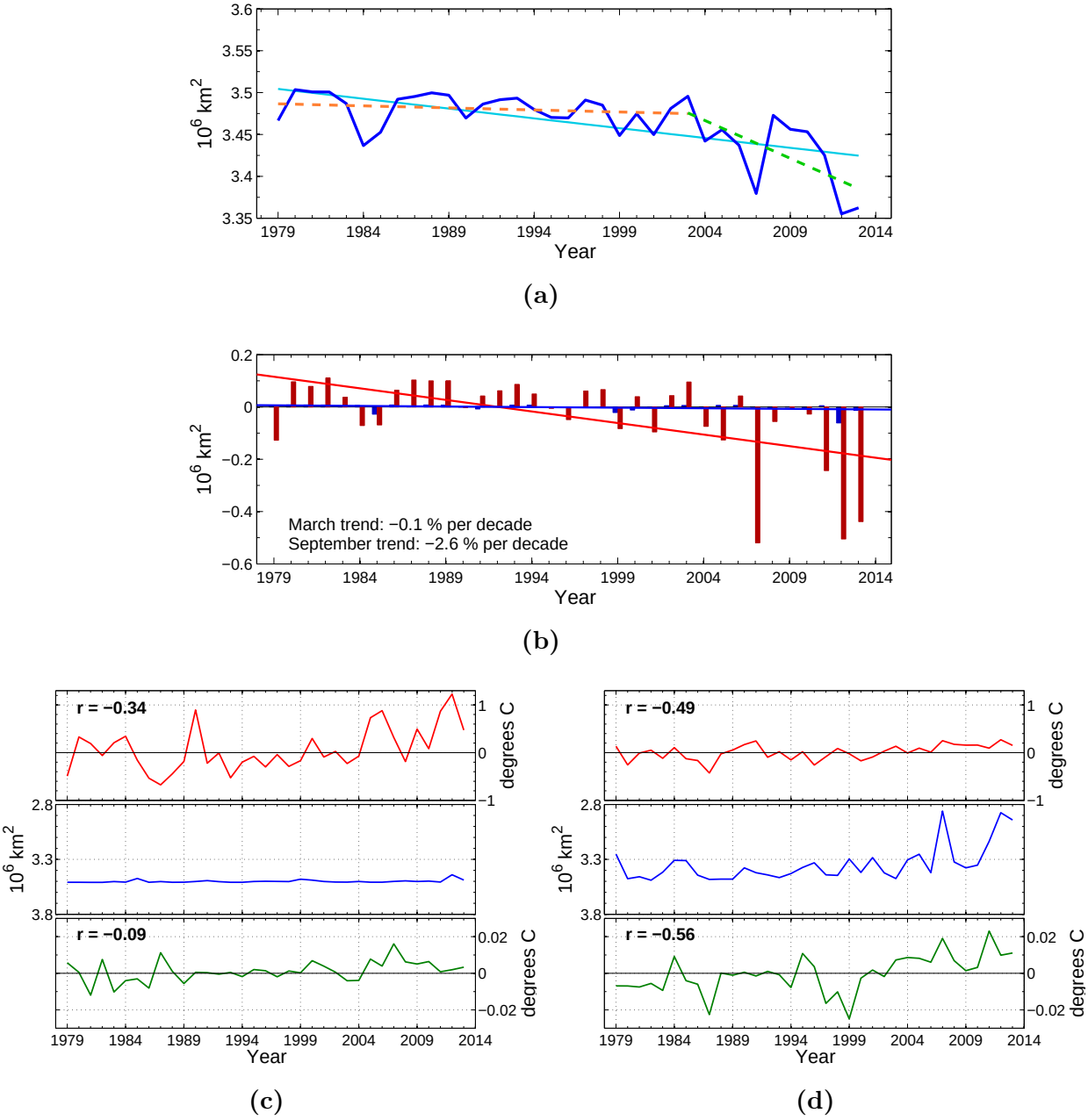

Figure 5.10: *Central Arctic sea ice extent, anomalies and temperatures. (a) Time series of annual mean sea ice extent with linear trends. (b) Anomalies of sea ice extent relative to the 1981-2010 mean. Bars show values for the month of March (blue) and September (red), while lines show the corresponding trends throughout the study period. Note that quantification of trends is given as percentage of the 1981-2010 climatology. (c) and (d) Air (2 m height) and ocean (upper 100 m) temperature anomalies (top and bottom panels respectively) compared with sea ice extent (mid panel) for March (c) and September (d). Temperatures from gridded data sets are spatially averaged over the region. Correlation, r, between temperatures and ice extent is indicated. Note that ice extent is inverted for easier comparison.*

5.5 Beaufort Sea

The Beaufort Sea generally experiences total freeze up from December trough April, as seen from the mean annual cycle in Figure 5.7b. The yearly minimum is usually reached in September, but on occasions this has happened as early as August. The figure of annual cycles also reveals that the minimum tends to drop lower more frequently in the years towards the end of the study period (lighter blue lines). A feature of which is manifested by the monthly mean trends in Figure 5.8b, where clear negative trends in all summer months is revealed. The total freeze up during winter ensures no noteworthy trends for the months December, January, February, March and April. The largest negative trend is regardless found in September, with a magnitude of -17.2 % per decade, as revealed in Figure 5.11b. In the later figure anomalies for September is displayed, while no anomalies are evident for the month of March. We note that a general shift in September anomalies, from positive to negative happens around the end of the 1990's. From this one can argue that a steeper trend may be more adequate for the latest decade, than the linear trend fitted to data for the entire time period. The same can be said for the yearly mean in Figure 5.11a, where segmented trend lines show that the later decade in fact corresponds to a more negative trend (green line).

Close to constant March values of ice extent (mid panel, Fig. 5.11c) provides few reference points for comparison with temperature anomalies. For the month of September on the other hand, Figure 5.11d indicates a good accordance between the inversed ice extent (mid panel) and the oceanic temperatures (bottom panel). Also the atmospheric temperatures (top panel) seems to vary in close compliance with the ice extent. These impressions are confirmed by correlation coefficients, r, of notable magnitude indicated in the panels.

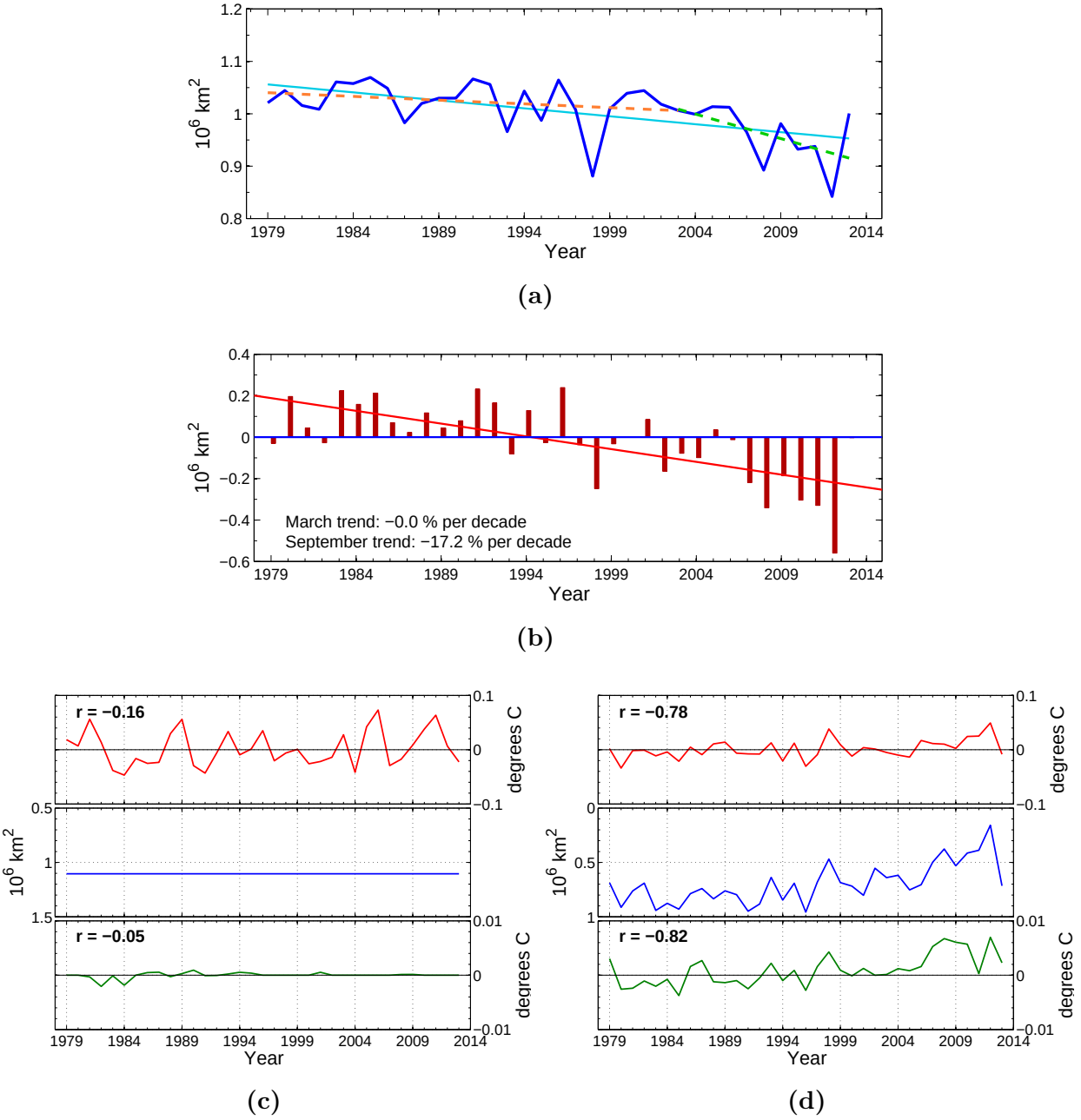

Figure 5.11: *Beaufort Sea ice extent, anomalies and temperatures. (a) Time series of annual mean sea ice extent with linear trends. (b) Anomalies of sea ice extent relative to the 1981-2010 mean. Bars show values for the month of March (blue) and September (red), while lines show the corresponding trends throughout the study period. Note that quantification of trends is given as percentage of the 1981-2010 climatology. (c) and (d) Air (2 m height) and ocean (upper 100 m) temperature anomalies (top and bottom panels respectively) compared with sea ice extent (mid panel) for March (c) and September (d). Temperatures from gridded data sets are spatially averaged over the region. Correlation, r, between temperatures and ice extent is indicated. Note that ice extent is inverted for easier comparison.*

5.6 Chukchi Sea

The Chukchi Sea experiences a total freeze up from January to April, as seen in the yearly cycle of ice extent in Figure 5.7c, where the mean yearly cycle (black line) is displayed along with the single years (blue lines). Some years the complete ice cover even lasts until May. The minimum of the mean yearly cycle is found in September. The minimum extent has tended to drop lower the later years (lighter colored), approaching zero and a completely ice free area. The monthly trends presented in Figure 5.8c are negative for all months with substantial variation. The steepest trend is found in September, August making a good second. In Figure 5.12a the time series of yearly mean (Jan-Dec) ice extent outlines a clear decreasing trend, although frequent year to year variations makes a pattern of sharp highs and lows. The absolute minimum occurred in 2007. In Figure 5.12b one can clearly see stronger negative anomalies for September the latest decade opposed to the preceding measurements, while there are no anomalies in March as the complete ice cover remains to the end of our study period.

Figure 5.12c and 5.12d outlines the inverted March and September ice extent values (mid panels) compared with corresponding air (2 m) and ocean (upper 100 m) temperatures (top and bottom panel). Correlations, as indicated in the panels, are irrelevant for the month of March (Fig. 5.12c), since there is no deviations in the March ice extent. In September (Fig. 5.12d) a steady decrease in ice cover is drawn out analogue to an increasing trend in atmospheric temperatures. The evolution of oceanic temperatures is not as unambiguously, and the correlation between ocean and ice cover is accordingly weaker.

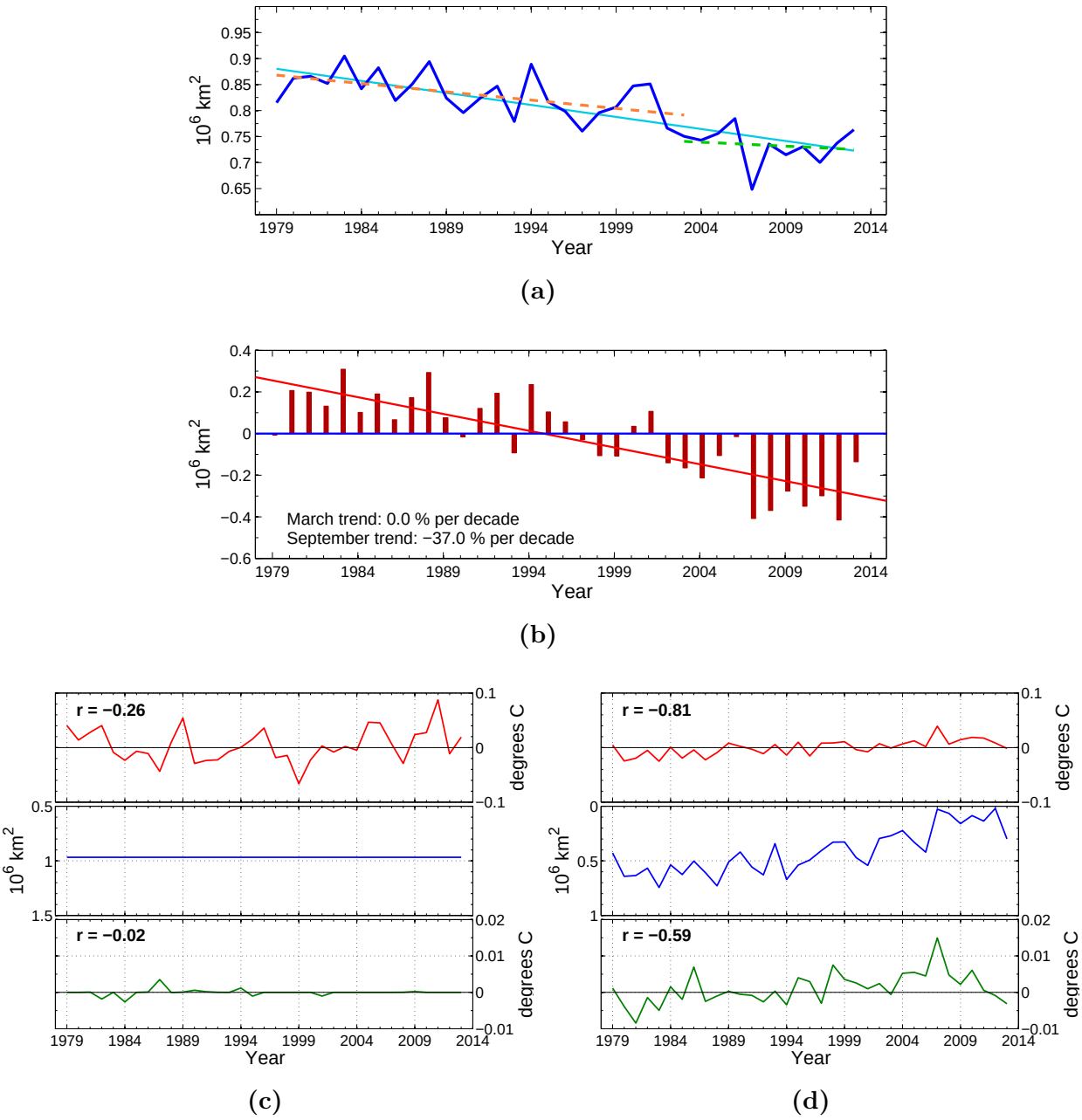

Figure 5.12: *Chukchi Sea ice extent, anomalies and temperatures. (a) Time series of annual mean sea ice extent with linear trends. (b) Anomalies of sea ice extent relative to the 1981-2010 mean. Bars show values for the month of March (blue) and September (red), while lines show the corresponding trends throughout the study period. Note that quantification of trends is given as percentage of the 1981-2010 climatology. (c) and (d) Air (2 m height) and ocean (upper 100 m) temperature anomalies (top and bottom panels respectively) compared with sea ice extent (mid panel) for March (c) and September (d). Temperatures from gridded data sets are spatially averaged over the region. Correlation, r, between temperatures and ice extent is indicated. Note that ice extent is inverted for easier comparison.*

5.7 East Siberian Sea

When viewing the ocean areas north of Eastern Siberia the yearly cycle of ice extent (Fig. 5.7d) shows that the region is totally ice covered from December to May. And for most years this period extends from November until July. The average minimum is found in September, but a few years deviates from this reaching the lowest extent already in August. These are also the two months where we have the clearest negative trends, as seen in Figure 5.8d. It also appears from this figure that the months January, March, April, May and June has small positive trends. This does though not represent any real significance, since the fact that we see a nearly continuous ice cover during the months in question means that just one small deviation from this total cover will be decisive for our trend output. From the yearly mean time series, as displayed in Figure 5.13a, it appears that there is a general tendency of lower ice extents towards the end of the time span. However noting the contours, a linear least square fit may not be the best way to describe the temporal evolution. The anomalies for September (Fig. 5.13b) fortifies this impression, even though there is no doubt that most negative anomalies are assembled in the latest decade.

March with its complete freeze up, has no anomalies, and hence it is also depicted as a straight line in the mid panel of Figure 5.13c. The September series (Fig. 5.13d) on the other hand has a much more dynamic variability. In the figure the inversed ice extent is put up with the regional air temperature (upper panel) and the regional oceanic temperature (lower panel). This collation visualizes the relation between less ice extent and higher atmospheric temperatures, quantified by the correlation coefficient, r. No obvious connection with oceanic temperatures stands out, and impression substantiated by a correlation of lower magnitude.

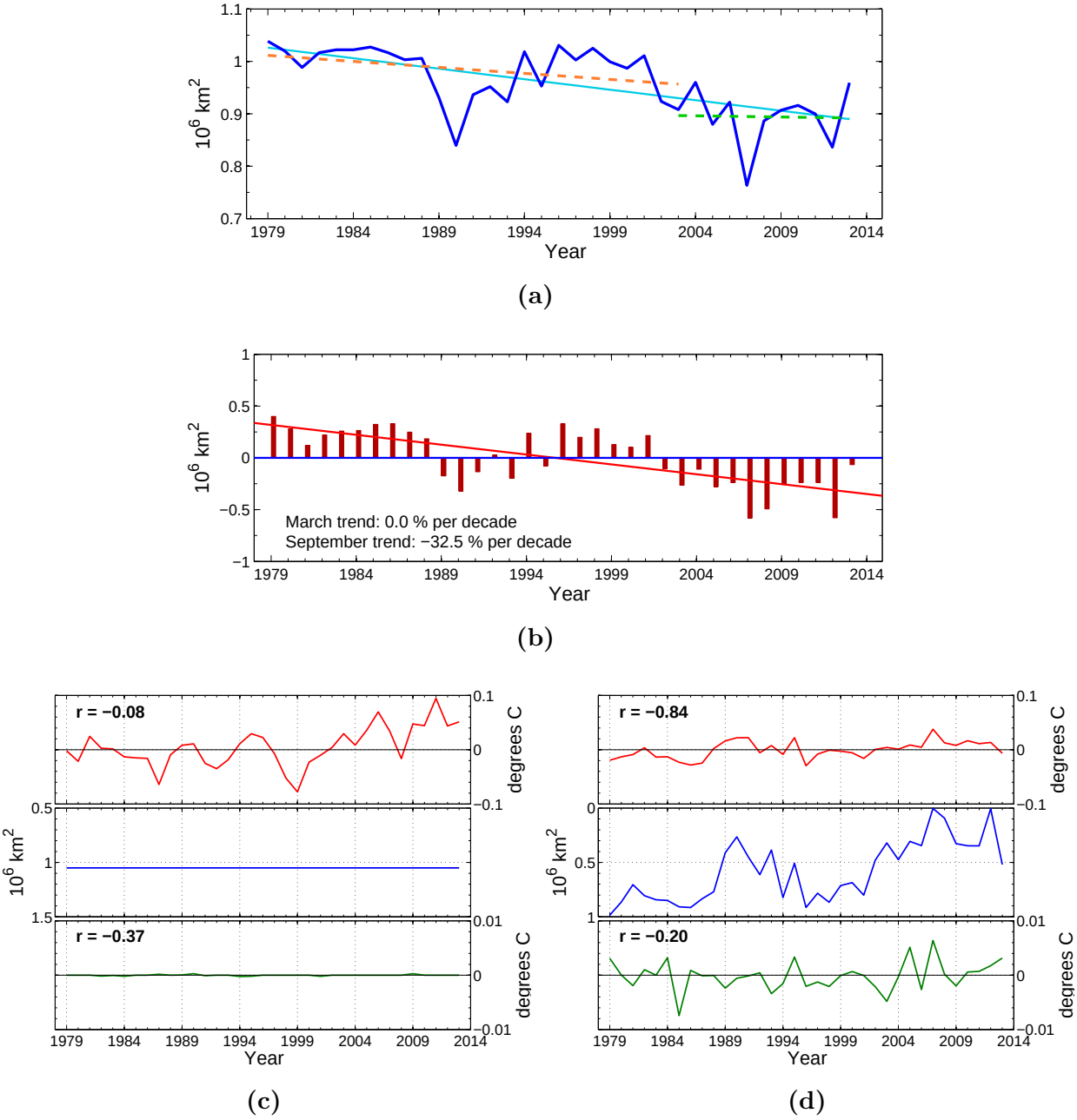

Figure 5.13: *East Siberian Sea ice extent, anomalies and temperatures. (a) Time series of annual mean sea ice extent with linear trends. (b) Anomalies of sea ice extent relative to the 1981-2010 mean. Bars show values for the month of March (blue) and September (red), while lines show the corresponding trends throughout the study period. Note that quantification of trends is given as percentage of the 1981-2010 climatology. (c) and (d) Air (2 m height) and ocean (upper 100 m) temperature anomalies (top and bottom panels respectively) compared with sea ice extent (mid panel) for March (c) and September (d). Temperatures from gridded data sets are spatially averaged over the region. Correlation, r, between temperatures and ice extent is indicated. Note that ice extent is inverted for easier comparison.*

5.8 Laptev Sea

From the yearly cycle of the Laptev Sea ice extent seen in Figure 5.7e one can see that the region is completely frozen already in November, a condition that retains until April, and for numerous years also until May or as long as June. The average extent (black line) has its minimum in September, but how low this minimum is varies greatly between the different years (blue lines). From the monthly trends viewed in Figure 5.8e it is clear there is an overall decrease in ice extent for all months not experiencing complete ice cover. That is the summer months from June to October. September shows the negative trend of largest magnitude, closely followed by August. In Figure 5.14b, where anomalies in ice extent for March and September are given as bars, reveals large interannual variations in September extent values. Regardless, all years since 2005 holds negative anomalies, ensuring a negative overall trend. There are no anomalies in Mach, which is also manifested in the mid panel of Figure 5.14c. In Figure 5.14d on the other hand, the variable September extent (inverted) is displayed in connection with analogous atmospheric (upper panel) and oceanic (lower panel) temperatures. Some distinct features are recognizable across the panels. But while the air temperature show signs of an increase towards the end of the time series, there is no notable trend in the oceanic temperatures.

5.9 Kara Sea

As can be seen in Figure 5.7f the Kara Sea usually experiences a complete freeze-up, from January to April. Nevertheless it is also apparent that there, some of the later years (lighter lines), has been intrusions to this long period of continuous total ice cover. This gives rise to emerging negative trends also during the winter months, as displayed in Figure 5.8f. The yearly mean (Fig. 5.15a) reveals a declining trend, although remarked variability. The rapid shifts can be illustrated by the drop down to a minimum in 2012, after witch it the ice extent increased again the following year, to a magnitude above that of 2011. However it is evident that the latest decade alone corresponds to a more negative linear trend (green line) than both the previous years (yellow) and the time series as a whole (cyan). Viewing extent anomalies in Figure 5.15b, although the intrusions to the March extent (blue bars) is traceable, the September anomalies (red bars) are dominating. It appears that, regardless of relatively frequent shifts early on in the period, the last decade is characterized by persistent negative September anomalies. This can be seen in connection with the flattening towards the end of the September ice extent time series (mid panel, Fig. 5.15d), which draws out to a nearly horizontal line the latest seven years.
Unlike the yearly mean, the time series of September extent does not show a clear negative trend. Despite the fact that oceanic temperatures (lower panel) outlines a steadily increasing trend. Although some perturbations to the March ice cover are already referred to, when seen relative to the variability in September extent (mid panels, Fig. 5.15c and 5.15d) they do not account for large areal extents. Where there are intrusions they seem to match with high atmospheric temperatures, as the correlation indicated is quite high.

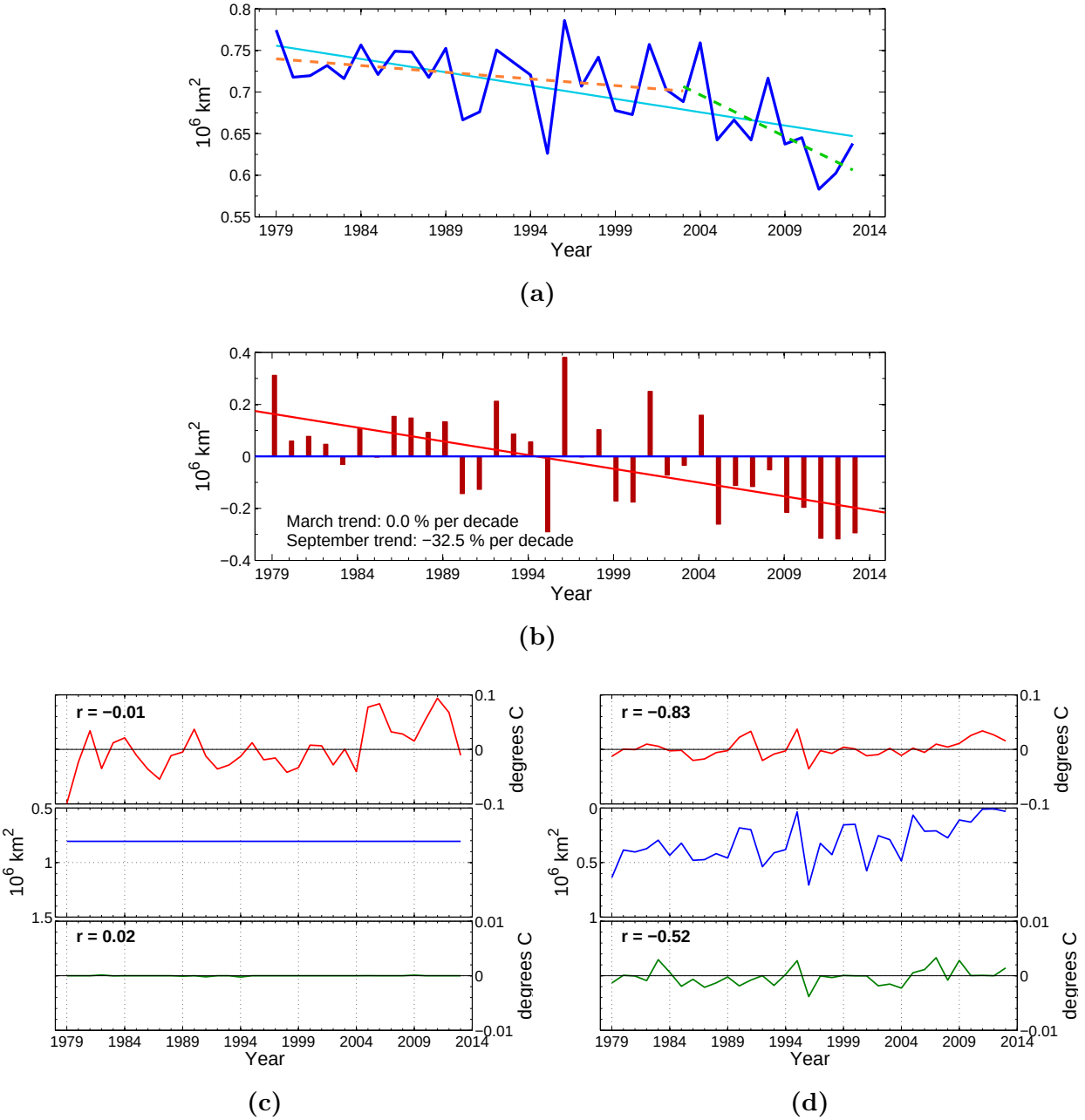

Figure 5.14: *Laptev Sea ice extent, anomalies and temperatures. (a) Time series of annual mean sea ice extent with linear trends. (b) Anomalies of sea ice extent relative to the 1981-2010 mean. Bars show values for the month of March (blue) and September (red), while lines show the corresponding trends throughout the study period. Note that quantification of trends is given as percentage of the 1981-2010 climatology. (c) and (d) Air (2 m height) and ocean (upper 100 m) temperature anomalies (top and bottom panels respectively) compared with sea ice extent (mid panel) for March (c) and September (d). Temperatures from gridded data sets are spatially averaged over the region. Correlation, r, between temperatures and ice extent is indicated. Note that ice extent is inverted for easier comparison.*

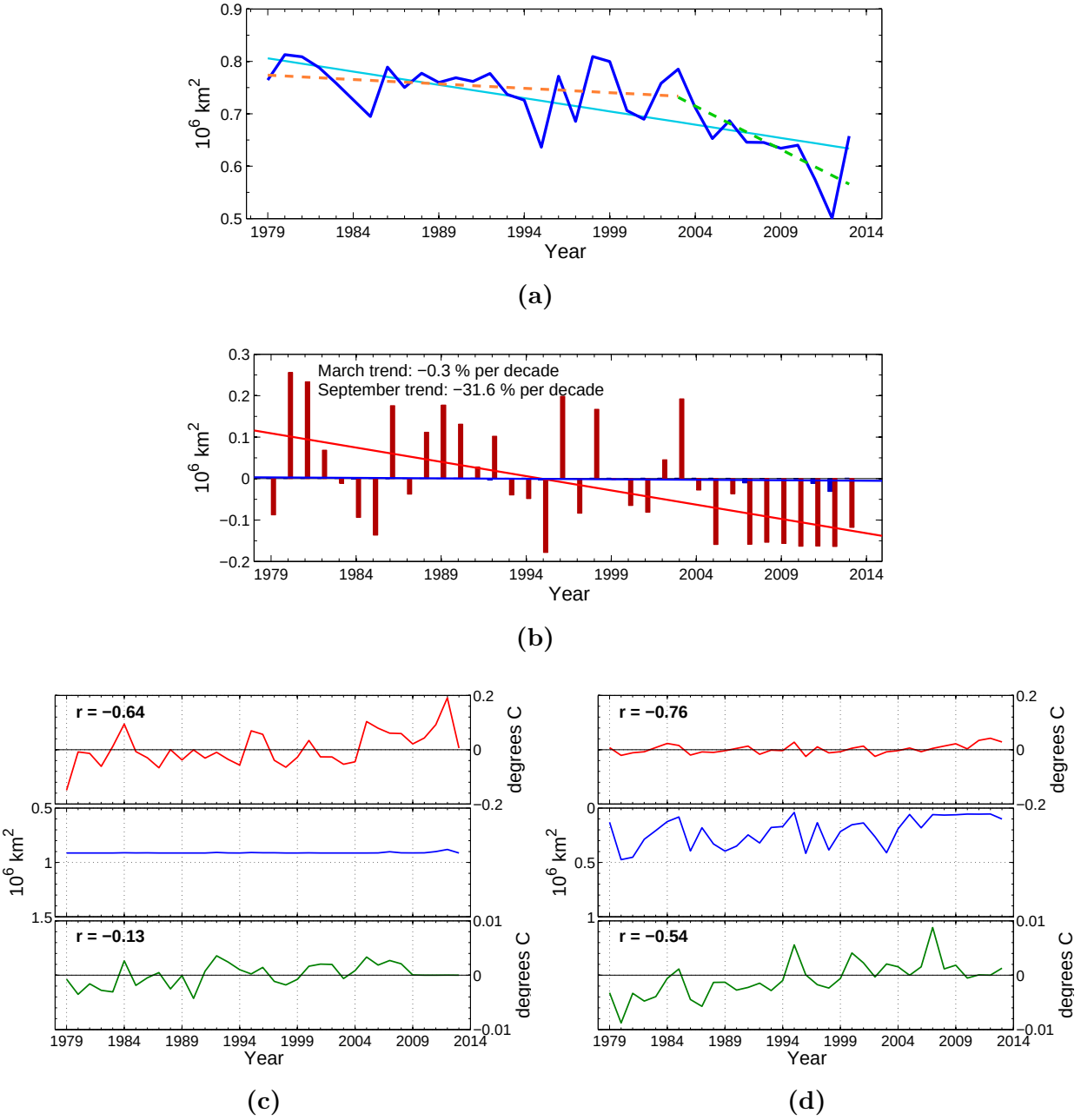

Figure 5.15: *Kara Sea ice extent, anomalies and temperatures. (a) Time series of annual mean sea ice extent with linear trends. (b) Anomalies of sea ice extent relative to the 1981-2010 mean. Bars show values for the month of March (blue) and September (red), while lines show the corresponding trends throughout the study period. Note that quantification of trends is given as percentage of the 1981-2010 climatology. (c) and (d) Air (2 m height) and ocean (upper 100 m) temperature anomalies (top and bottom panels respectively) compared with sea ice extent (mid panel) for March (c) and September (d). Temperatures from gridded data sets are spatially averaged over the region. Correlation, r, between temperatures and ice extent is indicated. Note that ice extent is inverted for easier comparison.*

5.10 Barents Sea

From Figure 5.7g it is known that the Barents Sea never sees a total ice cover, but the ice commonly retreats to an nearly ice free condition during the summer period. As seen from the mean average cycle (black line), the transition between maximum and minimum ice extent is relatively gradual. From a peak in April, it is steadily diminishing until hitting the lowest extent in September. The spread between single years is here greatest during winter months. And considering the monthly trends in Figure 5.8g, the months between November and June is also where we have the most pronounced negative trends. The anomalies for March and September shown in Figure 5.16b clearly illustrates that the variability and trend is more pronounced during the high extent winter months exemplified by March (blue bars) than during the summer minimum of September (red bars). This is in contrast to the regions of total winter cover, as described earlier (Sec. 5.4-5.9), which had no March anomalies. Even though March anomalies for the Barents Sea is larger in magnitude, when scaled compared to the monthly climatology the September trend depicts the strongest, reading -41.3% (Fig. 5.16b). This discrepancy between March and September trends is only due to that the climatological base for September is close to zero.

The time series of yearly mean ice extent (Fig. 5.16a) is clearly similar in evolution to that of the March extent (mid panel, Fig. 5.16c). (Note that the latest figure show inverted extent.) The March extent also seems to be closely coupled with the regional air temperature (upper panel). Similarities are also seen with the oceanic temperatures (lower panel). The September extent (mid panel, Fig. 5.16d) is low, and keeps at or close to zero for most of the years. The figure further divulges that episodes of enhanced ice cover are quite regularly distributed in time. These events does though not reveal any obvious relation to temperatures in air or ocean (upper and lower panel respectively).

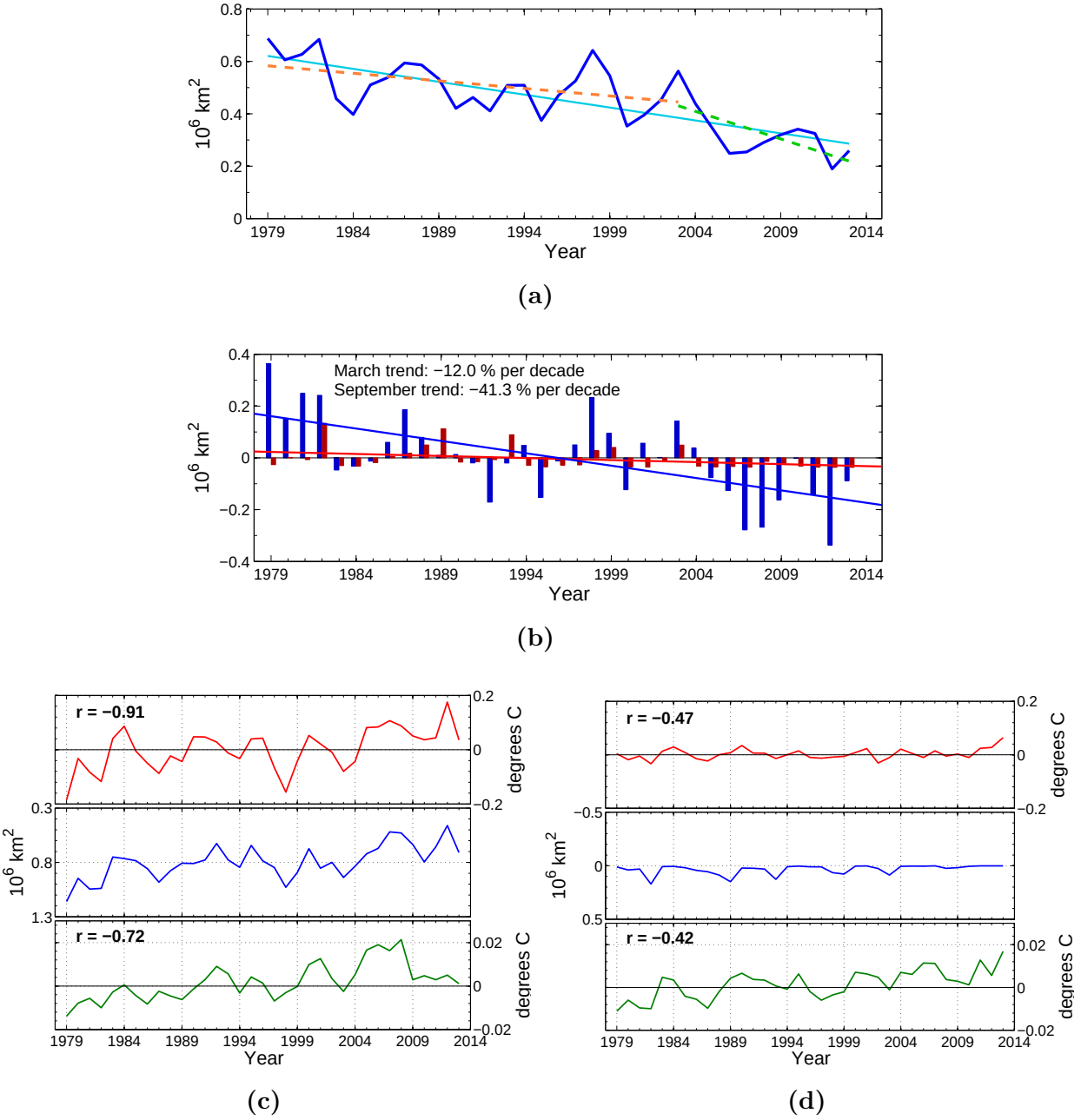

Figure 5.16: *Barents Sea ice extent, anomalies and temperatures. (a) Time series of annual mean sea ice extent with linear trends. (b) Anomalies of sea ice extent relative to the 1981-2010 mean. Bars show values for the month of March (blue) and September (red), while lines show the corresponding trends throughout the study period. Note that quantification of trends is given as percentage of the 1981-2010 climatology. (c) and (d) Air (2 m height) and ocean (upper 100 m) temperature anomalies (top and bottom panels respectively) compared with sea ice extent (mid panel) for March (c) and September (d). Temperatures from gridded data sets are spatially averaged over the region. Correlation, r, between temperatures and ice extent is indicated. Note that ice extent is inverted for easier comparison.*

5.11 Greenland Sea

In the Greenland Sea region the case of total regional ice cover does not occur, nor does the region experience complete ice free conditions. The yearly mean cycle of ice extent (Fig. 5.7h) has a sinusoidal pattern, alternating from a maximum in March to a minimum in September. But the lines for each year (blue lines) is found to be less uniform in terms of the shape than for most other regions. Although all years reaches their minimum extent in either August or September the evolution during winter months is far more irregular, and yearly maximums can be found where ever in the interval from January to June. Hence the average yearly cycle has a broad peak, with a little defined maximum. The monthly trends, as presented in Figure 5.8h, are all negative, with the largest magnitudes during the first months of the year. The trends are gradually moderated when approaching summer months, and the least pronounced trend is found in September. From the continuous time series of yearly mean ice extent (Fig. 5.17a) remarked variation can be seen over time spans of a few years. The linear trend is regardlessly negative. However, for the last ten years alone,the trend (green line) is positive.

In Figure 5.17b we see pronounced anomalies for both March and September, of comparable magnitudes. In Figures 5.17c and 5.17d the evolution of March and September extent can be seen in context of air and ocean temperatures. In March the decreasing trend in ice extent resembles the increasing tendency in oceanic temperatures. Also the atmospheric temperatures has an increasing trend over the study period. Although the overall decrease, variations in the ice extent appears to have dampened the latest decade. In September the trend in ice cover is less prominent, but variations seems to match relatively well with variations in air temperature, as indicated by the correlation coefficient, r, in the panel.

5.12 Baffin Bay

Baffin Bay is, after the Central Arctic region, the region of largest extent during winter time. The annual mean cycle (Fig. 5.7i) is peaking in March with a value of $2.8 \cdot 10^6$ km^2. Despite this its ice cover is almost vanished when reaching the months of August to October, implying that the rate of decay during spring is the highest of all regions, and equally that the regain in autumn also happens at a very high rate. Monthly trends, as seen in Figure 5.8i, are all negative. The most outstanding being those of July, October and November.

In Figure 5.18b it can be seen that the anomalies are larger in March than in September, although both acquires negative characteristics in the later half of the time series, ensuring negative trends in both cases. This is found again in Figures 5.18c and 5.18d, where time series for March and September ice extent are presented along with time series for atmospheric and oceanic temperatures. There are far larger amplitudes in the interannual variations in the March ice extent than what is found in September. This is further accompanied by more pronounced year-to-year variability in both atmospheric and oceanic temperatures.

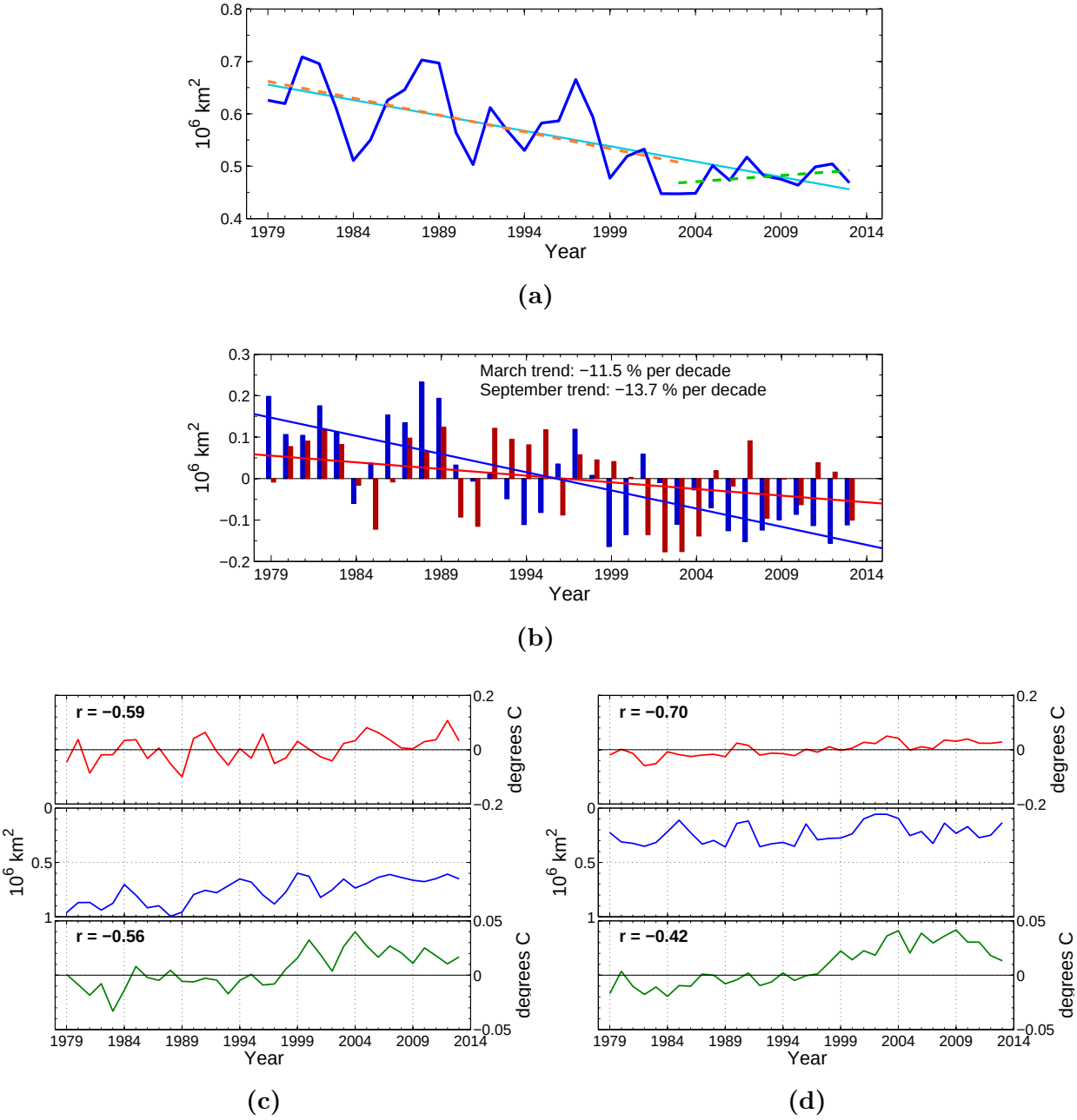

Figure 5.17: *Greenland Sea ice extent, anomalies and temperatures. (a) Time series of annual mean sea ice extent with linear trends. (b) Anomalies of sea ice extent relative to the 1981-2010 mean. Bars show values for the month of March (blue) and September (red), while lines show the corresponding trends throughout the study period. Note that quantification of trends is given as percentage of the 1981-2010 climatology. (c) and (d) Air (2 m height) and ocean (upper 100 m) temperature anomalies (top and bottom panels respectively) compared with sea ice extent (mid panel) for March (c) and September (d). Temperatures from gridded data sets are spatially averaged over the region. Correlation, r, between temperatures and ice extent is indicated. Note that ice extent is inverted for easier comparison.*

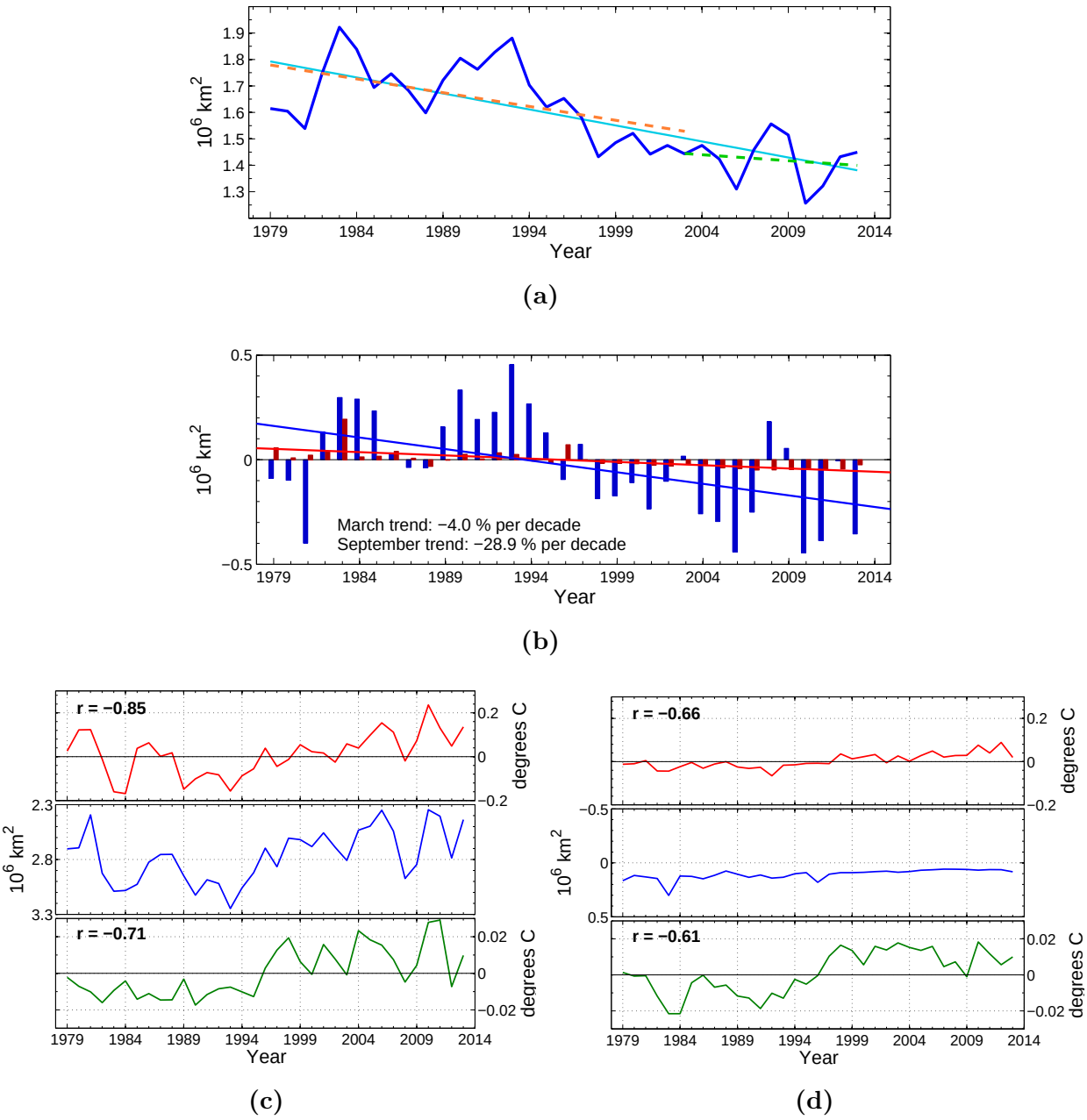

Figure 5.18: *Baffin Bay region ice extent, anomalies and temperatures. (a) Time series of annual mean sea ice extent with linear trends. (b) Anomalies of sea ice extent relative to the 1981-2010 mean. Bars show values for the month of March (blue) and September (red), while lines show the corresponding trends throughout the study period. Note that quantification of trends is given as percentage of the 1981-2010 climatology. (c) and (d) Air (2 m height) and ocean (upper 100 m) temperature anomalies (top and bottom panels respectively) compared with sea ice extent (mid panel) for March (c) and September (d). Temperatures from gridded data sets are spatially averaged over the region. Correlation, r, between temperatures and ice extent is indicated. Note that ice extent is inverted for easier comparison.*

5.13 Canadian Archipelago

The sea surface of the Canadian Archipelago gets completely ice covered during winter time, and hence the mean yearly cycle (black line) in Figure 5.7j is drawn as a straight line from December to April. The average minimum ice extent falls in September, but for certain years it occurs already in August. Trends for each month can be seen in Figure 5.8j, and as a consequence of the persistent winter ice throughout the data record only trends for months not experiencing a total ice cover are visible. These are all negative. Looking at the entire time series of yearly mean values (Fig. 5.19a) the interannual fluctuations are remarked, while a trend throughout the time series is less clearly depicted. Nevertheless the segmented trend line for 2003-2013 depicts a more negative trend than seen for both 1979-2003 and the entire span of 1979-2013. In Figure 5.19b frequent variations in September anomalies can be observed. It can though be seen explicitly that the heaviest load of negative anomalies falls between the years 2006 and 2012.

The March and September time series are presented and set up for comparison with temperatures of the atmosphere and ocean in Figures 5.19c and 5.19d. While the persistent total ice cover in March (mid panel, Fig. 5.19c) is not suited for any substantial comparison, the September ice extent (mid panel, Fig. 5.19d) reveals a good coherence with atmospheric temperatures (upper panel). Oceanic temperatures (lower panel) on the other hand does not appear as closely related.

5.14 Bering Sea

In the Bering Sea the ice cover nearly vanishes completely during the period from July to October, reaching the minimum in August. This appears from Figure 5.7k, where the yearly cycle of monthly mean ice extent is portrayed (black line) along with cycles for the individual years (blue lines). The maximum of the mean yearly cycle is found in March, and the widest spread of yearly values can be traced to the winter months January, February, March and April. This indicates that most of the variability seen in the yearly mean of the Bering Sea ice extent (Fig.5.20a, upper panel) can be explained by year-to-year variations in winter ice extent. In the Bering Sea we observe positive trends (Fig. 5.8k) for the five first months of the year, while the remaining months show negative trends. The anomalies for March (Fig. 5.20b) underlines the origin of the trends, as positive anomalies of high values are seen frequently after the year 2007.

In Figure 5.20c the year-to-year variations in March ice extent (mid panel) and atmospheric temperatures (upper panel) appears to follow each other quite well, and low temperature anomalies towards the end of the time series are accompanied by some of the highest ice extent values on record.

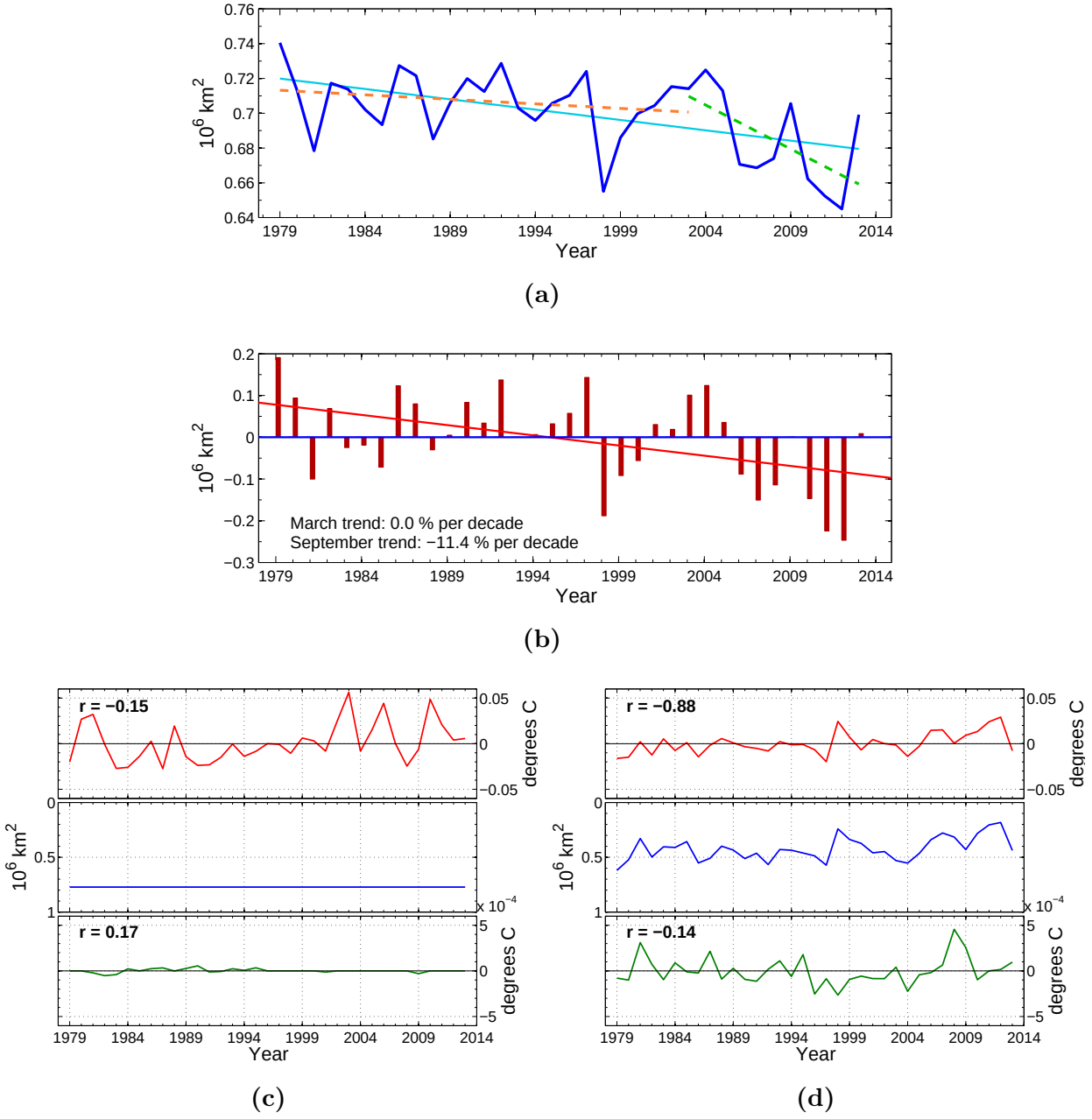

Figure 5.19: *Canadian Arctic Archipelago ice extent, anomalies and temperatures. (a) Time series of annual mean sea ice extent with linear trends. (b) Anomalies of sea ice extent relative to the 1981-2010 mean. Bars show values for the month of March (blue) and September (red), while lines show the corresponding trends throughout the study period. Note that quantification of trends is given as percentage of the 1981-2010 climatology. (c) and (d) Air (2 m height) and ocean (upper 100 m) temperature anomalies (top and bottom panels respectively) compared with sea ice extent (mid panel) for March (c) and September (d). Temperatures from gridded data sets are spatially averaged over the region. Correlation, r, between temperatures and ice extent is indicated. Note that ice extent is inverted for easier comparison.*

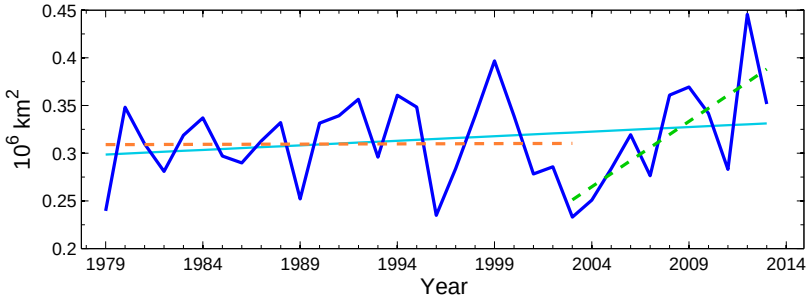

(a)

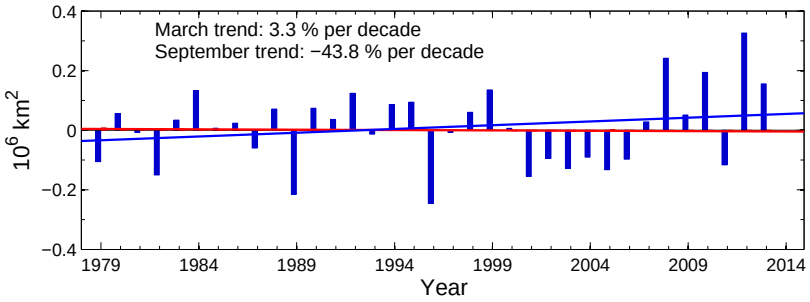

(b)

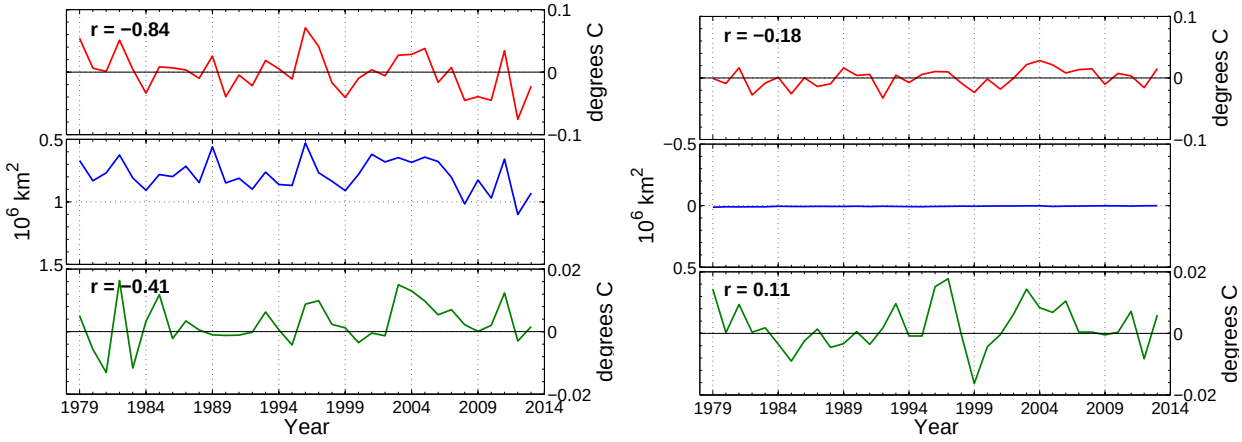

(c) **(d)**

Figure 5.20: *Bering Sea ice extent, anomalies and temperatures. (a) Time series of annual mean sea ice extent with linear trends. (b) Anomalies of sea ice extent relative to the 1981-2010 mean. Bars show values for the month of March (blue) and September (red), while lines show the corresponding trends throughout the study period. Note that quantification of trends is given as percentage of the 1981-2010 climatology. (c) and (d) Air (2 m height) and ocean (upper 100 m) temperature anomalies (top and bottom panels respectively) compared with sea ice extent (mid panel) for March (c) and September (d). Temperatures from gridded data sets are spatially averaged over the region. Correlation, r, between temperatures and ice extent is indicated. Note that ice extent is inverted for easier comparison.*

5.15 Okhotsk Sea

It is known from the yearly mean cycle in Figure 5.7l that the Okhotsk Sea region is seasonally ice free, as it does not have any presence of ice from July to September. This has persistently been the case throughout our data record. Hence there are not any trends to detect for these months in Figure 5.8l. While during first four months of the year the figure reveals the strongest decreasing trends. This is the reason for there not being any anomalies for September in Figure 5.21b, while the anomalies for March are pronounced, facilitating a decreasing linear trend. A feature revealed when viewing the March anomalies from the monthly climatology, which is not detectable by the linear trend, is the temporary upswing in the period of late nineties and early noughties. The same feature can also be observed in the time series of yearly mean (Fig. 5.21a).

In Figure 5.21c it can be seen that for the month of March the temporary peak in ice extent (mid panel) coincides with a drop in air temperatures (upper panel). Ocean temperatures (lower panel) does not reflect this same feature. The overall development of ice extent for these 35 years is heavily characterized by this upswing, and also by the high values seen at the beginning of the data record.

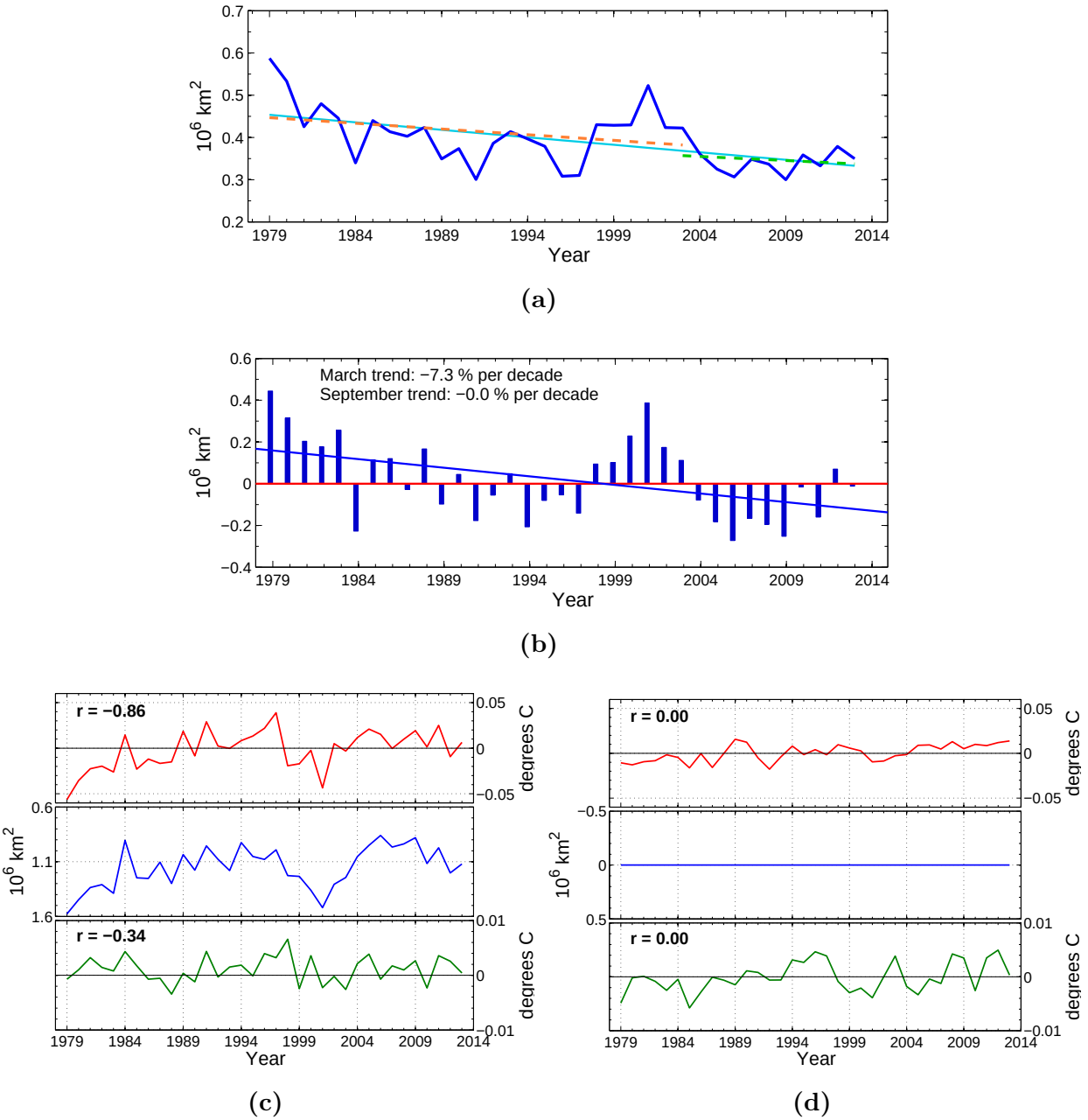

Figure 5.21: *Okhotsk Sea ice extent, anomalies and temperatures. (a) Time series of annual mean sea ice extent with linear trends. (b) Anomalies of sea ice extent relative to the 1981-2010 mean. Bars show values for the month of March (blue) and September (red), while lines show the corresponding trends throughout the study period. Note that quantification of trends is given as percentage of the 1981-2010 climatology. (c) and (d) Air (2 m height) and ocean (upper 100 m) temperature anomalies (top and bottom panels respectively) compared with sea ice extent (mid panel) for March (c) and September (d). Temperatures from gridded data sets are spatially averaged over the region. Correlation, r, between temperatures and ice extent is indicated. Note that ice extent is inverted for easier comparison.*

5.16 Regional comparison

In Table 5.1, 5.2 and 5.3 correlation coefficients between the temporal evolution of sea ice extent in the different regions are presented, respectively for yearly mean, March and September values. Upper right triangles are devoted to original time series, while lower left triangles (italic) contains values for detrended and standardized time series. The compared data includes time series for the entire Northern Hemisphere (NH), as well as the regions Central Arctic (CA), Beaufort Sea (BS), Chukchi Sea (CS), East Siberian Sea (ESS), Laptev Sea (LS), Kara Sea (KS), Barents Sea (BAR), Greenland Sea (GS), Baffin Bay (BB), Canadian Archipelago (CAN), Bering Sea (BER) and Okhotsk Sea (OS).

Flowingly, in Tables 5.4 and 5.5, correlation coefficients between sea ice extent and, respectively, atmospheric and oceanic temperatures are presented. The coefficients are calculated for March and September time series, and for each of these with original (upper row) and detrended (lower row, italic) time series.

Table 5.1: *Correlation between time series of yearly mean sea ice extent (Jan-Dec) for the different regions. Lower left triangular of the table (italic) are based on detrended and standardized time series, wile the upper right is computed from the original series. Correlations statistically significant to a level of 0.05 are emphasized in bold face.*

	NH	**CA**	**BS**	**CS**	**ESS**	**LS**	**KS**	**BAR**	**GS**	**BB**	**CAN**	**BER**	**OS**
NH	-	**0.74**	**0.60**	**0.84**	**0.74**	**0.75**	**0.81**	**0.84**	**0.72**	**0.75**	**0.59**	-0.21	**0.56**
CA	***0.50***	-	**0.40**	**0.55**	**0.48**	**0.56**	**0.73**	**0.74**	**0.55**	**0.47**	**0.48**	**-0.29**	0.29
BS	*0.22*	*0.04*	-	**0.61**	**0.48**	**0.44**	**0.55**	0.32	0.23	**0.51**	**0.68**	**-0.36**	0.17
CS	***0.48***	*0.11*	*0.95*	-	**0.75**	**0.54**	**0.59**	**0.57**	**0.57**	**0.59**	**0.35**	-0.07	**0.50**
ESS	***0.57***	*0.14*	*0.19*	***0.55***	-	**0.66**	**0.56**	**0.66**	**0.45**	0.33	**0.37**	-0.13	**0.48**
LS	***0.56***	*0.25*	*0.11*	*0.08*	***0.43***	-	**0.70**	**0.65**	**0.47**	**0.52**	**0.52**	**-0.44**	**0.40**
KS	***0.58***	***0.50***	*0.25*	*0.06*	*0.21*	***0.44***	-	**0.81**	**0.48**	**0.47**	**0.50**	-0.30	**0.43**
BAR	***0.52***	***0.50***	*-0.23*	*-0.09*	***0.37***	*0.32*	***0.58***	-	**0.65**	**0.39**	**0.43**	**-0.37**	**0.59**
GS	*0.11*	*0.15*	***-0.36***	*-0.03*	*-0.02*	*-0.01*	*-0.12*	*0.19*	-	**0.50**	0.27	-0.19	**0.34**
BB	*0.25*	*-0.01*	*0.16*	*0.02*	*-0.24*	*0.09*	*-0.12*	***-0.41***	*-0.10*	-	**0.56**	0.03	0.15
CAN	***0.37***	*0.24*	***0.55***	*-0.10*	*0.07*	*0.29*	*0.22*	*0.06*	*-0.20*	*0.32*	-	**-0.43**	0.25
BER	*-0.04*	*-0.20*	*-0.30*	***0.38***	*-0.01*	***-0.40***	*-0.23*	*-0.33*	*-0.06*	*0.18*	***-0.39***	-	-0.13
OS	*0.20*	*-0.08*	*-0.20*	*0.16*	*0.22*	*0.09*	*0.09*	***0.33***	*-0.10*	***-0.43***	*-0.03*	*-0.02*	-

Table 5.2: *Correlation between time series of sea ice extent in March for the different regions. Lower left triangular of the table (italic) are based on detrended and standardized time series, wile the upper right is computed from the original series. Correlations statistically significant to a level of 0.05 are emphasized in bold face.*

	NH	**CA**	**BS**	**CS**	**ESS**	**LS**	**KS**	**BAR**	**GS**	**BB**	**CAN**	**BER**	**OS**
NH	-	0.17	**0.41**	0.09	0.05	-0.04	0.32	**0.66**	**0.72**	**0.57**	0.13	-0.00	**0.63**
CA	*-0.25*	-	-0.14	-0.11	-0.15	-0.19	**0.67**	**0.44**	**0.39**	-0.01	-0.20	**-0.53**	-0.04
BS	***0.48***	*-0.22*	-	0.26	0.17	0.12	-0.13	0.05	0.03	0.27	**0.48**	**0.36**	0.29
CS	*0.29*	*-0.09*	*0.28*	-	-0.00	**0.39**	0.05	0.14	-0.22	-0.11	0.10	0.32	0.19
ESS	*0.10*	*-0.16*	*0.18*	*-0.00*	-	**0.61**	-0.09	0.15	0.08	-0.21	**0.34**	0.01	0.17
LS	*0.14*	*-0.15*	*0.15*	***0.38***	***0.62***	-	-0.03	0.20	-0.13	-0.31	0.23	-0.05	0.14
KS	*-0.02*	***0.62***	*-0.22*	*0.08*	*-0.10*	*0.02*	-	**0.57**	**0.35**	0.08	-0.14	**-0.38**	0.13
BAR	*0.30*	*0.30*	*-0.09*	*0.24*	*0.19*	***0.38***	***0.45***	-	**0.64**	-0.07	-0.10	**-0.41**	**0.55**
GS	*0.22*	*0.21*	*-0.18*	*-0.25*	*0.13*	*-0.04*	*0.09*	*0.32*	-	0.20	-0.11	**-0.39**	**0.49**
BB	***0.36***	*-0.20*	*0.21*	*-0.09*	*-0.23*	*-0.29*	*-0.13*	***-0.53***	*-0.27*	-	0.10	0.17	-0.05
CAN	*0.32*	*-0.19*	***0.49***	*0.10*	***0.34***	*0.22*	*-0.13*	*-0.09*	*-0.12*	*0.13*	-	**0.35**	0.15
BER	*0.33*	***-0.50***	***0.41***	*0.31*	*0.01*	*-0.07*	***-0.34***	***-0.37***	***-0.38***	*0.30*	***0.35***	-	-0.13
OS	***0.52***	*-0.23*	*0.24*	*0.25*	*0.19*	*0.23*	*-0.06*	***0.38***	*0.24*	*-0.33*	*0.19*	*-0.05*	-

Table 5.3: *Correlation between time series of sea ice extent in September for the different regions. Lower left triangular of the table (italic) are based on detrended and standardized time series, wile the upper right is computed from the original series. Correlations statistically significant to a level of 0.05 are emphasized in bold face.*

	NH	**CA**	**BS**	**CS**	**ESS**	**LS**	**KS**	**BAR**	**GS**	**BB**	**CAN**	**BER**	**OS**
NH	-	**0.71**	**0.83**	**0.90**	**0.83**	**0.74**	**0.65**	**0.36**	0.25	**0.65**	**0.62**	**0.68**	-
CA	***0.55***	-	**0.47**	**0.60**	**0.47**	**0.43**	**0.56**	**0.47**	0.14	0.31	**0.44**	**0.38**	-
BS	***0.64***	*0.15*	-	**0.87**	**0.64**	**0.47**	**0.43**	0.06	0.05	**0.58**	**0.58**	**0.55**	-
CS	***0.69***	*0.31*	***0.73***	-	**0.75**	**0.49**	**0.47**	0.21	0.31	**0.60**	**0.45**	**0.68**	-
ESS	***0.63***	*0.13*	*0.31*	***0.46***	-	**0.63**	**0.37**	0.11	0.15	**0.56**	**0.42**	**0.57**	-
LS	***0.56***	*0.15*	*0.12*	*0.02*	***0.37***	-	**0.53**	0.27	0.04	**0.45**	**0.51**	**0.41**	-
KS	***0.46***	***0.38***	*0.12*	*0.08*	*0.00*	*0.31*	-	**0.48**	0.07	**0.36**	0.33	0.32	-
BAR	*0.09*	***0.34***	*-0.28*	*-0.17*	*-0.22*	*0.07*	***0.37***	-	**0.34**	0.11	0.14	0.22	-
GS	*-0.10*	*-0.07*	*-0.28*	*0.03*	*-0.14*	*-0.23*	*-0.15*	*0.24*	-	0.21	-0.09	**0.49**	-
BB	*0.18*	*-0.11*	*0.21*	*0.10*	*0.15*	*0.08*	*-0.00*	*-0.20*	*-0.05*	-	**0.37**	**0.63**	-
CAN	***0.48***	*0.24*	***0.40***	*0.14*	*0.14*	*0.32*	*0.11*	*-0.04*	*0.31*	*0.08*	-	**0.38**	-
BER	*-0.11*	*-0.18*	*-0.05*	*-0.00*	*-0.05*	*-0.20*	*-0.25*	*-0.17*	*0.38*	*0.15*	*-0.03*	-	-
OS	-	-	-	-	-	-	-	-	-	-	-	-	-

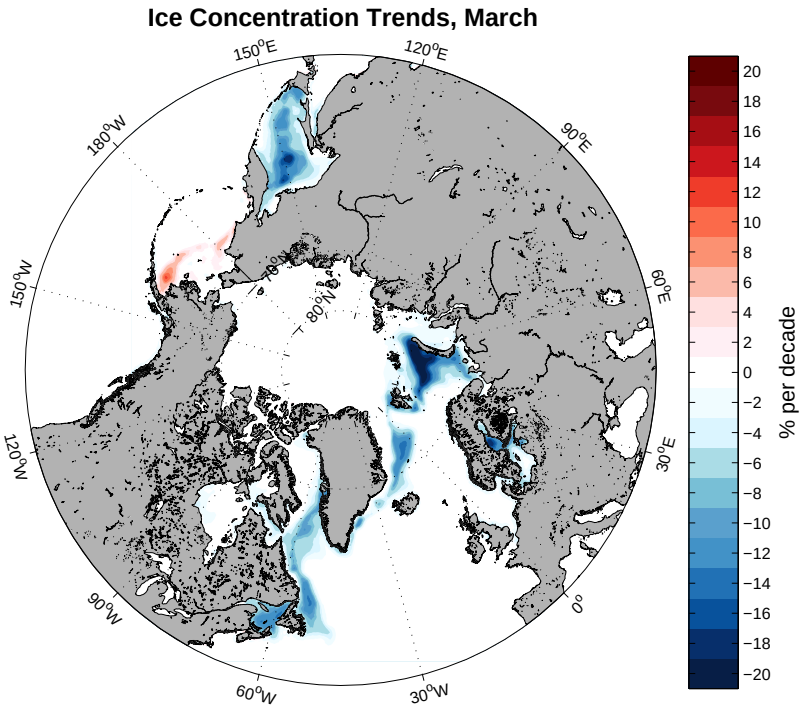

(a)

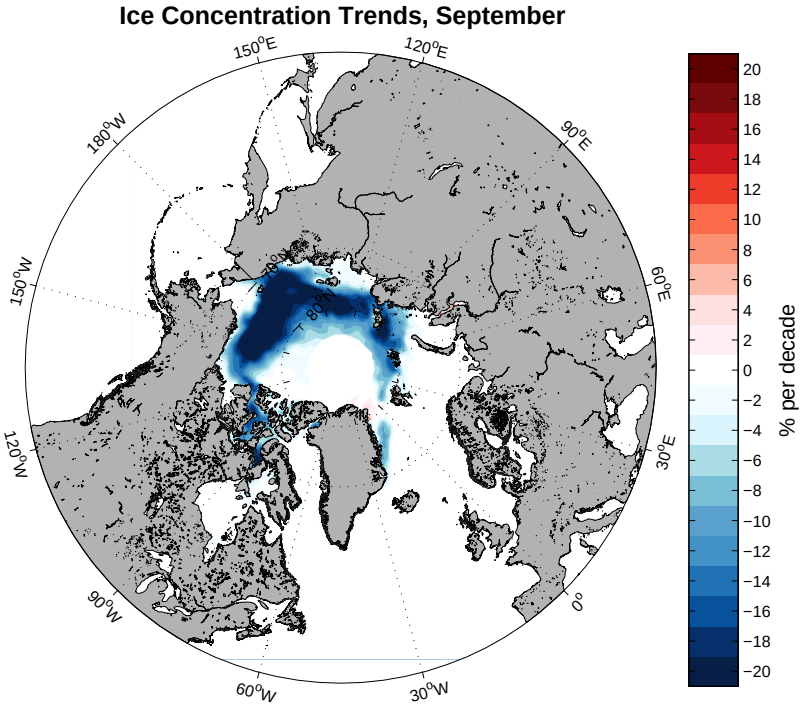

(b)

Figure 5.2: *Linear trends in monthly mean sea ice concentration from 1979-2013 for the months of March (a) and September (b).*

Table 5.4: *Correlation between time series of sea ice extent and corresponding atmospheric temperatures for the region in subject. Correlation coefficients are computed both for original time series and detrended series (italic). Values within a statistical significance level of 0.05 are emphasized in bold face.*

	NH	CA	BS	CS	ESS	LS	KS	BAR	GS	BB	CAN	BER	OS
March	**-0.68**	**-0.34**	-0.16	-0.26	-0.08	-0.01	**-0.64**	**-0.91**	**-0.59**	**-0.85**	-0.15	**-0.84**	**-0.86**
	-0.44	*-0.21*	*-0.15*	*-0.27*	*-0.09*	*-0.10*	***-0.56***	***-0.87***	***-0.43***	***-0.82***	*-0.17*	***-0.83***	***-0.83***
Sept	**-0.85**	**-0.49**	**-0.78**	**-0.81**	**-0.84**	**-0.83**	**-0.76**	**-0.47**	**-0.70**	**-0.66**	**-0.88**	-0.18	-
	-0.72	*-0.32*	***-0.73***	***-0.65***	***-0.81***	***-0.83***	***-0.71***	***-0.41***	***-0.70***	*-0.31*	***-0.84***	*0.18*	-

Table 5.5: *Correlation between time series of sea ice extent and corresponding ocean temperatures for the region in subject. Correlation coefficients are computed both for original time series and detrended series (italic). Values within a statistical significance level of 0.05 are emphasized in bold face.*

	NH	CA	BS	CS	ESS	LS	KS	BAR	GS	BB	CAN	BER	OS
March	**-0.80**	-0.09	-0.05	-0.02	**-0.37**	0.02	-0.13	**-0.72**	**-0.56**	**-0.71**	0.17	**-0.41**	**-0.34**
	-0.37	*0.06*	*-0.00*	*-0.02*	***-0.37***	*0.01*	*0.05*	***-0.53***	*-0.00*	***-0.61***	*0.17*	***-0.49***	***-0.36***
Sept	**-0.78**	**-0.56**	**-0.82**	**-0.59**	-0.20	**-0.52**	**-0.54**	**-0.42**	**-0.42**	**-0.61**	-0.14	0.11	-
	-0.05	***-0.38***	***-0.70***	***-0.41***	*-0.13*	***-0.48***	***-0.31***	*-0.25*	*-0.24*	*-0.27*	*-0.13*	*0.32*	-

Chapter 6

Discussion

The results obtained in this study describe the variability of the Arctic sea ice cover and quantify its evolution during the 35 years of satellite monitoring 1979-2013. These are presented in Chapter 5, along with data for some related variables. In the current chapter the results are interpreted further, elucidated by previous studies and physical theory, in order to identify possible connections and mechanisms driving the evolution of the Arctic ice cover.

6.1 Regional and seasonal differences

As the total Northern Hemisphere ice cover has proven to manifest negative trends for all months of the year during the satellite era (1979 to present) (Fig. 5.6b), one aim of this study has been to evaluate the most recent data available in terms of spatial and seasonal origins of these trends. As the ice covered Arctic encompasses a large region in meteorological and oceanographic scale, the evolution is not thought to be uniform for all parts of the ice cover. From the results presented in this study we try to outline a pattern of how the decline is distributed in time and space. By first addressing the regional time series we now highlight some of the characteristic features observed.

Of the regions in this study the Central Arctic, Beaufort Sea, Laptev Sea, Kara Sea, Barents Sea and Canadian Archipelago have yearly mean extent time series (Fig. 5.10a, 5.11a, 5.14a, 5.15a, 5.16a and 5.19a) with a steeper trend the latest decade of our records than for the preceding years, indicating an accelerated decline. Except the Barents Sea these regions all belong to the group C1, consisting of regions with a total winter ice cover (cf. Sec. 5.2 and Fig. 5.7), and hence the March extent does not resemble the development of the yearly mean throughout the data record. For the Central Arctic, Beaufort Sea and Canadian Archipelago the outline of the September ice extent (Fig. 5.10d, 5.11d and 5.19d) resembles the evolution of the yearly mean. Hence, we infer that the shrinking summer minimum explains the evolution of yearly mean ice extent in these regions.

In Laptev and Kara Sea however, the reduction in September extent (Fig. 5.14d and 5.15d)

recedes at the end of the time series. For the Kara Sea the September extent the last seven years displays considerably lower values with minimal variations, an evolution suggesting that a further decrease may not be possible. However, the fact that the extent does not reach zero does not quite agree with this. A closer look at maps of ice concentration in September (e.g. Fig.1.3) reveals that the remaining ice confines to the Gulf of Ob, an elongated bay holding the mouth of Ob river, and the Kara Sea can in regard to the analyses in this study be regarded as ice free under these conditions. This means that the acceleration in the yearly mean decrease does not origin from a further diminishing minimum extent. As the ice cover in March is continuous, it is clear that the accelerating decline is neither due to changes in minimum nor maximum extent. As discovered from the monthly trends of the Kara Sea (Fig. 5.8f), standing out from other C1 regions, the period of low ice extent has been prolonging over the span of our time series. This does hence manifest as the reason for our observed intensified decline. The profile of monthly trends for Laptev Sea (Fig. 5.8e) does also stand out compared to other C1 regions, not having an equally pronounced negative trend in September relative to other months. In context of the flattening of September extents this indicates a modification in the seasonal cycle similar to that of Kara Sea, although the Laptev Sea is not yet as far in the transition towards a seasonally ice free region.

The Barents Sea does not have substantial ice extent in September compared to the winter ice cover of the region. From our records the September extent (Fig. 5.16d) depicts for a decreasing trend. However constrained occurrences of September ice are not large enough to have any notable impact on the yearly mean. While clearly in decline, neither the March extent (Fig. 5.16c) can fully account for the accelerated ice loss of the yearly mean, and hence it is clear that other months of the year must account for the observed acceleration. As the Barents Sea also shows signs of an expanding period of minimum extent (cf. Fig. 5.8g), we infer that while a reduced March extent (i.e. lack of freezing) to a large degree accounts for the overall decrease, the prolongation of the summer season is an important reason for the accelerated decline evident the later years.

Chukchi Sea, East Siberian Sea, Baffin Bay and Okhotsk Sea all have time series of yearly mean ice extent (Fig. 5.12a, 5.13a, 5.18a and 5.21a) where the trend for the latest decade is moderated towards a lesser decline compared to the linear trend for the preceding years. Chukchi and East Siberian Sea, as C1 regions, does not have any trend in March (Fig. 5.12c and 5.13c). However the fact that, for both regions, the deceleration in the yearly mean is seen again in the September extent (Fig. 5.12d and 5.13d), where it is nearing zero, invokes that the nearing extinction of the summer ice extent is the reason for the yearly mean extent leveling out.

Baffin Bay sees almost no ice cover during summer, but still the modest variations seen in the first part of the time series of September extent in Figure 5.18d is almost eliminated after 1997, and the last 15 years depicts more constricted in terms of variation. However, as the March extent resembles the yearly mean quite well the main source for the flattening of yearly mean extent is believed to be found in the winter period. In the Okhotsk Sea it is hard to pinpoint any trend profile in the yearly mean extent (Fig. 5.21a), and its mediocre correlation to the remaining ice regions in March (Tab. 5.2) indicates that a large part of

the variation seen here is determined by local processes.

In the Bering Sea and Greenland Sea positive trends for 2003-2013 is seen. In fact in the Bering Sea the overall trend for the entire record is positive. The March extent time series (Fig. 5.20c) reflects the yearly mean well, and as the region is ice free during summer an increased rate of freezing must be the reason for the observed trends. (Sullivan et al., 2014) stated that winds are the primary driver of formation and advection of ice in the Bering Sea, and from this we can infer that changes in wind conditions to a certain extent is related to the changes seen in the ice cover. Greenland Sea has a larger negative trend in March than in September (Fig. 5.8h), but both time series (Fig. 5.17c and 5.17d) show substantial interannual variability. In March though this variability is dampened the last decade, and at the same time the decline tends to level out. Hence the deceleration of the decline in yearly mean ice extent is to a large extent due to processes during winter time.

6.1.1 Relations to other studies

The negative trends comes forward as an important feature for the interregional correlations (Tab. 5.1, 5.2 and 5.3). When trends are removed the magnitude of correlation coefficients are in general heavily reduced. The overall diminishing of ice cover is hence an important common aspect for most regions. Additionally an accelerated decline towards the end of the data record has been observed in several regions.

Cavalieri and Parkinson (2012) have previously addressed the regional evolution of the Arctic sea ice extent. Although our regional division consists of regional merging deviating from theirs, the data presented in this thesis can nevertheless be used for an update of their work. When comparing the linear trends of this study with those found by Cavalieri and Parkinson (2012) for the period 1979-2010, we get an impression of how the latest years affects our overall picture of the evolution. For the yearly average the trends have grown increasingly negative for most regions, confirming our suggestions of accelerated decline. Exceptions are the Bering Sea, where the positive trend has become larger, and the Greenland Sea, where a transition to a less pronounced negative trend is seen compared to the findings of Cavalieri and Parkinson (2012). The regions where the trends have become less negative are the same regions believed an ice cover where the variability to a large extent is responding to wind conditions.

Overland and Wang (2007) investigated the evolution in regional ice extent from the perspective of climate models. By starting with the model assembly from the Fourth Assessment Report (AR4) of the International Panel on Climate Change (IPCC), models of adequate compliance were selected to make projections for the 21st century. In the resulting projections most regions were expected to undergo substantial decline in ice extent up to 2050. Overland and Wang (2007) suggested a future summer sea ice area loss of more than 40% by 2050 in the marginal seas of the Arctic basin. Also in the adjacent seas of Bering, Okhotsk and Barents, although with less confidence, their results suggested a similar decline of 40% by 2050 in winter sea ice area. The simulated Greenland Sea showed less decline than other

regions, but was not represented by a sufficient selection of models to make a clear statement. Baffin Bay revealed, as the only region, no pronounced change compared to conditions at the time of investigation. The data set presented in this thesis is mainly in agreement with the projection of Overland and Wang (2007). With seven years of new observations since their projections were made, it is interesting to review their results in the light of todays ice conditions. It is found that, in most regions, there are no reasons to suggest that their projected decline was an over estimation. With the exception of the Bering Sea, of which the development the later years stands out. The increasing trend seen her does not quite coincide with the continuing decreasing tendency of Overland and Wang (2007).

6.2 Summer melting vs. lack of winter freezing

In this study two important mechanisms for diminishing of Arctic sea ice are advocated. A net loss of ice in the Northern Hemisphere can either come from an enhanced rate of melting or from reduced regain by freezing. With this as a base the question of relative importance between the two mechanisms arises. Knowing that different regions of the Arctic can be associated with locally defined patterns in their ice evolution, as throughly outlined in Section 6.1, the relation between melting and freezing in each region is consequently of interest. The question arising is consequently if we can define areas of the Arctic Ocean and adjacent seas to be classified as melting or non-freezing regions, targeting a principal reason for moderation of the ice extent.

6.2.1 Seasonal regimes

To investigate the co-variability between ice extent and temperatures in atmosphere and ocean correlation coefficients were calculated, with results as presented in Table 5.4 and 5.5. Even though the correlation is easily quantified, complex physical coupling makes conclusions about causality less straight forward. But based on a physical line of reasoning we will in this section show that there in some cases is acceptable to make assumptions about drivers of ice extent variability. By firstly addressing the summer scenario, and consequently the winter scenario, we here discuss the thermal interactions of atmosphere and ocean in both cases.

In late summer we typically have surface air temperatures that are higher than the ocean temperature, and hence heat fluxes are directed from atmosphere towards ocean (Screen and Simmonds, 2010). The underlying surface is important for the magnitude of the heat flux, and when the alternatives are ice contrary to open ocean, the less ice implies a smaller heat loss from the atmosphere. This stems from the fact that the ocean is warmer than ice, and hence the heat transfer coefficient is smaller at an air-ocean interface than at an air-ice interface. However, as summer is the time of year with the least pronounced temperature differences, this heat flux response to a lessened ice cover is limited (Deser et al., 2010). The warm air enables melting from the upper interface of the ice (cf. Sec.2.3), meaning that the atmospheric temperature is decisive for the ice condition. A warmer atmosphere will also

enhance direct warming of the ocean in the ice free areas. Additionally less ice cover will allow more radiative heating of the ocean (e.g. Perovich et al., 2008). This means that even though the ocean temperatures contribute to the melt of ice, the extent of the ice cover during summer is in turn highly decisive for the heating of the ocean (Comiso and Hall, 2014).

During winter the atmospheric temperature is usually below the freezing point, while the ocean is not colder than this. From Section 2.2 it is known that the air temperature has significance for the efficiency of ice growth. But it is also clear that the extent of the ice cover is decisive for the heat flux to the atmosphere from the ocean, and therefor an observed connection between atmospheric temperatures and ice cover makes it likely there is reciprocal influence. The ocean temperature on the other hand is highly decisive for the formation and growth of ice (cf. Sec. 2.2), but is to a lesser extent influenced by the ice cover. Based on this physical reasoning we can gain knowledge of the system from the following statements:

- A significant negative correlation between atmospheric temperatures and ice extent during summer suggests that the air temperature is a driver for melting of the ice cover.
- A significant negative correlation between oceanic temperature and ice extent during summer can not tell us whether the main reason is the oceans influence on the ice cover or the ice covers implications for the ocean, only that the two are connected.
- In the case of significant negative correlation between atmospheric temperatures and ice extent during winter we can only infer that the two are strongly coupled.
- A significant negative correlation between oceanic temperature and ice extent during winter indicates that a warmer ocean prevents ice growth.

As these statements origins from the theory of melting and freezing (Sec. 2), it is claimed that they enable assumptions about causality that are physically founded. Tietsche et al. (2011) suggests that in summer lack of ice cover enhances an oceanic heat anomaly (radiative heating), but in winter excess oceanic heat is lost to the atmosphere as a consequence of less ice, increasing the atmospheric temperature anomaly. The data in this study can be seen to support this statement.

6.2.2 What happens where when?

The Marginal Ice Zone (MIZ) shifts its location throughout the year (cf. Sec. 2.4). By exploiting what is know of the ice cover in March and September regions holding the MIZ in winter and summer can be identified exemplified by these months. During mid winter the ice edge is essentially found in the regions belonging to the C2 class based on their annual cycle (cf. Sec. 5.2), as they never sees a total ice cover. Pacific MIZ-regions are Bering Sea and Okhotsk Sea, and Atlantic MIZ-regions are Barents Sea, Greenland Sea and the Baffin Bay region. The remaining are regions classified as C1 regions (cf. Sec. 5.2) based on their annual mean cycle (Fig. 5.7), having a total or close to total ice cover during winter months.

During summer, when the MIZ retreats to the inner Arctic Ocean, the MIZ resides in C1 class regions. With one exception being the Greenland Sea, the only C2 region with substantial ice extent also in September. We now define the MIZ-regions after which water mass they are predominantly influenced by (cf. Fig. 2.1). Then Pacific MIZ-regions becomes Chukchi Sea, Beaufort Sea and the Canadian Archipelago. While Atlantic MIZ-regions are Greenland Sea, Kara Sea, Laptev Sea and the Central Arctic region. While the East Siberian Sea lies in the outskirts of the reach for both Atlantic and Pacific currents. In September the remaining regions are free or nearly free of ice.

In March the Northern Hemisphere as a whole shows a correlation of -0.80 between ice extent and ocean temperature (Tab. 5.5). The regions holding the MIZ at this time of year are the same regions whose ice cover show significant negative correlations with ocean temperatures. The East Siberian Sea is the only one of the non-MIZ regions revealing a significant correlation. When taking a closer look at the time series in question though (Fig. 5.13a), it is clear that there are only minor deviations, not even visible at the current scale, accounting for the variance in a seemingly straight line. However these intrusions are alone responsible for the retrieved correlation, while it is understood that they have little significance for the Arctic ice cover as a whole. In the Greenland Sea there is an outstandingly large discrepancy between the correlation coefficients calculated from trended and detrended time series. Despite a significant correlation of -0.56 for the original time series, the ice extent and ocean temperature series with removed trends does not reveal any traceable connection. This can be seen to indicate that other mechanisms are dominant in governing the variability of ice extent in this region. As the Fram Strait is known to be the main gate for ice export by drift (c.f. Sec. 2.6), and Smedsrud et al. (2011) showed the ice area export through the Fram Strait to a large extent relies on the variability of geostrophic wind, this can be the reason for a lesser reliance on oceanic heat. In general the ice-ocean correlations for March reveals a stronger relation between oceanic temperatures and ice extent on the Atlantic side than on the Pacific side (cf. Tab. 5.5). Indicating that the ocean temperatures are more important for the ice extent in the region receiving the warm water masses through the North Atlantic Current. Årthun et al. (2012) showed that the ice extent in the Barents Sea is closely related to the oceanic heat flux, and that a decreasing ice cover is bot related to higher temperatures of the incoming water and increased speeds of the currents carrying it into the region.

There are also significant negative correlations between ice extent and atmospheric temperatures in March (Tab. 5.4). The Northern Hemisphere as a whole has a correlation coefficient of -0.68, and even stronger correlations are found in most of the MIZ-regions. But as mentioned the strong coupling between atmosphere and open sea area makes us unable to assume anything about what caused what. Remaining regions do not show significant correlation coefficients. Exceptions form this are the Central Arctic and the Kara Sea. The correlations here are based on minor intrusions to what is predominantly total regional ice covers (cf. Fig. 5.10c and 5.15c), and is hence not of any real physical significance.

In September the MIZ-regions all have ice extent that is significantly negatively correlated to atmospheric temperature (Tab. 5.4). Suggesting that changes in air temperature initiates variation in the ice extent. The Central Arctic region is the MIZ-region with a correlation

coefficient of lowest absolute value. As it is situated in the midst of the ice cover intrusions to the summer ice extent comes alternating from the different surrounding regions. The regional temperature on the other hand is influenced of overlying the inner of the ice masses. One can therefor think it likely that the ice edge is more influenced by the air temperature in the surrounding regions. This might be a reason for the lower co-variability than seen in the other regions. The nearly ice free regions Barents Sea and Baffin Bay are also listed with significant correlation coefficients. As seen from the time series for Baffin Bay in Figure 5.18d the variance in September ice extent here is confined. Hence one may presume that the physical relevance of the air-ice relationship is less significant than the numbers indicate. In the Barents Sea it is known that the September ice extent is either a prolongation of the Central Arctic ice cover through the Svalbard-Franz Josef Land gate, or an intrusion from the Kara Sea between Franz-Josef Land and Novaya Zemlya. Correlation with averages over the entire spatial coverage of the Barents Sea may therefore not be of highest relevance in this regard.

The oceanic temperatures are also accountable for significant correlations with ice extent in September (Tab. 5.5), although generally not as prominent as for the atmospheric temperatures. As previously argued it is not hereby said that this is because incoming warm water masses controls the ice edge retreat. Attention is hereunder to be drawn to the the East Siberian Sea and the Canadian Arctic Archipelago. These regions, both lying in the fringes of their respective influential ocean currents, has little remarked correlations between ice extent and ocean temperature. This can be seen to indicate that the heat introduced by the ocean currents are actually initiating the ice edge retreat.

In general the detrended time series gives less pronounced correlations with atmosphere and ocean data than the original time series. For the regions already emphasized as substantially correlated variations are to a large extent explained. However, since the higher correlation coefficients are seen for the time series with trends removed, this indicates that the overall decrease in ice extent is clearly connected to an increase in temperatures both in atmosphere and ocean over the same period.

Chapter 7

Concluding remarks

7.1 Regional and seasonal differences

This thesis gives an in-depth description of the geographical distribution of observed changes in the Arctic sea ice extent. Linear trends were used as a tool to evaluate and compare the development.
It was found that the ice loss has accelerated towards the end of our data record for six of twelve regions. In the Central Arctic, Beaufort Sea and Canadian Archipelago this decrease is caused by an increasingly smaller summer ice cover. In the Laptev, Kara and Barents Sea a prolongation of the summer period is the main reason for the observed acceleration. Four regions reveals that the loss in ice extent has subsided the later years. In Chukchi and East Siberian Sea this is because the summer ice extent has been nearing or reaching zero the later years and is reaching it natural limit of declination. The last two regions, Greenland Sea and Bering Sea, show positive trends for the last decade, evolving from winter ice covers of increasing extents. The ice extent in these are both believed to be heavily subjected to wind conditions.

7.2 Melting vs. lack of freezing

As the regional variability of sea ice extent is examined in the light of seasonal temperature anomalies in atmosphere and ocean, the present work suggests that a general increase in atmospheric and oceanic temperatures is highly connected with a diminishing ice cover. In particular cases it is argued that the increasing temperatures can be identified as initial drivers for the sea ice retreat. This is the case for the Barents Sea and Baffin Bay region in in winter, when high ocean temperatures are believed to prevent the process of freezing. It is further argued that during summer the ice cover of Bering Sea, Chukchi Sea, East Siberian Sea, Laptev Sea, Kara Sea and the Canadian Archipelago is highly affected by melting initiated by a warm atmosphere.

In the Bering Sea and Greenland Sea, the two regions where the linear trends for the last decade is positive, we argue that thermal forcing is not the dominating factor driving the evolution of ice extent. It is however beyond this study to take the conclusion any further, as we have not taken ice thickness or transport of ice by drift into account.

Bibliography

Aagaard, K. and Carmack, E. (1989). The role of sea ice and other fresh water in the arctic circulation. *Journal of Geophysical Research: Oceans (1978–2012)*, 94(C10):14485–14498.

Aagaard, K., Coachman, L., and Carmack, E. (1981). On the halocline of the arctic ocean. *Deep Sea Research Part A. Oceanographic Research Papers*, 28(6):529–545.

Agnew, T., Lambe, A., and Long, D. (2008). Estimating sea ice area flux across the canadian arctic archipelago using enhanced amsr-e. *Journal of Geophysical Research: Oceans (1978–2012)*, 113(C10).

Andersen, S., Tonboe, R., Kaleschke, L., Heygster, G., and Pedersen, L. T. (2007). Intercomparison of passive microwave sea ice concentration retrievals over the high-concentration arctic sea ice. *Journal of Geophysical Research: Oceans (1978–2012)*, 112(C8).

Årthun, M., Eldevik, T., Smedsrud, L. H., Skagseth, Ø., and Ingvaldsen, R. (2012). Quantifying the influence of atlantic heat on barents sea ice variability and retreat. *Journal of Climate*, 25(13):4736–4743.

Årthun, M. and Schrum, C. (2010). Ocean surface heat flux variability in the barents sea. *Journal of Marine Systems*, 83(1):88–98.

Babb, D. G., Galley, R. J., Asplin, M. G., Lukovich, J. V., and Barber, D. G. (2013). Multiyear sea ice export through the bering strait during winter 2011–2012. *Journal of Geophysical Research: Oceans*, 118(10):5489–5503.

Berrisford, P., Dee, D., Poli, P., Brugge, R., Fielding, K., Fuentes, M., Kallberg, P., Kobayashi, S., Uppala, S., and Simmons, A. (2011). The era-interim archive. `http://www.ecmwf.int/en/research/climate-reanalysis/era-interim`. Accessed: 16.09.2014.

Beszczynska-Möller, A., Woodgate, R. A., Lee, C., Melling, H., and Karcher, M. (2011). A synthesis of exchanges through the main oceanic gateways to the arctic ocean. *in: The Changing Arctic Ocean: Special Issue on the International Polar Year (20072009), Oceanography, 24 (3) 99.*, 82.

Björk, G., Söderkvist, J., Winsor, P., Nikolopoulos, A., and Steele, M. (2002). Return of the cold halocline layer to the amundsen basin of the arctic ocean: Implications for the sea ice mass balance. *Geophysical Research Letters*, 29(11):8–1.

Cavalieri, D. and Parkinson, C. (2012). Arctic sea ice variability and trends, 1979-2010. *The Cryosphere, Volume 6, Issue 4, 2012, pp. 881-889*, 6:881–889.

Cavalieri, D., Parkinson, C., Gloersen, P., and Zwally, H. J. (1996). Sea ice concentrations from nimbus-7 smmr and dmsp ssm/i-ssmis passive microwave data. `http://nsidc.org/data/docs/daac/nsidc0051_gsfc_seaice.gd.html`. Accessed: 24.08.2014.

Chepurin, G. A. and Carton, J. A. (2012). Subarctic and arctic sea surface temperature and its relation to ocean heat content 1982–2010. *Journal of Geophysical Research: Oceans (1978–2012)*, 117(C6).

Comiso, J. C. (2002). Correlation and trend studies of the sea-ice cover and surface temperatures in the arctic. *Annals of Glaciology*, 34(1):420–428.

Comiso, J. C. (2003). Warming trends in the arctic from clear sky satellite observations. *Journal of Climate*, 16(21):3498–3510.

Comiso, J. C. (2012). Large decadal decline of the arctic multiyear ice cover. *Journal of Climate*, 25(4):1176–1193.

Comiso, J. C. and Hall, D. K. (2014). Climate trends in the arctic as observed from space. *Wiley Interdisciplinary Reviews: Climate Change*, 5(3):389–409.

Comiso, J. C., Parkinson, C. L., Gersten, R., and Stock, L. (2008). Accelerated decline in the arctic sea ice cover. *Geophysical Research Letters*, 35(1).

Curry, J. A., Schramm, J. L., Rossow, W. B., and Randall, D. (1996). Overview of arctic cloud and radiation characteristics. *Journal of Climate*, 9(8):1731–1764.

Deser, C., Tomas, R., Alexander, M., and Lawrence, D. (2010). The seasonal atmospheric response to projected arctic sea ice loss in the late twenty-first century. *Journal of Climate*, 23(2):333–351.

Eicken, H. (2003). From the microscopic, to the macroscopic, to the regional scale: growth, microstructure and properties of sea ice. *Sea ice: an introduction to its physics, chemistry, biology and geology*, pages 22–81.

Eisenman, I. and Wettlaufer, J. (2009). Nonlinear threshold behavior during the loss of arctic sea ice. *Proceedings of the National Academy of Sciences*, 106(1):28–32.

Ekman, V. W. (1905). On the influence of the earth\'s rotation on ocean currents. *Ark. Mat. Astron. Fys.*, 2:1–53.

Ekwurzel, B., Schlosser, P., Mortlock, R. A., Fairbanks, R. G., and Swift, J. H. (2001). River runoff, sea ice meltwater, and pacific water distribution and mean residence times in the arctic ocean. *Journal of Geophysical Research: Oceans (1978–2012)*, 106(C5):9075–9092.

Fetterer, F., Savoie, M., Helfrich, S., and Clemente-Colón, P. (2010). Multisensor analyzed sea ice extent - northern hemisphere, masie-nh. http://dx.doi.org/10.7265/N5GT5K3K. Accessed: 17.01.2014.

Francis, J. A. and Hunter, E. (2006). New insight into the disappearing arctic sea ice. *Eos, Transactions American Geophysical Union*, 87(46):509–511.

Hansen, E., Gerland, S., Granskog, M., Pavlova, O., Renner, A., Haapala, J., Løyning, T. B., and Tschudi, M. (2013). Thinning of arctic sea ice observed in fram strait: 1990–2011. *Journal of Geophysical Research: Oceans*, 118(10):5202–5221.

IHO (1953). *Limits of Oceans and Seas*. Number 23. International Hydrographic Organization.

Ivanova, N., Johannessen, O. M., Pedersen, L. T., and Tonboe, R. T. (2014). Retrieval of arctic sea ice parameters by satellite passive microwave sensors: A comparison of eleven sea ice concentration algorithms.

Jahn, A., Tremblay, B., Mysak, L. A., and Newton, R. (2010). Effect of the large-scale atmospheric circulation on the variability of the arctic ocean freshwater export. *Climate dynamics*, 34(2-3):201–222.

Jones, E. P. (2001). Circulation in the arctic ocean. *Polar Research*, 20(2):139–146.

Kapsch, M.-L., Graversen, R. G., and Tjernström, M. (2013). Springtime atmospheric energy transport and the control of arctic summer sea-ice extent. *Nature Climate Change*, 3(8):744–748.

Kikuchi, T., Hatakeyama, K., and Morison, J. H. (2004). Distribution of convective lower halocline water in the eastern arctic ocean. *Journal of Geophysical Research: Oceans (1978–2012)*, 109(C12).

Kwok, R. (2006). Exchange of sea ice between the arctic ocean and the canadian arctic archipelago. *Geophysical Research Letters*, 33(16).

Kwok, R., Cunningham, G., and Pang, S. (2004). Fram strait sea ice outflow. *Journal of Geophysical Research: Oceans (1978–2012)*, 109(C1).

Kwok, R., Cunningham, G., Wensnahan, M., Rigor, I., Zwally, H., and Yi, D. (2009). Thinning and volume loss of the arctic ocean sea ice cover: 2003–2008. *Journal of Geophysical Research: Oceans (1978–2012)*, 114(C7).

Kwok, R., Toudal Pedersen, L., Gudmandsen, P., and Pang, S. (2010). Large sea ice outflow into the nares strait in 2007. *Geophysical Research Letters*, 37(3).

Leppäranta, M. (1993). A review of analytical models of sea-ice growth. *Atmosphere-Ocean*, 31(1):123–138.

Leppäranta, M. (2011). *The drift of sea ice*. Springer.

Levitus, S., Antonov, J. I., Boyer, T. P., Baranova, O. K., Garcia, H. E., Locarnini, R. A., Mishonov, A. V., Reagan, J., Seidov, D., Yarosh, E. S., et al. (2012). Global ocean heat and salt content. `https://www.nodc.noaa.gov/OC5/3M_HEAT_CONTENT`. Accessed: 24.09.2014.

Li, L., McClean, J. L., Miller, A. J., Eisenman, I., Hendershott, M. C., and Papadopoulos, C. A. (2014). Processes driving sea ice variability in the bering sea in an eddying ocean/sea ice model: mean seasonal cycle. *Ocean Modelling*, 84:51–66.

Løvås, G. G. (2013). *Statistikk for universiteter og høgskoler*. Universitetsforlaget.

Maslanik, J., Fowler, C., Stroeve, J., Drobot, S., Zwally, J., Yi, D., and Emery, W. (2007). A younger, thinner arctic ice cover: Increased potential for rapid, extensive sea-ice loss. *Geophysical Research Letters*, 34(24).

Maslanik, J., Stroeve, J., Fowler, C., and Emery, W. (2011). Distribution and trends in arctic sea ice age through spring 2011. *Geophysical Research Letters*, 38(13).

Maykut, G. A. (1978). Energy exchange over young sea ice in the central arctic. *Journal of Geophysical Research: Oceans (1978–2012)*, 83(C7):3646–3658.

McGeehan, T. and Maslowski, W. (2012). Evaluation and control mechanisms of volume and freshwater export through the canadian arctic archipelago in a high-resolution pan-arctic ice-ocean model. *Journal of Geophysical Research: Oceans (1978–2012)*, 117(C8).

McPhee, M. and Morison, J. (2001). Under-ice boundary layer. *Encyclopedia of Ocean Sciences*, pages 3069–3076.

McPhee, M., Morison, J., and Nilsen, F. (2008). Revisiting heat and salt exchange at the ice-ocean interface: Ocean flux and modeling considerations. *Journal of Geophysical Research: Oceans (1978–2012)*, 113(C6).

McPhee, M. G. (1992). Turbulent heat flux in the upper ocean under sea ice. *Journal of Geophysical Research: Oceans (1978–2012)*, 97(C4):5365–5379.

Münchow, A., Melling, H., and Falkner, K. K. (2006). An observational estimate of volume and freshwater flux leaving the arctic ocean through nares strait. *Journal of Physical Oceanography*, 36(11).

Nghiem, S., Rigor, I., Perovich, D., Clemente-Colon, P., Weatherly, J., and Neumann, G. (2007). Rapid reduction of arctic perennial sea ice. *Geophysical Research Letters*, 34(19).

Notz, D. (2009). The future of ice sheets and sea ice: Between reversible retreat and unstoppable loss. *Proceedings of the National Academy of Sciences*, 106(49):20590–20595.

Ogi, M., Rigor, I. G., McPhee, M. G., and Wallace, J. M. (2008). Summer retreat of arctic sea ice: Role of summer winds. *Geophysical Research Letters*, 35(24).

Ogi, M., Yamazaki, K., and Wallace, J. M. (2010). Influence of winter and summer surface wind anomalies on summer arctic sea ice extent. *Geophysical Research Letters*, 37(7).

Onarheim, I. H., Smedsrud, L. H., Ingvaldsen, R. B., and Nilsen, F. (2014). Loss of sea ice during winter north of svalbard. *Tellus A*, 66.

Overland, J. E. and Guest, P. S. (1991). The arctic snow and air temperature budget over sea ice during winter. *Journal of Geophysical Research: Oceans (1978–2012)*, 96(C3):4651–4662.

Overland, J. E. and Wang, M. (2007). Future regional arctic sea ice declines. *Geophysical Research Letters*, 34(17).

Parkinson, C. and Cavalieri, D. (2008). Arctic sea ice variability and trends, 1979-2006. *Journal of Geophysical Reserch: Oceans, Volume 113, Issue C7, july 2008*, 113.

Parkinson, C. L. and Comiso, J. C. (2013). On the 2012 record low arctic sea ice cover: Combined impact of preconditioning and an august storm. *Geophysical Research Letters*, 40(7):1356–1361.

Pease, C. H. (1980). Eastern bering sea ice processes. *Monthly Weather Review*, 108(12):2015–2023.

Perovich, D. K., Richter-Menge, J. A., Jones, K. F., and Light, B. (2008). Sunlight, water, and ice: Extreme arctic sea ice melt during the summer of 2007. *Geophysical Research Letters*, 35(11).

Pfirman, S., Haxby, W. F., Colony, R., and Rigor, I. (2004). Variability in arctic sea ice drift. *Geophysical Research Letters*, 31(16).

Polyakov, I. V., Alekseev, G. V., Bekryaev, R. V., Bhatt, U. S., Colony, R., Johnson, M. A., Karklin, V. P., Walsh, D., and Yulin, A. V. (2003). Long-term ice variability in arctic marginal seas. *Journal of Climate*, 16(12):2078–2085.

Polyakov, I. V., Bhatt, U. S., Walsh, J. E., Abrahamsen, E. P., Pnyushkov, A. V., and Wassmann, P. F. (2013). Recent oceanic changes in the arctic in the context of long-term observations. *Ecological Applications*, 23(8):1745–1764.

Polyakov, I. V., Timokhov, L. A., Alexeev, V. A., Bacon, S., Dmitrenko, I. A., Fortier, L., Frolov, I. E., Gascard, J.-C., Hansen, E., Ivanov, V. V., et al. (2010). Arctic ocean warming contributes to reduced polar ice cap. *Journal of Physical Oceanography*, 40(12):2743–2756.

Rothrock, D. (1975). The steady drift of an incompressible arctic ice cover. *Journal of Geophysical Research*, 80(3):387–397.

Rudels, B., Anderson, L., and Jones, E. (1996). Formation and evolution of the surface mixed layer. *Journal of Geophysical Research*, 101(C4):8807–8821.

Screen, J. A. and Simmonds, I. (2010). The central role of diminishing sea ice in recent arctic temperature amplification. *Nature*, 464(7293):1334–1337.

Serreze, M. C., Barrett, A. P., Slater, A. G., Woodgate, R. A., Aagaard, K., Lammers, R. B., Steele, M., Moritz, R., Meredith, M., and Lee, C. M. (2006). The large-scale freshwater cycle of the arctic. *Journal of Geophysical Research: Oceans (1978–2012)*, 111(C11).

Serreze, M. C., Holland, M. M., and Stroeve, J. (2007). Perspectives on the arctic's shrinking sea-ice cover. *science*, 315(5818):1533–1536.

Shimada, K., Kamoshida, T., Itoh, M., Nishino, S., Carmack, E., McLaughlin, F., Zimmermann, S., and Proshutinsky, A. (2006). Pacific ocean inflow: Influence on catastrophic reduction of sea ice cover in the arctic ocean. *Geophysical Research Letters*, 33(8).

Smedsrud, L., Sirevaag, A., Kloster, K., Sorteberg, A., and Sandven, S. (2011). Recent wind driven high sea ice area export in the fram strait contributes to arctic sea ice decline. *The Cryosphere*, 5(4):821–829.

Smedsrud, L. H., Ingvaldsen, R., Nilsen, J. E. Ø., and Skagseth, Ø. (2010). Heat in the barents sea: Transport, storage, and surface fluxes.

Smedsrud, L. H., Sorteberg, A., and Kloster, K. (2008). Recent and future changes of the arctic sea-ice cover. *Geophysical Research Letters*, 35(20).

Spreen, G., Kwok, R., and Menemenlis, D. (2011). Trends in arctic sea ice drift and role of wind forcing: 1992–2009. *Geophysical Research Letters*, 38(19).

Squire, V. (2007). Of ocean waves and sea-ice revisited. *Cold Regions Science and Technology*, 49(2):110–133.

Steele, M. and Boyd, T. (1998). Retreat of the cold halocline layer in the arctic ocean. *Journal of Geophysical Research: Oceans (1978–2012)*, 103(C5):10419–10435.

Stocker, T. and Qin, D. (2013). Climate change 2013: The physical science basis. *Working Group I Contribution to the Fifth Assessment Report of the Intergovernmental Panel on Climate Change, Summary for Policymakers, IPCC*.

Stroeve, J., Holland, M. M., Meier, W., Scambos, T., and Serreze, M. (2007). Arctic sea ice decline: Faster than forecast. *Geophysical research letters*, 34(9).

Stroeve, J. C., Serreze, M. C., Holland, M. M., Kay, J. E., Malanik, J., and Barrett, A. P. (2012). The arctic's rapidly shrinking sea ice cover: a research synthesis. *Climatic Change*, 110(3-4):1005–1027.

Sullivan, M. E., Kachel, N. B., Mordy, C. W., Salo, S. A., and Stabeno, P. J. (2014). Sea ice and water column structure on the eastern bering sea shelf. *Deep Sea Research Part II: Topical Studies in Oceanography*.

Swift, J., Aagaard, K., Timokhov, L., and Nikiforov, E. G. (2005). Long-term variability of arctic ocean waters: Evidence from a reanalysis of the ewg data set. *Journal of Geophysical Research: Oceans (1978–2012)*, 110(C3).

Thomas, D. N. and Dieckmann, G. S. (2009). *Sea ice*. John Wiley & Sons.

Thorndike, A. and Colony, R. (1982). Sea ice motion in response to geostrophic winds. *Journal of Geophysical Research: Oceans (1978–2012)*, 87(C8):5845–5852.

Tietsche, S., Notz, D., Jungclaus, J., and Marotzke, J. (2011). Recovery mechanisms of arctic summer sea ice. *Geophysical Research Letters*, 38(2).

Wadhams, P. (1986). The seasonal ice zone. In *The geophysics of sea ice*, pages 825–991. Springer.

Wang, M. and Overland, J. E. (2009). A sea ice free summer arctic within 30 years? *Geophysical Research Letters*, 36(7).

Wang, M. and Overland, J. E. (2012). A sea ice free summer arctic within 30 years: An update from cmip5 models. *Geophysical Research Letters*, 39(18).

Wang, X. and Zhao, J. (2012). Seasonal and inter-annual variations of the primary types of the arctic sea-ice drifting patterns. *Adv Polar Sci*.

Wendler, G., Chen, L., and Moore, B. (2013). Recent sea ice increase and temperature decrease in the bering sea area, alaska. *Theoretical and Applied Climatology*, pages 1–6.

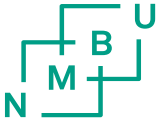

Norwegian University
of Life Sciences

Postboks 5003
NO-1432 Ås, Norway
+47 67 23 00 00
www.nmbu.no